Palestine Polytechnic University

Deanship of Graduate Studies and Scientific Research

Master of Civil Engineering

# Numerical Investigation of Reinforced Concrete Deep Beams with Web Openings Strengthened Using UHPC and CFRP

Done By

Mahmoud Ibrahim Hasan Mahariq

Supervisor

Dr. Belal Almassri

Thesis submitted in partial fulfillment of requirements
of the degree Master of Civil Engineering

May, 2026

The undersigned hereby certify that they have read, examined and recommended to the Deanship of *Graduate Studies and Scientific Research* at Palestine Polytechnic University:

Numerical Investigation of Reinforced Concrete Deep Beams with Web Openings Strengthened Using UHPC and CFRP

Mahmoud Ibrahim Hasan Mahariq

In partial fulfillment of the requirements for the degree of Master in Civil Engineering.

Graduate Advisory Committee:

Prof./Dr. ...Belal...ALMASSRI... University ...,PPU.....

Signature: _____ Date:07/05/2026

Prof./Dr. ..... University ...,.....

Signature: _____ *Date:07/05/2026*

Prof./Dr. ..Haitham...Ayyad..... University ...,..P.P.U.....

Signature: _____ Date:07/05/2026

Prof./Dr. ...Mahmoud Shalan... University ..P.A.U.....

Signature: _____ Date:07/05/2026

Thesis Approved by:

Name:

Dean of Graduate Studies & Scientific Research

Palestine Polytechnic University

*Signature :* .....

Date : 07/05/2026

**Numerical Investigation of Reinforced Concrete Deep Beams with Web Openings Strengthened Using UHPC and CFRP**

(Mahmoud Ibrahim Hasan Mahariq)

ABSTRACT

Reinforced concrete deep beams are widely used in structural applications where loads are transferred over short spans, such as transfer girders, pile caps, and other heavily loaded members. Unlike slender beams, deep beams resist loads primarily through a diagonal compression strut, which governs their overall structural behavior. In practical applications, web openings are often introduced to accommodate mechanical and electrical services. However, such openings disturb the natural load-transfer path, leading to stress concentration, earlier cracking, lower stiffness, and a significant reduction in ultimate load capacity. This makes the evaluation of strengthening techniques essential for improving the performance of deep beams with openings.

This study investigates the behavior of reinforced concrete deep beams with and without web openings using nonlinear finite element analysis in ABAQUS. The numerical model was first validated against available experimental results in terms of load–displacement response, ultimate load, and failure mode. After achieving acceptable agreement, the validated model was used to conduct a detailed parametric study. The investigated parameters included opening size, opening location, strengthening technique, transverse reinforcement ratio, concrete compressive strength, and reinforcement yield strength. In addition, the effectiveness of ultra-high-performance concrete (UHPC) and carbon-fiber-reinforced polymer (CFRP) was assessed as strengthening methods for beams weakened by openings.

The results showed that the introduction of web openings caused a substantial reduction in the ultimate load capacity, ranging from 62.42% to 65.69% compared with the solid reference beam, depending on the size and location of the opening. Beams with openings located near the edge of the shear span performed better than those with openings at the center of the shear span, while larger openings resulted in more severe reductions in strength. The strengthening results indicated that UHPC was the most effective technique, increasing the ultimate load capacity by approximately 24.34% to 32.61%, whereas CFRP provided more moderate improvements ranging from about 11.9% to 15.35%. The parametric study further showed that concrete compressive strength had the greatest influence on beam response, followed by the transverse reinforcement ratio, while the effect of reinforcement yield strength was comparatively limited.

Overall, the study confirms that the structural behavior of reinforced concrete deep beams is governed mainly by the integrity of the diagonal compression strut. Therefore, any parameter or strengthening technique that enhances or restores this load-transfer mechanism has the greatest impact on structural performance. The findings of this study provide a clearer understanding of the behavior of deep beams with openings and offer useful guidance for their analysis, strengthening, and design using advanced materials such as UHPC and CFRP.

# دراسة عددية للسلوك الإنشائي للكمرات العميقة الخرسانية المسلحة ذات الفتحات في الجذع والمقواة باستخدام الخرسانة فائقة الأداء (UHPC) والبوليمرات المسلحة بألياف الكربون(CFRP)

محمود ابراهيم حسن محاريق

الملخص:

تُعدّ الكمرات العميقة الخرسانية المسلحة من العناصر الإنشائية المهمة التي تُستخدم على نطاق واسع في التطبيقات التي تنتقل فيها الأحمال عبر بحور قصيرة، مثل الجوائز الناقلة، وقواعد الخوازيق، وغيرها من العناصر المعرضة لأحمال كبيرة. وعلى خلاف الكمرات النحيفة، فإن الكمرات العميقة تقاوم الأحمال بصورة رئيسية من خلال دعامة ضغط قطرية تتحكم في سلوكها الإنشائي العام. وفي التطبيقات العملية، غالبًا ما يتم عمل فتحات في جسم الكمرة لتمرير الخدمات الميكانيكية والكهربائية. إلا أن هذه الفتحات تؤدي إلى إعاقة مسار انتقال الحمل الطبيعي داخل الكمرة، مما ينتج عنه تركّز في الإجهادات، وظهور مبكر للتشققات، وانخفاض في الصلابة، وتراجع ملحوظ في الحمولة القصوى. لذلك، يصبح تقييم تقنيات التقوية أمرًا ضروريًا لتحسين أداء الكمرات العميقة المحتوية على فتحات.

تتناول هذه الدراسة سلوك الكمرات العميقة الخرسانية المسلحة بوجود الفتحات وبدونها باستخدام التحليل العددي غير الخطي من خلال برنامج .ABAQUS وقد تم أولًا التحقق من صحة النموذج العددي من خلال مقارنته بالنتائج العملية المتاحة من حيث منحنيات الحمل–الإزاحة، والحمولة القصوى، ونمط الفشل. وبعد الوصول إلى توافق مقبول، استُخدم النموذج المعتمد لإجراء دراسة بارامترية تفصيلية. وشملت المتغيرات المدروسة حجم الفتحة، وموقعها، ونوع التقوية، ونسبة التسليح العرضي، ومقاومة الخرسانة للضغط، وإجهاد خضوع حديد التسليح. كما تم تقييم فعالية كلٍّ من الخرسانة فائقة الأداء (UHPC) والبوليمرات المسلحة بألياف الكربون (CFRP) كوسيلتين لتقوية الكمرات المتأثرة بوجود الفتحات.

أظهرت النتائج أن وجود الفتحات أدى إلى انخفاض كبير في الحمولة القصوى، حيث تراوحت نسبة الانخفاض بين **62.42%و65.69 %**مقارنة بالكمرة المرجعية المصمتة، وذلك تبعًا لحجم الفتحة وموقعها. كما تبيّن أن الكمرات التي تقع فتحاتها بالقرب من حافة بحر القص أظهرت أداءً أفضل من تلك التي تقع فتحاتها في مركز بحر القص، في حين أدت الفتحات الأكبر إلى انخفاض أشد في المقاومة. وأوضحت نتائج التقوية أن استخدام **UHPC**كان الأكثر فاعلية، إذ أدى إلى زيادة في الحمولة القصوى تراوحت بين **24.34%و32.61%**، بينما حقق **CFRP**تحسينات أكثر اعتدالًا تراوحت بين **11.9%و15.35%**. كذلك أظهرت الدراسة البارامترية أن مقاومة الخرسانة للضغط كانت العامل الأكثر تأثيرًا في استجابة الكمرة، تلتها نسبة التسليح العرضي، في حين كان تأثير إجهاد خضوع حديد التسليح محدودًا نسبيًا.

وبوجه عام، تؤكد هذه الدراسة أن السلوك الإنشائي للكمرات العميقة الخرسانية المسلحة تحكمه بصورة رئيسية سلامة دعامة الضغط القطرية. وعليه، فإن أي متغير أو أسلوب تقوية يسهم في تحسين أو استعادة آلية انتقال الحمل هذه سيكون له الأثر الأكبر في الأداء الإنشائي. وتوفر نتائج هذه الدراسة فهمًا أوضح لسلوك الكمرات العميقة ذات الفتحات، كما تقدم دلالات مفيدة لتحليلها وتقويتها وتصميمها باستخدام مواد متقدمة مثل **UHPC**و **CFRP**

.

## DECLARATION

I declare that the Master Thesis entitled" Numerical Investigation of Reinforced Concrete Deep Beams with Web Openings Strengthened Using UHPC and CFRP" is my own original work, and herby certify that unless stated, all work contained within this thesis is my own independent research and has not been submitted for the award of any other degree at any institution, except where due acknowledgement is made in the text.

Student Name: Mahmoud Ibrahim Hasan Mahariq

Signature: ———————————— Date: 07/05/2026

# DEDICATION

Thanks be to God Who is always helping us to success

To the soul of my beloved father, may he rest in peace, who was a source of support and inspiration, and whose memory will forever remain in my heart.

To my dear mother, for her endless love, prayers, and unwavering support

To my wife, for her patience, encouragement, and constant support throughout this journey.

To my dear daughter, who has been a source of joy and hope, adding meaning and light to my life.

To my sisters, for their love and sincere support.

To my friends and colleagues, for their support and companionship along this path.

To my teachers, for their guidance, knowledge, and inspiration.

To all of them, I dedicate this work with deep gratitude and appreciation.

ACKNOWLEDGEMENT

I would like to express my sincere gratitude to my supervisor, **Dr. Belal Almassri**, Head of the Civil Engineering Department, for his continuous support, guidance, and motivation throughout the preparation of this work, as well as for his dedicated efforts in establishing the Master's Degree program in Civil Engineering.

My sincere thanks are also due to **Dr. Haitham Ayyad** and **Dr. Maher Amro**, from whom I have learned a great deal through their knowledge, guidance, and academic support.

I would like to especially acknowledge **Prof. Nabil Al-Joulani (may he rest in peace)**, whose teaching and influence had a lasting impact on my academic journey, and whose legacy will always remain a source of inspiration.

# Contents

## List of Tables

## List of Figures

## List of Symbols Used in This Thesis

| Symbol | Description | Unit |
|---|---|---|
| a | Shear span | mm |
| d | Effective depth of beam | mm |
| a/d | Shear span-to-depth ratio | — |
| $b_w$ | Width of beam web | mm |
| h | Overall beam depth | mm |
| L | Beam length / clear span, depending on context | mm |
| $f'_c$ | Concrete compressive strength | MPa |
| $f_t$ | Concrete tensile strength | MPa |
| $E_c$ | Modulus of elasticity of concrete | MPa |
| $E_s$ | Modulus of elasticity of steel reinforcement | MPa / GPa |
| $f_y$ | Yield strength of steel reinforcement | MPa |
| $A_v$ | Area of transverse reinforcement within spacing s | mm² |
| s | Spacing of stirrups | mm |
| $A_v/s$ | Transverse reinforcement ratio per unit spacing | mm²/mm |
| $\rho_s$ | Longitudinal reinforcement ratio | — |
| $\rho_{sv}$ | Vertical web reinforcement ratio | — |
| $\rho_{sh}$ | Horizontal web reinforcement ratio | — |
| $P_u$ | Ultimate load capacity | kN |
| $P_{cr}$ | First-cracking load | kN |
| $\Delta$ | Mid-span deflection / displacement | mm |
| $\Delta_u$ | Ultimate displacement | mm |
| $\Delta_{0.75Pu}$ | Displacement corresponding to 75% of ultimate load | mm |
| $\eta$ | Ductility index | — |
| $\sigma_c$ | Concrete compressive stress | MPa |
| $\sigma_t$ | Concrete tensile stress | MPa |
| $\varepsilon_c$ | Concrete compressive strain | — |
| $\varepsilon_t$ | Concrete tensile strain | — |
| $\varepsilon_0$ | Strain corresponding to peak compressive stress | — |
| $\varepsilon_u$ | Ultimate compressive strain | — |
| $\varepsilon_{in}$ | Compressive inelastic strain used in CDP input | — |
| $\varepsilon_{cr}$ | Tensile cracking strain used in CDP input | — |

| | | |
|---|---|---|
| $d_c$ | Concrete compression damage parameter | — |
| $d_t$ | Concrete tension damage parameter | — |
| $\psi$ | Dilation angle in Concrete Damaged Plasticity model | degree |
| e | Eccentricity parameter in Concrete Damaged Plasticity model | — |
| $f_{b0}/f_{c0}$ | Ratio of biaxial to uniaxial compressive strength in CDP | — |
| K | Parameter defining the shape of the deviatoric plane in CDP | — |
| $\mu$ | Viscosity parameter in Concrete Damaged Plasticity model | — |
| $E_{11}$ | Elastic modulus of CFRP in fiber direction | GPa |
| $E_{22}$ | Elastic modulus of CFRP transverse to fiber direction | GPa |
| $G_{12}$ | In-plane shear modulus of CFRP | GPa |
| $G_{13}$ | Shear modulus of CFRP | GPa |
| $G_{23}$ | Transverse shear modulus of CFRP | GPa |
| $\nu_{12}$ | Major Poisson's ratio of CFRP | — |
| $t_{CFRP}$ | Thickness of CFRP sheet | mm |
| $f_{fu}$ | Ultimate tensile strength of CFRP | MPa |
| $t_{UHPC}$ | Thickness of UHPC strengthening layer | mm |
| $f'_{UHPC}$ | Compressive strength of UHPC | MPa |
| $E_{UHPC}$ | Modulus of elasticity of UHPC | GPa |
| $\theta$ | Inclination angle of the diagonal compression strut / crack path | degree |
| % | Strength reduction, strength recovery, or percentage difference | % |
| c | Concrete cover used in effective-depth calculation | mm |
| $\phi$ | Bar diameter | mm |
| z | Internal lever arm of the STM mechanism | mm |
| $A_s$ | Area of bottom longitudinal reinforcement | $mm^2$ |
| $T_n$ | Nominal tensile resistance of the bottom tie | kN |
| $P_{tie}$ | Total applied load corresponding to the tie-based STM capacity | kN |
| $f_{ce}$ | Effective compressive stress in strut or nodal zone | MPa |
| $\beta_s$ | Strut efficiency factor | — |
| $\beta_n$ | Nodal efficiency factor | — |
| $A_n$ | Effective bearing area of the nodal zone | $mm^2$ |
| $F_{nn}$ | Nominal nodal force capacity | kN |

## List of Abbreviations Used in This Thesis

| Abbreviation | Full Term |
|---|---|
| RC | Reinforced Concrete |
| FE | Finite Element |
| FEM | Finite Element Method |
| FEA | Finite Element Analysis |
| CDP | Concrete Damaged Plasticity |
| UHPC | Ultra-High-Performance Concrete |
| UHPFRC | Ultra-High-Performance Fiber-Reinforced Concrete |
| CFRP | Carbon Fiber Reinforced Polymer |
| FRP | Fiber Reinforced Polymer |
| STM | Strut-and-Tie Model |
| ACI | American Concrete Institute |

| | |
|---|---|
| ASCE | American Society of Civil Engineers |
| ACI-ASCE | American Concrete Institute – American Society of Civil Engineers |
| ABAQUS | Finite Element Analysis Software |
| LVDT | Linear Variable Differential Transformer |
| MEP | Mechanical, Electrical, and Plumbing |
| EB | Externally Bonded |
| NSM | Near-Surface-Mounted |
| WWM | Welded Wire Mesh |
| FHWA | Federal Highway Administration |
| PCI | Precast/Prestressed Concrete Institute |
| DAMAGEC | Concrete compression damage variable in ABAQUS |
| DAMAGET | Concrete tension damage variable in ABAQUS |
| DP-S2 | Solid reference deep beam specimen |
| O1 | Small square web opening, 200 × 200 mm |
| O2 | Large square web opening, 230 × 230 mm |
| C | Central opening location |
| E | Edge / inner-edge opening location |
| C-C-T | Compression–Compression–Tension nodal zone |
| C-C-C | Compression–Compression–Compression nodal zone |

# Chapter1 Introduction

## 1.1 General Introduction

Reinforced concrete deep beams are widely used in structural applications where heavy loads must be transferred over relatively short spans, such as transfer girders, pile caps, bridge bent caps, and wall-beam systems. ACI Committee 318 (2019) classifies these members within the category of discontinuity regions, where the assumptions of ordinary sectional analysis are no longer fully valid. Typical practical applications of reinforced concrete deep beams are illustrated in **Figure 1.1**, highlighting their role in transferring


Figure 1. 1 Typical applications of reinforced concrete deep beams.

Instead of flexural action, load transfer in deep beams is primarily achieved through a **direct compression mechanism**, in which forces are transmitted along a diagonal path between the loading point and the support. This behavior results in a highly nonlinear stress distribution and necessitates special analytical and design approaches. For this reason, conventional beam theory is not applicable, and alternative methods such as the **strut-and-tie model** are commonly used to represent the internal force flow in these structural members (Schlaich et al., 1987).

In modern construction, the need to accommodate mechanical, electrical, and plumbing systems has led to the introduction of web openings in deep beams. Although these openings are often unavoidable, they significantly alter the internal load-transfer mechanism by interrupting the continuity of the compression strut. As a result, deep beams with web openings tend to exhibit reduced stiffness, earlier crack initiation, and a considerable decrease in load-carrying capacity.

To overcome these challenges, various strengthening techniques have been developed to enhance the structural performance of deep beams with openings. Among these techniques, fiber-reinforced polymer (FRP) systems—particularly carbon fiber-reinforced polymer (CFRP)—have been widely used due to their high strength-to-weight ratio and ease of application. In addition, ultra-high-performance concrete (UHPC) and its fiber-reinforced variants (UHPFRC) have emerged as promising materials capable of providing superior mechanical performance and improved crack resistance.

Despite the availability of these strengthening methods, the relative effectiveness of different techniques under varying conditions—such as opening size, opening location, and material properties—remains an important area of investigation. Furthermore, the increasing use of advanced numerical tools, such as nonlinear finite element analysis, has enabled more accurate simulation of deep beam behavior, providing new opportunities for comprehensive parametric studies.

Accordingly, there is a growing need for systematic research that integrates the effects of geometric discontinuities and advanced strengthening materials within a unified analytical framework, in order to better understand and improve the performance of reinforced concrete deep beams with web openings.

### 1.2 Structural Behavior of Reinforced Concrete Deep Beams

Reinforced concrete deep beams transfer loads primarily through a **diagonal compression strut mechanism**, rather than through conventional flexural action. This fundamental difference arises because deep beams do not satisfy the classical assumption of linear strain distribution. Instead, their structural response is governed predominantly by shear forces and direct load transfer between the applied load and the supports.

Experimental investigations by Subedi et al. (1986) confirmed that shear behavior dominates the response of deep beams, while Schlaich et al. (1987) formalized this concept through the development of the **strut-and-tie model**, which provides a rational framework for analyzing disturbed regions. Further studies by Tuchscherer et al. (2011) illustrated the internal stress flow mechanism, demonstrating that stresses are concentrated along a well-defined compression path.

As illustrated in Figure 1.2, the load is transmitted along a compressed diagonal path between the loading point and the support. Tan et al. (1995) showed that failure is typically governed by **diagonal compression**, whereas Tan et al. (1997) highlighted the important role of web reinforcement in stabilizing the compression strut and delaying failure.

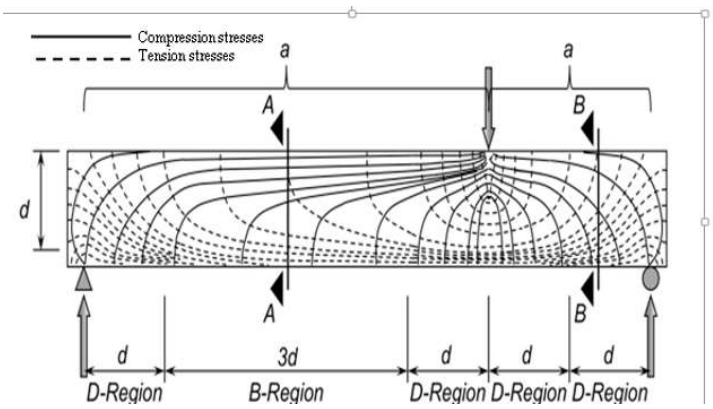


Figure 1. 2 Stress flow and diagonal compression strut behavior in deep beams.
Source: Adapted from Tuchscherer, R. G., Birrcher, D. B., & Bayrak, O. (2011).

### 1.3 Effect of Web Openings on Deep Beam Behavior

In practical applications, web openings are often introduced in deep beams to accommodate mechanical and service systems. However, these openings significantly alter the internal load-transfer mechanism by disrupting the continuity of the diagonal compression strut.

Mansur and Alwis (1984) were among the first to demonstrate experimentally that web openings lead to a considerable reduction in structural capacity. This effect was later quantified by Yang et al. (2006), who reported strength reductions in the range of **40–60%**, while Jasim et al. (2018) observed that large openings located within the shear span can result in reductions of up to **66%**.

In addition to opening size, the **location of the opening** plays a critical role. Campione and Minafò (2012) emphasized that openings located within the principal stress path are significantly more detrimental than those positioned away from the critical shear zone.

Figure 1.3 illustrates how the presence of openings modifies cracking patterns and leads to localized stress concentrations, ultimately resulting in premature failure due to the interruption of the compression field (Jasim et al., 2020).


Figure 1. 3: Failure of reinforced concrete deep beams: (left) from Mansur and Alwis (1984); (right) from Jasim et al. (2020).
Source: Mansur and Alwis (1984); Jasim et al. (2020).

### 1.4 Strengthening of Deep Beams with Web Openings

To mitigate the adverse effects of web openings, strengthening techniques are commonly employed to restore or enhance the disrupted load-transfer mechanism. Among the available methods, **CFRP** and **UHPC/UHPFRC** have received considerable attention due to their distinct mechanical characteristics.

CFRP strengthening primarily enhances structural performance through **crack control and tensile reinforcement**. Chen and Teng (2003) demonstrated that the effectiveness of CFRP systems is governed by bond behavior and resistance to debonding. Experimental work by El Maaddawy and Sherif (2009) confirmed that CFRP can significantly improve shear capacity, while Rahim et al. (2020) reported strength increases ranging between **15% and 40%**, depending on the strengthening configuration.

In contrast, UHPC-based systems provide a more **comprehensive structural enhancement** by improving both the tensile and compressive behavior of the member. Li (2004) explained the role of fiber bridging in controlling crack propagation, whereas Graybeal (2014) highlighted the superior mechanical properties of UHPC, including high compressive strength and enhanced durability. Experimental studies by Elghany et al. (2025), Al-Enezi et al. (2023), and Yousef et al. (2023) reported improvements ranging between **25% and 60%**.

Unlike CFRP, which mainly improves post-cracking behavior, UHPC has the potential to **restore the continuity of the compression strut**, making it particularly effective for strengthening deep beams with disrupted load paths.

## 1.5 Research Problem

Despite extensive research on reinforced concrete deep beams, the behavior of deep beams with web openings remains a complex structural problem. This complexity arises primarily from the disruption of the principal internal load-transfer path caused by the presence of openings.

While previous studies have investigated the effects of opening size, opening location, and strengthening techniques individually, the **combined influence of these parameters** has not been sufficiently addressed within a unified analytical framework. In particular, limited research has been conducted to directly compare the effectiveness of **UHPC and CFRP strengthening systems** under consistent conditions.

Furthermore, the interaction between geometric parameters (such as opening size and location) and material properties (such as concrete strength and reinforcement characteristics) introduces additional complexity that requires systematic investigation. Therefore, there remains a clear need for a **comprehensive nonlinear numerical study** to evaluate these factors simultaneously and to better understand their combined influence on structural performance (Jasim et al., 2018; Al-Osta et al., 2018).

## 1.6 Aim and Objectives of the Study

### 1.6.1 Aim of the Study

The main aim of this study is to investigate the structural behavior of reinforced concrete deep beams with web openings and to evaluate the effectiveness of **UHPC and CFRP strengthening systems** using nonlinear finite element analysis in ABAQUS.

### 1.6.2 Objectives of the Study

The objectives of this study are:

1. To develop and validate a nonlinear finite element model for reinforced concrete deep beams using ABAQUS.
2. To investigate the effect of opening size and opening location on beam behavior.

3. To evaluate the effectiveness of UHPC and CFRP as strengthening techniques.
4. To study the influence of transverse reinforcement ratio, concrete compressive strength, and reinforcement yield strength.
5. To interpret the results in relation to the diagonal compression strut mechanism.

## 1.7 Research Significance

The significance of this study lies in its contribution to improving the understanding of the structural behavior of reinforced concrete deep beams containing web openings, as well as in assessing the efficiency of advanced strengthening materials such as UHPC and CFRP. The findings of this study may also provide useful guidance for the analysis, strengthening, and design of such structural members.

## 1.8 Scope of the Study

This study is limited to the nonlinear numerical investigation of reinforced concrete deep beams using ABAQUS. The work includes validating the numerical model against available experimental results, followed by the analysis of beams with and without web openings. The study examines the effects of opening size, opening location, UHPC strengthening, CFRP strengthening, transverse reinforcement ratio, concrete compressive strength, and reinforcement yield strength. The structural response is evaluated mainly in terms of load-displacement behavior, ultimate load capacity, and damage distribution (Jasim et al., 2018).

## 1.9 Research Methodology

The methodology adopted in this study begins with selecting suitable experimental benchmark specimens from the published literature. Based on these specimens, a finite element model is developed in ABAQUS and then validated by comparing its results with the corresponding experimental data. After the validation stage, the verified model is extended to carry out a parametric study covering the main variables considered in this research. The numerical response is assessed mainly through load-displacement behavior, ultimate load capacity, and damage patterns (Jasim et al., 2018).

## 1.10 Organization of the Thesis

This thesis is organized into five chapters. Chapter 1 introduces the research background and presents the research problem, objectives, significance, scope, and methodology. Chapter 2 provides a review of the relevant literature related to reinforced concrete deep beams, web openings, and strengthening techniques. Chapter 3 describes the finite element modeling procedures adopted in ABAQUS, including material modeling, interaction assumptions, boundary conditions, and model validation. Chapter 4 presents the numerical results and discusses the effects of the studied parameters.

Finally, Chapter 5 summarizes the main conclusions of the study and provides recommendations for future work.

# Chapter2 :LITERATURE REVIEW

## 2.1 Introduction

Reinforced concrete deep beams occupy a distinct position among structural concrete members because their load-transfer mechanism differs fundamentally from that assumed in ordinary beam theory. ACI Committee 318 (2019) classifies such members within discontinuity regions, where conventional sectional assumptions are no longer fully applicable. Subedi et al. (1986) demonstrated experimentally that deep beams transfer loads mainly through direct compression fields rather than through flexure-dominated stress distribution. Schlaich et al. (1987) later provided the theoretical basis for this interpretation through the strut-and-tie model, showing that the internal response of deep beams is governed by the interaction of compression struts, tension ties, and nodal zones.

Deep beams are widely used in transfer girders, pile caps, bridge bent caps, and wall-beam systems, where heavy loads must be transmitted over short spans. Their structural importance is closely related to the brittle nature of shear-dominated failure. Subedi et al. (1986) observed that deep beams often fail through diagonal splitting associated with instability of the compression field. Tan et al. (1995) further showed that diagonal compression can govern the ultimate response, while Tan et al. (1997) highlighted the contribution of reinforcement in delaying such failure. Kong and Evans (1987) also emphasized that the behavior of deep beams should be interpreted through arching action rather than conventional flexural theory.

Accordingly, this literature review does more than introduce deep beams as a structural form. It establishes the mechanical basis required for the later discussion of web openings, material parameters, and strengthening systems. Schlaich et al. (1987) showed that any change in the member configuration must be assessed in relation to its effect on the internal strut-and-tie mechanism, while Abbood (2023) reaffirmed in a modern review that the behavior of deep beams is best understood through the continuity and stability of the internal load-transfer path

### 2.1.1 Definition and engineering applications of deep beams

According to ACI Committee 318 (2019), a structural member is classified as a deep beam when the clear span-to-overall depth ratio is sufficiently small or when concentrated loads act close to the supports, creating a discontinuity region in which ordinary sectional assumptions are no longer valid. Schlaich et al. (1987) explained that this classification reflects a change in structural behavior rather than a purely geometric condition, because once the member enters the deep-beam regime, the internal force path shortens and becomes more direct between the loading and support regions.

In practical engineering applications, deep beams are used where high stiffness and efficient short-span load transfer are required. ACI-ASCE Committee 426 (1974) discussed their relevance in regions governed by disturbed stress flow, while Subedi et al. (1986) showed experimentally that such

members are suitable for heavily loaded structural zones. For this reason, deep beams are commonly used in transfer girders, pile caps, bridge bent caps, and wall-beam systems. To clarify the fundamental differences between shallow beams and deep beams, the main distinctions in structural behavior, strain distribution, load-transfer mechanism, and failure tendency are summarized in **Table 2.1**.

| Characteristic | Shallow beam | Deep beam |
|---|---|---|
| Span-to-depth behavior | Slender; sectional behavior dominates | Short/deep; discontinuity-region behavior dominates |
| Strain distribution | Approximately linear over depth | Markedly non-linear |
| Main load-transfer mechanism | Flexure with conventional shear action | Arching action through compression struts and ties |
| Typical governing model | Sectional analysis | Strut-and-Tie Model or related D-region idealization |
| Typical failure tendency | Flexural yielding or diagonal shear | Diagonal tension, strut crushing, nodal distress, anchorage-related failure |
| Role of web reinforcement | Important but interpreted through sectional shear design | Still important, yet its efficiency depends strongly on crack orientation and a/d ratio |

Table 2. 1: Key distinctions between shallow and deep beams as synthesized from the reviewed literature.

As shown in **Table 2.1**, a deep beam should not be viewed as a shallow beam with increased depth only. Rather, it is a fundamentally different structural member in which response is governed by discontinuity-region behavior, arching action, and the stability of alternative force paths. Schlaich et al. (1987) provided the theoretical explanation for this distinction, while Abbood (2023) reaffirmed in a recent review that deep-beam behavior must be interpreted through disturbed stress fields rather than ordinary flexural assumptions.

### 2.1.2 Structural behavior and the role of arching action

The defining feature of reinforced concrete deep beams is the formation of a diagonal compression field that transfers load directly from the applied force to the support. Subedi et al. (1986) demonstrated experimentally that this arching mechanism governs the response of deep beams, making their behavior fundamentally different from that of slender beams. Kong and Evans (1987) also explained that deep-beam action is controlled by direct load transfer through the web rather than by the flexural stress distribution assumed in ordinary beam theory.

Later studies refined this interpretation by focusing on the geometry and continuity of the internal force path. Park and Kuchma (2007) showed that the prediction of deep-beam strength becomes more rational when the compression strut and nodal regions are represented explicitly. Similarly, Lu et al. (2013) demonstrated that the structural response of deep beams can be interpreted more reliably when the internal load flow is treated as a concentrated force path rather than as a simplified sectional shear problem.

From a serviceability point of view, cracking in deep beams also follows a different pattern from that observed in slender beams. Kong and Evans (1987) noted that cracks tend to localize along the future diagonal crack path, while Mansur and Alwis (1984) showed that any disturbance in this path can significantly weaken the member. Campione and Minafò (2012) further explained that when the compression field is interrupted, the beam is forced to develop a less efficient alternative load-transfer mechanism. This point is especially important for the present study, because it provides the mechanical basis for understanding the behavior of beams with web openings.

### 2.1.3 Strut-and-Tie Model (STM) as the governing interpretive framework

Among the available analytical approaches, the Strut-and-Tie Model (STM) is the most widely accepted framework for interpreting the behavior of reinforced concrete deep beams. Schlaich et al. (1987) established STM as a lower-bound plasticity-based idealization for discontinuity regions, in which the complex stress field is represented by a rational system of compression struts, tension ties, and nodal zones. This contribution is fundamental because it provides the theoretical basis for understanding how forces are transmitted through deep beams when ordinary sectional assumptions are no longer applicable.

Subsequent studies extended STM from a conceptual framework into a practical tool for prediction and assessment. Park and Kuchma (2007) showed that STM can provide reliable strength estimates when the geometry of the internal force path is represented carefully. Liu and Mihaylov (2016) later compared different strength-prediction approaches and concluded that mechanics-based models generally capture deep-beam behavior more reliably than purely empirical formulations. More recent studies, such as Karimzadeh and Arabzadeh (2021), Abbood (2023), and Alhayani and Almssad (2026), confirmed that STM remains an effective interpretive framework even in beams containing openings and other stress disturbances.

For clarity, the principal references that support the discussion of deep-beam behavior and STM-based interpretation are summarized in **Table 2.2**.

| Reference | Primary contribution to this thesis |
|---|---|
| Abbood (2023) | Modern review consolidating STM applications in RC deep beams and supporting the theoretical framework. |
| Liu & Mihaylov (2016) | Comparative assessment of strength-prediction models; useful for positioning mechanics-based versus empirical approaches.. |
| Subedi et al. (1986); Tan et al. (1995) | Experimental evidence for arching action, diagonal splitting, and the influence of geometry on deep-beam response. |
| Kong & Evans (1987) | Classical behavioral background on arching action, load transfer, and serviceability in deep beams. |
| Schlaich et al. (1987) | Foundational STM reference for disturbed regions and idealized force-flow modeling. |
| Park & Kuchma (2007); Liu & Mihaylov (2016) | Support STM-based strength prediction and comparative evaluation of mechanics-based versus empirical models. |

Table 2. 2: Main references supporting deep-beam behavior and STM-based interpretation

As indicated in **Table 2.2**, the significance of STM in the present thesis goes beyond general background theory. Schlaich et al. (1987) provide the foundational framework, Park and Kuchma (2007) support its predictive application, and Liu and Mihaylov (2016) position it against alternative models. More recent references, including Karimzadeh and Arabzadeh (2021), Abbood (2023), and Alhayani and Almssad (2026), show that STM remains highly relevant when evaluating openings, disturbed stress trajectories, and changes in force-transfer efficiency. For this reason, STM serves in the present study as the main interpretive framework for explaining the influence of opening position, reinforcement arrangement, and strengthening systems on the behavior of deep beams.

## **2.2** Effect of Web Openings on the Structural Behavior of Deep Beams

Web openings are often introduced in reinforced concrete deep beams to accommodate mechanical, electrical, and plumbing services. Ashour and Rishi (2000) noted that such openings may be required for practical design and service integration, while Campione and Minafò (2012) showed that their presence cannot be treated as a simple geometric modification because deep beams depend strongly on continuity of stress flow. El Maaddawy and Sherif (2009) further emphasized that when an opening is introduced into a deep beam, its effect must be evaluated in relation to the disturbed

load-transfer path rather than only the reduction in concrete area. More recent work by Augustino et al. (2022) confirmed that openings alter the internal force path in a manner that can significantly affect stiffness, cracking, and strength.

The literature also shows that the behavior of deep beams with openings cannot be explained by a single geometric parameter. Hu et al. (2007) demonstrated that the structural response depends on how the opening modifies the compression field and the remaining concrete ligaments. Jasim et al. (2018) showed experimentally and numerically that opening size and location both influence the severity of strength reduction. Jasim et al. (2020) later extended this understanding by relating cracking and failure progression to the disturbed load path around the opening. Similarly, Karimzadeh and Arabzadeh (2021) and Khalaf et al. (2021) highlighted that opening shape, local detailing, and interaction between adjacent disturbed regions must also be considered when interpreting the response of deep beams with web openings.

### 2.2.1 Necessity of openings and general structural implications

Openings may be classified according to whether they are planned during the design stage or introduced later after construction. Ashour and Rishi (2000) explained that pre-planned openings allow the designer to provide suitable reinforcement and detailing around the disturbed region, thereby reducing their adverse structural effect. In contrast, Augustino et al. (2022) showed that post-planned or drilled openings are usually more critical because they may cut existing reinforcement and interrupt a load-transfer path that was not originally designed to accommodate such discontinuity. Karimzadeh and Arabzadeh (2021) likewise emphasized that the structural effect of an opening depends not only on its dimensions, but also on whether the surrounding reinforcement is detailed to preserve continuity of internal force flow.

At the member level, the most important consequence of an opening is the disturbance of the diagonal compression path. Campione and Minafò (2012) explained that once the principal compression field is interrupted, stresses are forced to deviate around the opening and become concentrated near its corners or edges. Yang et al. (2006) quantified the severity of this effect in high-strength concrete deep beams and reported strength reductions in the range of about 40% to 60%. Jasim et al. (2018) further showed that when large openings are located within the shear span, the reduction in load-carrying capacity may reach about 66%. Jasim et al. (2020) confirmed that this disturbed mechanism also leads to earlier cracking and greater deformation compared with solid beams.

### 2.2.2 Effect of opening shape

Opening shape directly influences how stresses are redistributed around the disturbed region. Ashour and Rishi (2000) showed that circular openings are generally less harmful than openings with sharp corners because curved boundaries reduce local stress concentration. Campione and Minafò (2012) supported this interpretation by explaining that square and rectangular openings tend to attract higher diagonal tensile stresses at their corners, which often become the starting points of crack initiation. El-Kassas et al. (2020) further observed that sharp-cornered openings are associated with

more severe cracking and less efficient alternative force paths. Karimzadeh and Arabzadeh (2021) likewise confirmed that opening geometry influences not only local cracking but also the overall redistribution of forces around the opening.

The effect of shape is therefore mechanical as well as geometric. Hu et al. (2007) showed that trapezoidal openings alter both the path and the effective width of the remaining compression field. El-Kassas et al. (2020) and Khalaf et al. (2021) also noted that elongated or rectangular openings may induce local Vierendeel-type action in the concrete chords above and below the opening. This means that opening shape affects not only where cracks start, but also how the beam develops a substitute load-transfer mechanism after the original diagonal compression path has been disturbed.

### 2.2.3 Effect of opening size

Opening size is one of the clearest indicators of structural degradation in deep beams with web openings. Rahim et al. (2020) reported that increasing the diameter of circular openings led to progressive strength losses of about 15%, 22%, and 30% for 150 mm, 200 mm, and 250 mm openings, respectively, relative to the corresponding solid beam. Yang et al. (2006) also showed that when the opening removes a substantial portion of the diagonal compression strut, the reduction in ultimate capacity may reach about 40% to 60%. Ashour and Rishi (2000) were among the early researchers to explain this trend by relating larger openings to more severe interruption of the principal load path, while Campione and Minafò (2012) confirmed that the loss of strength becomes especially critical when the opening occupies a major part of the shear-transfer zone.

The significance of opening size should not be interpreted in absolute terms only. Campione and Minafò (2012) explained that the severity of an opening depends on its proportion relative to the beam depth and to the width of the compression field. Similarly, Yang et al. (2006) and Rahim et al. (2020) showed that openings approaching a significant fraction of the member depth are more likely to remove an essential portion of the strut mechanism. For this reason, the literature consistently interprets opening size as a measure of how severely the main diagonal compression path has been disturbed rather than as a geometric dimension alone.

### 2.2.4 Effect of opening location

Opening location is often more critical than opening size because it determines whether the opening intersects the dominant diagonal compression path. Campione and Minafò (2012) showed that openings positioned within the shear span directly interfere with the principal load-transfer mechanism and therefore cause more severe loss of strength. Hu et al. (2007) similarly demonstrated that the same opening may have very different structural consequences depending on whether it is located along or away from the stress trajectory. Augustino et al. (2022) also confirmed that openings placed close to the critical shear zone produce greater stiffness reduction and more severe cracking than those located

in less sensitive regions. Jasim et al. (2018) further showed experimentally that openings intersecting the strut region result in significantly lower capacity than openings placed away from the main compression path.

The reviewed studies are highly consistent on this issue. Campione and Minafò (2012) related the severity of the response to the interaction between opening position and low shear span-to-depth ratio behavior. El-Kassas et al. (2020) showed that openings within the critical shear zone produce more severe local damage and less efficient force redistribution. Jasim et al. (2020) likewise linked failure development to the extent of interference between the opening and the strut path. More recently, Alhayani and Almssad (2026) reinforced this conclusion by showing that opening location remains one of the most decisive variables governing the structural response of deep beams with openings.

### 2.2.5 Reinforcement detailing around openings

Once the original diagonal compression strut is interrupted, the beam requires an alternative force-transfer mechanism to preserve structural efficiency. Hu et al. (2007) showed that local reinforcement around openings can partially restore this mechanism when it is placed in directions compatible with the disturbed stress trajectory. Jasim et al. (2018) demonstrated that diagonal bars at the opening corners are especially effective because they intercept the diagonal tensile stresses that tend to develop in these regions. Jasim et al. (2020) further confirmed that vertical and horizontal bars adjacent to the opening help tie the disturbed concrete chords above and below the opening and improve load redistribution around the removed concrete zone.

The effectiveness of reinforcement detailing depends on orientation as much as on quantity. Hu et al. (2007) explained that reinforcement contributes most efficiently when it is aligned with the likely crack path and force trajectory. Jasim et al. (2018) and Jasim et al. (2020) both showed that inclined or corner-oriented reinforcement can outperform a larger amount of steel placed in less favorable directions. Karimzadeh and Arabzadeh (2021) also supported this interpretation, showing that the benefit of reinforcement around openings is best understood as restoration of disturbed force flow rather than simple addition of steel area.

### 2.2.6 Multiple openings and opening interaction

When more than one opening is introduced, the structural problem becomes more severe because the remaining concrete ligaments may be insufficient to develop an effective diagonal compression field. El-Kassas et al. (2020) showed that multiple openings can cause disproportionately large strength loss when the concrete between adjacent openings is too narrow to transfer compression efficiently. Augustino et al. (2022) likewise noted that the interaction between neighboring openings is not simply additive, because one disturbed region may intensify the local stresses caused by another. Khalaf et al.

(2021) further demonstrated that elongated or clustered penetrations may prevent the formation of a stable intermediate compression strut, leading to pronounced loss of stiffness and capacity.

These findings have direct practical implications. El-Kassas et al. (2020) recommended maintaining sufficient clear spacing between adjacent openings to preserve the integrity of the remaining concrete web. Karimzadeh and Arabzadeh (2021) similarly emphasized that grouped service openings should not be evaluated independently when they occupy the same disturbed region. Khalaf et al. (2021) confirmed that clustered penetrations may divide the web into isolated and structurally weak segments, making the member more vulnerable to premature failure.

### 2.2.7 Cracking pattern and failure sequence

Deep beams with web openings typically exhibit a recognizable progression of cracking and failure. Ashour and Rishi (2000) showed that initial cracks may appear at relatively low loads, but critical cracking soon localizes around the opening corners because of stress concentration. Campione and Minafò (2012) further explained that as loading increases, the principal diagonal crack extends toward the loading and support regions, forcing the beam to develop a less efficient load-transfer path around the opening. Jasim et al. (2018) observed that this process is accompanied by progressive weakening of the remaining compression strut, while Jasim et al. (2020) related ultimate failure to widening of the main diagonal crack and deterioration of the shear-transfer mechanisms that remain active after cracking.

This cracking sequence is also important for understanding strengthening effectiveness. El Maaddawy and Sherif (2009) showed that CFRP strengthening can delay crack initiation at critical regions and reduce crack widening after cracking begins. Jasim et al. (2020) further indicated that strengthening does not eliminate the disturbed stress field, but can improve post-cracking performance by enhancing confinement and redistributing stresses. Al-Osta (2018) and Li (2004) also supported the broader idea that high-performance strengthening materials improve the disturbed region by enhancing crack control, tension transfer, and local confinement around the modified compression path.

Before presenting the concluding synthesis of this section, the main opening-related parameters discussed in the reviewed studies are summarized in **Table 2.3**, including their general trends, representative references, and implications for the interpretation adopted in the present thesis.

| Variable | General trend | Representative supporting studies | Implication for thesis interpretation |
|---|---|---|---|
| Shape | Circular openings are usually less harmful than sharp-cornered openings of similar size. | Ashour & Rishi (2000); Hu et al. (2007); El-Kassas et al. (2020) | Supports comparing crack concentration and force redistribution around square versus smoother openings. |
| Size | Larger openings remove a larger portion of the effective compression path and cause greater capacity loss. | Rahim et al. (2020); Yang et al. (2006); Jasim et al. (2018); Campione & Minafò (2012) | Supports interpreting larger openings as a more severe disturbance to the diagonal strut. |
| Location | Openings in the shear span or along the strut path are most critical; openings away from the principal load path are generally less severe. | El-Kassas et al. (2020); Campione & Minafò (2012); Jasim et al. (2020); Alhayani & Almssad (2026) | Supports ranking opening cases by degree of interference with the main load path. |
| Detailing | Diagonal and strategically oriented reinforcement can partly recover lost performance. | Augustino et al. (2022); Hu et al. (2007); Karimzadeh & Arabzadeh (2021) | Supports discussing reinforcement detailing as restoration of force transfer rather than steel addition alone. |
| Multiple openings | Interaction between adjacent voids can be disproportionately harmful when the remaining concrete ligaments are insufficient. | El-Kassas et al. (2020); Khalaf et al. (2021); Karimizadeh & Arabzadeh (2021) | Supports caution when interpreting clustered openings or elongated penetrations. |

Table 2. 3:Comparative synthesis of the main opening-related variables discussed in the reviewed studies.

As shown in **Table 2.3**, the reviewed literature consistently indicates that the structural effect of web openings is best interpreted in relation to the degree of disturbance introduced into the original diagonal compression path. The table also clarifies that shape, size, location, detailing, and interaction between multiple openings should not be treated as isolated variables, since each of them influences the efficiency of the alternative force-transfer mechanism that remains after the opening is introduced.

Overall, the reviewed literature shows that the effect of web openings should be interpreted as a force-path problem rather than as a simple reduction in concrete area. Ashour and Rishi (2000) first established that openings disturb the internal stress field in a fundamental way. Campione and Minafò (2012) clarified that the severity of this disturbance depends on whether the opening interferes with the principal compression path. Jasim et al. (2018) and Jasim et al. (2020) further demonstrated that opening size, location, and local detailing influence not only ultimate capacity, but also cracking sequence and failure development. Taken together, these findings justify evaluating openings in the present thesis in mechanical terms, that is, according to the extent to

which they disturb the original diagonal compression strut and the efficiency of the alternative load-transfer mechanism.

## 2.3 Key Factors Influencing the Shear Capacity of Deep Beams

Unlike shallow beams, the shear capacity of reinforced concrete deep beams cannot be explained through a single sectional parameter. Subedi et al. (1986) demonstrated experimentally that deep-beam behavior is governed by arching action rather than flexural stress distribution. Schlaich et al. (1987) provided the theoretical framework for this interpretation through the strut-and-tie model, showing that the diagonal compression strut and the longitudinal tension tie form the principal load-transfer system. Liu and Mihaylov (2016) later confirmed through comparative studies that prediction approaches are most reliable when they explicitly account for the continuity and stability of this internal force path.

The interaction among parameters is equally important. Liu and Mihaylov (2016) emphasized that the apparent effect of one variable depends on the level of other parameters. Ma et al. (2022), based on a large database, showed that variables such as reinforcement ratio, concrete strength, and member depth do not contribute equally under all conditions. Abbood (2023) further highlighted that the influence of each parameter must be interpreted in relation to the governing failure mechanism and the integrity of the diagonal compression strut. Accordingly, the following subsections examine the main influencing factors in terms of their governing mechanisms and relative importance.

### 2.3.1 Shear Span-to-Depth Ratio (a/d)

The shear span-to-depth ratio is one of the most influential geometric parameters governing deep-beam behavior. Subedi et al. (1986) showed experimentally that small a/d ratios promote a pronounced arching mechanism, allowing loads to be transferred directly through the compression field. Tan et al. (1995) further explained that this leads to higher shear capacity because the compression strut becomes shorter and steeper, reducing tensile demand in the system.

As the a/d ratio increases, the efficiency of the compression strut decreases. Tan et al. (1995) observed that increasing a/d gradually shifts the behavior toward a more flexure-influenced response. Hu and Wu (2018) confirmed that this transition is associated with flatter compression struts, higher tensile stresses, and more extensive diagonal cracking. Liu and Mihaylov (2016) also showed that a/d is one of the key variables responsible for variation among prediction models because it directly controls the governing load-transfer mechanism.

The same trend applies to high-performance materials. Deng et al. (2021) showed that UHPC deep beams still experience reduced shear resistance with increasing a/d, despite their higher strength. Mirzaaghabeik et al. (2025) further demonstrated that fiber reinforcement can mitigate, but not

eliminate, this effect. From an STM perspective, Schlaich et al. (1987) explained that smaller a/d produces a shorter and stronger strut, while Park and Kuchma (2007) showed that prediction accuracy depends on correctly representing this geometry.

To summarize the general influence of a/d on structural behavior, its effect on load-transfer mechanism and failure mode is presented in **Table 2.4**.

| a/d range | Dominant mechanism | Typical response | Common failure tendency |
|---|---|---|---|
| < 1.0 | Direct arching action | High shear resistance; steep compression strut; limited stress redistribution | Strut crushing, nodal distress, splitting of the compression field |
| 1.0–2.5 | Combined arch-and-truss action | Gradual reduction in strength; increased diagonal cracking; partial redistribution | Diagonal tension followed by shear-compression or strut crushing |
| > 2.5 | Shallow-beam-like action | Arching weakens; flexural effects become more significant | Conventional shear or flexural failure |

Table 2. 4:Generalized influence of the shear span-to-depth ratio on the structural response of deep beams.

As shown in **Table 2.4**, decreasing a/d enhances arching action and shear resistance, whereas increasing a/d leads to a transition toward flexure-dominated behavior and more pronounced cracking.

### 2.3.2 Concrete Compressive Strength (f'c)

Concrete compressive strength plays a significant role in the behavior of deep beams, particularly when the diagonal compression strut remains intact. Tan et al. (1995) showed that higher compressive strength increases both stiffness and ultimate load when the compression field is stable. Tan et al. (1997) further explained that when failure shifts toward splitting or anchorage-related mechanisms, the benefit of increasing concrete strength becomes less pronounced.

This effect is more evident in high-performance materials. Chen et al. (2022) demonstrated that increasing compressive strength in UHPC significantly improves shear capacity. Deng et al. (2021) also showed that this improvement is associated with enhanced matrix integrity and better crack control. Mirzaaghabeik et al. (2025) confirmed that fiber reinforcement further improves performance by enhancing tensile resistance and crack-bridging behavior.

However, Liu and Mihaylov (2016) emphasized that compressive strength should not be treated as an independent predictor of capacity. Abbood (2023) further clarified that its effectiveness depends on whether the compression strut remains the governing load-transfer mechanism. When other weaknesses dominate, increasing concrete strength provides only limited improvement.

### 2.3.3 Longitudinal Reinforcement Ratio (ρs)

The longitudinal reinforcement in deep beams acts as the primary tension tie within the internal strut-and-tie system. Subedi et al. (1986) showed that this reinforcement is essential for maintaining internal equilibrium and resisting tensile forces. Tan et al. (1995) and Tan et al. (1997) further demonstrated that increasing the longitudinal reinforcement ratio improves structural resistance, particularly in cases where failure is influenced by combined tie action and diagonal cracking.

However, the improvement is not linear. Liu and Mihaylov (2016) showed that beyond a certain level, increasing reinforcement produces diminishing returns because failure shifts toward concrete-controlled modes. Ma et al. (2022) confirmed this trend using a large database, showing that once the tension tie is sufficiently strong, additional reinforcement does not significantly increase capacity.

This behavior is also observed in high-performance beams. Erfan et al. (2021), Deng et al. (2021), and Mirzaaghabeik et al. (2025) showed that even large increases in longitudinal reinforcement result in moderate capacity gains compared with the influence of geometric and material parameters.

### 2.3.4 Web Reinforcement: Vertical and Horizontal Ratios

Web reinforcement in deep beams is provided mainly to control diagonal cracking, restrain transverse splitting of the compression strut, and improve structural stability after cracking. Schlaich et al. (1987) explained that its contribution should be interpreted within the strut-and-tie mechanism rather than through ordinary sectional shear concepts. Tan et al. (1997) further showed that the efficiency of web reinforcement depends on the orientation of the reinforcement relative to the crack pattern. Liu and Mihaylov (2016) confirmed that this role is strongly influenced by the geometry of the load path and the governing failure mode.

#### *2.3.4.1 Vertical Web Reinforcement (ρsv)*

Vertical web reinforcement acts as a supplementary tie system that intercepts inclined cracks and helps sustain load after cracking begins. Tan et al. (1997) showed that its effectiveness depends strongly on the inclination of the diagonal crack pattern, which in turn is related to the shear span-to-depth ratio. Tan et al. (2004) further explained that when the beam is very deep and the diagonal cracks are steep, vertical stirrups are not ideally oriented to cross the principal cracks, which limits their direct contribution to ultimate strength.

Although its effect on peak load is sometimes moderate, vertical web reinforcement still plays an important role in serviceability and post-cracking behavior. Liu and Mihaylov (2016) showed that its contribution becomes more noticeable when the crack angle is more favorable for stirrup engagement. Ma et al. (2022) likewise confirmed, through a broad comparative database, that vertical web reinforcement generally improves crack control and ductility even when its influence on ultimate capacity is less pronounced than that of other parameters.

#### *2.3.4.2 Horizontal Web Reinforcement (ρsh)*

Horizontal web reinforcement is often identified as the more effective web-reinforcement component in deep beams. Tan et al. (1997) showed that because diagonal cracks in deep beams are typically steep, horizontal bars intersect them at more favorable angles than vertical stirrups. Tan et al. (2004) further demonstrated that this makes horizontal reinforcement more effective in restraining crack propagation and stabilizing the compression field. Schlaich et al. (1987) also supported this interpretation by relating horizontal reinforcement to improved confinement of the disturbed compression strut.

Later studies reached similar conclusions in both conventional and high-performance deep beams. Yousef et al. (2018) showed that horizontal reinforcement improves crack distribution and delays brittle failure. Mirzaaghabeik et al. (2025) further confirmed that increasing horizontal web reinforcement enhances the stability of the compression field and improves structural resistance. Together, these findings indicate that the role of horizontal reinforcement is not merely additive, but mechanically linked to the restraint of transverse splitting and the preservation of strut continuity.

To clarify the distinct roles of vertical and horizontal web reinforcement, their primary structural functions and relative efficiencies are compared in **Table 2.5**.

| Parameter | Primary structural role | Typical efficiency in deep beams | Why the effect changes |
|---|---|---|---|
| ρsv | Intercepts inclined cracks and provides suspension action after cracking | Moderate and strongly dependent on a/d | Becomes less effective when diagonal cracks are steep and nearly parallel to the stirrups |
| ρsh | Restrains splitting of the compression strut and improves crack distribution | Often more effective than ρsv in deep beams | Intersects steep diagonal cracks more efficiently and stabilizes the compression field |

Table 2. 5: Comparative interpretation of vertical and horizontal web reinforcement in deep beam behavior.

As shown in **Table 2.5**, vertical reinforcement mainly contributes through crack interception and suspension action after cracking, whereas horizontal reinforcement is often more effective in restraining splitting of the compression strut and stabilizing the diagonal load path.

### 2.3.5 Size Effect and Member Depth

Member depth has a direct influence on the nominal shear strength of deep beams. Liu and Mihaylov (2016) showed that specimens with different depths do not fail at the same normalized shear stress even when reinforcement ratio and a/d are kept approximately constant. Li et al. (2021) further demonstrated that increasing depth leads to more localized cracking and a more brittle failure process because the principal crack extends over a longer path and becomes more susceptible to unstable propagation. Ma et al. (2022) confirmed, through comparative evidence, that size effect remains one of the important variables governing the difference between laboratory-scale specimens and full-scale structural members.

These findings are particularly important for design interpretation. Li et al. (2021) explained that equations calibrated on smaller specimens may overestimate the resistance of larger structural members if the size effect is ignored. Ma et al. (2022) also showed that although web reinforcement can reduce the severity of localization, it does not eliminate the phenomenon completely. Therefore, member depth should be treated as a governing parameter rather than as a secondary dimensional feature.

### 2.3.6 Integrated Statistical Evidence and Comparative Databases

Large comparative databases provide an important bridge between individual experiments and broader design-oriented interpretation. Ma et al. (2022) compiled and analyzed 833 reinforced concrete deep beam specimens, showing that database-based synthesis can distinguish recurring behavioral trends from isolated test outcomes. Liu and Mihaylov (2016) likewise demonstrated that comparative assessment is essential for identifying the strengths and limitations of different strength-prediction models.

The conclusions drawn from these databases are broadly consistent with the experimental literature. Ma et al. (2022) showed that increasing the shear span-to-depth ratio has the strongest negative effect on capacity, whereas concrete strength and longitudinal reinforcement generally contribute positively but with different levels of influence. Li et al. (2021) further highlighted the significance of member depth, while Erfan et al. (2021) confirmed that the contribution of longitudinal reinforcement tends to diminish once a sufficient tie capacity is achieved. Together, these studies support a mechanics-based interpretation in which the relative influence of each parameter is understood through its effect on the stability and continuity of the diagonal compression field.

A condensed synthesis of the principal parameters affecting deep-beam shear capacity is presented in **Table 2.6**.

| Parameter | General trend | Relative influence | Interpretive note | Representative sources |
|---|---|---|---|---|
| a/d | Increase in a/d reduces shear strength | Highest | Controls the geometry and efficiency of the diagonal strut | Hu et al. (2018); Ma et al. (2022); Tan et al. (1995, 1997) |
| f'c | Increase in f'c generally increases capacity | Very high | Most effective when the diagonal strut remains continuous and well confined | Liu & Mihaylov (2016); Li et al. (2021); Chen et al. (2022); Deng et al. (2021) |
| ρs | Increase improves tie action, then shows diminishing returns | Moderate | Once the tie becomes sufficient, failure shifts toward concrete-controlled modes | Liu & Mihaylov (2016); Erfan et al. (2021); Ma et al. (2022) |
| ρsv | Positive but variable effect | Moderate to low | Depends strongly on crack inclination and the shear span-to-depth ratio | Tan et al. (1997); Tan et al. (2004); Ma et al. (2022) |
| ρsh | Positive and often stronger than ρsv | High among web-reinforcement variables | Improves strut stability and restrains steep diagonal cracking | Tan et al. (1997); Smarzewski (2020); Mirzaaghabeik et al. (2025) |
| Member depth | Larger depth reduces nominal shear strength | Negative | Reflects fracture localization and the quasi-brittle size effect | Li et al. (2021); Ma et al. (2022); Liu & Mihaylov (2016) |
| Member depth | Larger depth reduces nominal shear strength | Negative | Reflects fracture localization and the quasi-brittle size effect | Li et al. (2021); Ma et al. (2022); Liu & Mihaylov (2016) |

Table 2. 6:Condensed synthesis of the principal factors affecting deep beam shear capacity.

As indicated in **Table 2.6**, the strongest negative influence is generally associated with increasing a/d, whereas concrete strength, horizontal reinforcement, and longitudinal reinforcement contribute positively but with different degrees of effectiveness depending on the governing structural mechanism.

### 2.3.7 Interaction Between a/d and Web Reinforcement

A more reliable interpretation of the literature emerges when the shear span-to-depth ratio and web reinforcement are considered as interacting variables rather than as isolated parameters. Tan et al. (1997) showed that at very low a/d ratios, deep beams transfer load mainly through direct arching action, which limits the extent to which additional web reinforcement can enhance ultimate capacity. Tan et al. (2004) further demonstrated that as a/d increases, the crack pattern becomes more favorable for reinforcement engagement, making both vertical and horizontal web reinforcement more effective.

Liu and Mihaylov (2016) supported this interpretation by showing that the contribution of reinforcement depends strongly on the governing crack geometry and load-transfer mechanism. Ma et al. (2022) likewise confirmed that apparently contradictory findings in the literature can often be reconciled when the interaction between geometry and reinforcement orientation is taken into account. Therefore, the most defensible conclusion is not that web reinforcement is always weak or always strong, but that its effectiveness depends on how well it engages the crack pattern produced by a given internal load path

### 2.3.8 Shear Strength Prediction Models

Because deep-beam behavior is governed by interacting geometric, material, and reinforcement variables, several approaches have been proposed to predict shear strength. ACI Committee 318 (2019) adopts a design-oriented strut-and-tie approach that provides a rational but conservative representation of the internal load-transfer mechanism. Schlaich et al. (1987) supplied the theoretical foundation for this method by establishing STM as a lower-bound plasticity-based model for discontinuity regions. Abbood (2023) further highlighted that the main advantage of such approaches lies in their physical interpretability and engineering applicability.

More refined analytical approaches attempt to improve predictive accuracy by representing cracking and redistribution more explicitly. Liu and Mihaylov (2016) showed that no single prediction model is universally superior, because model accuracy varies with geometry, specimen type, and calibration range. Park and Kuchma (2007) demonstrated that compatibility-based STM can achieve improved predictive consistency when the internal force path is modeled carefully. For beams with openings, Karimzadeh and Arabzadeh (2021) further showed that STM-based modeling can provide reasonably accurate predictions when the disturbed load path is represented explicitly.

Recent data-driven studies also show promise. Megahed (2024) reported that machine-learning models can achieve high predictive accuracy when trained on sufficiently broad databases. However, Ma et al. (2022) and Liu and Mihaylov (2016) make it clear that predictive accuracy alone is not enough in a research context. Mechanics-based interpretation remains necessary to explain why the variables influence behavior in the first place. For this reason, machine-learning approaches should be regarded as complementary tools rather than substitutes for physically grounded models.

### 2.3.9 Critical Synthesis

Because deep-beam behavior is governed by interacting geometric, material, and reinforcement variables, several approaches have been proposed to predict shear strength. ACI Committee 318 (2019) adopts a design-oriented strut-and-tie approach that provides a rational but conservative representation of the internal load-transfer mechanism. Schlaich et al. (1987) supplied the theoretical foundation for this method by establishing STM as a lower-bound plasticity-based model for discontinuity regions. Abbood (2023) further highlighted that the main advantage of such approaches lies in their physical interpretability and engineering applicability.

More refined analytical approaches attempt to improve predictive accuracy by representing cracking and redistribution more explicitly. Liu and Mihaylov (2016) showed that no single prediction model is universally superior, because model accuracy varies with geometry, specimen type, and calibration range. Park and Kuchma (2007) demonstrated that compatibility-based STM can achieve improved predictive consistency when the internal force path is modeled carefully. For beams with openings, Karimzadeh and Arabzadeh (2021) further showed that STM-based modeling can provide reasonably accurate predictions when the disturbed load path is represented explicitly.

Recent data-driven studies also show promise. Megahed (2024) reported that machine-learning models can achieve high predictive accuracy when trained on sufficiently broad databases. However, Ma et al. (2022) and Liu and Mihaylov (2016) make it clear that predictive accuracy alone is not enough in a research context. Mechanics-based interpretation remains necessary to explain why the variables influence behavior in the first place. For this reason, machine-learning approaches should be regarded as complementary tools rather than substitutes for physically grounded models.

## 2.4 Strengthening Deep Beams with Web Openings Using CFRP

The significant reduction in shear capacity caused by web openings has led to increasing interest in external strengthening techniques. Chen and Teng (2003) established that CFRP provides high tensile resistance with minimal added weight, making it suitable for retrofit applications. El Maaddawy and Sherif (2009) further showed that in deep beams, CFRP does not act as a replacement for the compression strut but instead contributes mainly through crack control and tensile resistance. Jasim et

al. (2020) confirmed that CFRP improves force transfer around disturbed regions, particularly after cracking initiates.

The effectiveness of CFRP strengthening depends strongly on the position of the opening. El Maaddawy and Sherif (2009) showed that strengthening is most effective when the opening lies within the critical shear zone, where the compression strut is interrupted. Rahim et al. (2020) demonstrated that CFRP efficiency is influenced by opening size and number of layers, while Khalaf et al. (2021) showed that fiber orientation and distribution affect the degree of recovery. Jasim et al. (2020) further confirmed that strengthening effectiveness depends on how well the CFRP layout aligns with the actual crack path.

### 2.4.1 Material Characteristics and Structural Role of CFRP

CFRP combines high tensile strength with low self-weight and excellent durability characteristics. Chen and Teng (2003) showed that CFRP is particularly effective in tension-dominated regions, while El Maaddawy and Sherif (2009) demonstrated that its role in deep beams becomes significant after cracking. Jasim et al. (2020) further explained that CFRP acts by bridging cracks, limiting crack widening, and maintaining residual tensile capacity after the initial diagonal cracking.

This explains why CFRP often improves serviceability more than ultimate capacity. El Maaddawy and Sherif (2009) observed that strengthened beams exhibit delayed crack initiation and reduced crack widths. Rahim et al. (2020) confirmed that CFRP leads to improved ductility and a less abrupt failure process, while Khalaf et al. (2021) showed that crack propagation becomes more controlled in strengthened beams.

Two main application techniques are commonly used. Chen and Teng (2003) described externally bonded (EB) systems, while Ibrahim et al. (2020) and Mansour and El Maaddawy (2021) showed that near-surface-mounted (NSM) systems provide improved bond behavior and reduced risk of debonding. The choice between these systems affects overall performance.

The effectiveness of CFRP also depends on its layout. El Maaddawy and Sherif (2009) showed that diagonal strips are more effective because they align with tensile stress trajectories. Jasim et al. (2020) and Khalaf et al. (2021) confirmed that proper orientation and anchorage significantly improve performance. Mansour and El Maaddawy (2021) further emphasized that anchorage quality is critical for mobilizing CFRP capacity.

Experimental studies provide direct evidence of CFRP effectiveness in deep beams with openings. Rahim et al. (2020) showed that externally bonded CFRP can recover approximately 10% to 40% of lost capacity, depending on opening size and number of layers. El Maaddawy and Sherif (2009) emphasized that bond quality governs the effectiveness of FRP systems, often limiting full utilization of material strength. Khalaf et al. (2021) demonstrated that in continuous deep beams, CFRP

improves structural response by about 15% to 35% while reducing crack width and deflection. Jasim et al. (2020) similarly reported strength gains of about 20% to 30% when CFRP sheets are properly aligned with the crack path.

Near-surface-mounted techniques have also shown strong performance. Ibrahim et al. (2020) reported gains of about 20% to 45%, while Mansour and El Maaddawy (2021) confirmed improved bond behavior and reduced debonding risk. Ali et al. (2023) further showed numerically that CFRP effectiveness increases with increasing opening ratio. Abadel and Alharbi (2025) demonstrated that hybrid strengthening systems can achieve even higher performance gains when combined with advanced materials.

To summarize the main findings from these studies, the representative experimental and numerical results are presented in **Table 2.7**.

| Study | System / specimen condition | Main strengthening variable | Reported outcome and interpretation |
|---|---|---|---|
| Rahim et al. (2020) | RC deep beams with circular openings | Externally bonded CFRP sheets; number of layers and opening size | Strength recovery was reported in an approximate range of **10%–40%**. The results showed that the effectiveness of CFRP depended strongly on both opening size and number of layers, with smaller openings requiring less intensive strengthening. |
| El-Maaddawy & Sherif (2009) | Deep beams with openings | Externally bonded FRP layout and bond development | Meaningful shear enhancement was achieved, but the effectiveness of the FRP system depended strongly on bond quality, anchorage, and strip development length. |
| Khalaf et al. (2021) | Continuous RC deep beams with large openings | CFRP strip orientation and distribution around openings | CFRP remained effective under the more complex stress state of continuous deep beams, with an improvement of about **17%** relative to the corresponding unstrengthened specimens with large openings. |

| | | | |
|---|---|---|---|
| Jasim et al. (2020) | Deep beams with web openings | CFRP sheets in regions surrounding the opening | Measurable gains in capacity and improved crack control were reported, although the degree of recovery depended strongly on whether the strengthened region coincided with the actual crack path. |
| Ibrahim et al. (2020) | RC deep beams strengthened with NSM hybrid FRP | Near-surface-mounted hybrid strips | The NSM hybrid strengthening scheme improved bond efficiency and reduced premature interface-related failure. A fixed percentage is better omitted here unless verified directly from the full paper. |
| Ali et al. (2022) | Finite-element study of beams with different opening ratios | Opening ratio and CFRP effectiveness | The numerical results indicated that the relative contribution of CFRP increased as the opening ratio became larger, confirming its greater importance in more severely disturbed load paths. |
| Abadel et al. (2025) | Deep beams with square openings | NSM-type CFRP versus conventional EB systems | The study supports the conclusion that NSM-type solutions can outperform conventional externally bonded systems and can provide a more stable strengthening response, but the percentage gain should not be fixed here without direct verification from the full article tables or text |

Table 2. 7: Condensed synthesis of representative CFRP strengthening studies on deep beams with openings

As shown in **Table 2.7**, CFRP strengthening provides moderate to significant recovery in shear capacity, with effectiveness strongly dependent on opening size, strengthening layout, and bond performance.

### 2.4.2 Bond Behavior, Debonding Modes, and Durability

Bond behavior is one of the most critical factors controlling the effectiveness of CFRP strengthening. Chen and Teng (2003) identified plate-end debonding, intermediate crack-induced

debonding, and concrete cover separation as the main failure modes. El Maaddawy and Sherif (2009) confirmed that these mechanisms limit the extent to which CFRP tensile capacity can be mobilized.

Mansour and El Maaddawy (2021) further showed that debonding is more likely when CFRP terminates in high-stress regions or near opening corners. Ibrahim et al. (2020) demonstrated that NSM systems reduce this risk by improving confinement and bond performance. These findings highlight the importance of anchorage and proper detailing.

Durability is also an important consideration. Chen and Teng (2003) noted that while CFRP itself is corrosion-resistant, the epoxy interface may degrade under environmental exposure. Ibrahim et al. (2020) and Mansour and El Maaddawy (2021) emphasized that protection of the bond interface is essential to ensure long-term performance.

## 2.5 Strengthening and Design Using UHPC and UHPFRC

Unlike CFRP, which mainly enhances the tensile response after cracking, UHPC and UHPFRC contribute at both the compressive and tensile levels of the structural response. Li (2004) introduced the concept of fiber bridging, showing that fibers improve post-cracking behavior and delay crack localization. Graybeal (2014) further demonstrated that the dense matrix and high compressive strength of UHPC enhance the compression field in structural members. Al-Osta (2018) confirmed that these materials improve both strength and ductility, while Elghany et al. (2025) showed that they can modify damage patterns and delay diagonal cracking in deep beams.

UHPC and UHPFRC are used either as full structural materials or as localized strengthening layers. Graybeal (2014) showed that UHPC jacketing can improve structural performance without increasing member size significantly. Al-Osta (2018) and Al-Enezi et al. (2023) demonstrated that these materials are particularly effective when applied in critical shear zones. Abadel and Alharbi (2025) and Yousef et al. (2023) further confirmed that UHPFRC-based strengthening can restore load-transfer continuity in beams with openings.

### 2.5.1 Material Characteristics and the Role of Fibers

The structural effectiveness of UHPC and UHPFRC depends primarily on compressive strength, fiber content, and post-cracking tensile behavior. Li (2004) showed that fibers bridge cracks and delay localization, allowing stress redistribution across cracked regions. Graybeal (2014) confirmed that this mechanism enhances both strength and durability. Mirzaaghabeik et al. (2025) further demonstrated that fiber reinforcement stabilizes the disturbed tensile field associated with diagonal cracking in deep beams.

Mirzaaghabeik et al. (2025) also showed that increasing fiber content improves shear performance, but the benefit does not increase linearly. Reported results indicate that increasing fiber content from 1% to 2% can enhance shear capacity by approximately 16.19%. Chen et al. (2022)

supported this conclusion by showing that the improvement in performance is linked to the combined effect of matrix strength and fiber bridging, and that an optimal fiber content exists beyond which gains become less significant.

### 2.5.2 Experimental Evidence for UHPC and UHPFRC in Deep Beams

Experimental studies provide strong evidence for the effectiveness of UHPC and UHPFRC in deep beams. Chen et al. (2022) showed that increasing compressive strength from about 132 MPa to 199 MPa leads to an increase in shear capacity of approximately 37.9%. This confirms that a stronger matrix directly enhances the compression strut when it remains continuous.

Al-Enezi et al. (2023) demonstrated that UHPFRC can compensate for the loss of capacity caused by openings, with reductions of about 40% being partially recovered by gains of 30% to 50%. Abadel and Alharbi (2025) further showed that hybrid systems combining UHPFRC with CFRP can significantly improve performance, achieving gains of up to about 63.8% after an initial loss of 56.5%.

Elghany et al. (2025) confirmed that thin UHPFRC layers applied as retrofit systems can improve shear resistance by about 25% to 35% while delaying diagonal cracking. Yousef et al. (2018) also showed that even in high-performance matrices, reinforcement detailing remains essential, as fibers alone do not eliminate the need for proper load-path control.

To summarize the main findings from these studies, the key experimental and analytical results are presented in **Table 2.8**.

| Study | Material / structural context | Primary variable | Reported outcome and structural implication |
|---|---|---|---|
| Mirzaaghabeik et al. (2025) | State-of-the-art review of UHPC deep beams | Fiber content, a/d ratio, reinforcement, and matrix strength | Confirmed the dominant influence of the shear span-to-depth ratio and highlighted the important role of fibers in maintaining post-cracking shear resistance and delaying damage localization. |
| Chen et al. (2022) | Experimental UHPC deep beams | Compressive strength within the UHPC range | An increase in compressive strength from about 132.3 MPa to 198.6 MPa was associated with an increase in shear capacity of roughly 37.9%, confirming the strong |

| | | | |
|---|---|---|---|
| | | | contribution of matrix strength to compression-strut resistance. |
| Al-Enezi et al. (2023) | UHPFRC deep beams with web openings | Presence of openings in a high-performance cementitious matrix | The adverse effect of openings was moderated because the crack-bridging matrix preserved a more effective load-transfer path than that typically observed in ordinary reinforced concrete beams. |
| Abd Elghany et al. (2025) | Existing RC deep beams strengthened with UHPFRC layers | Thin strengthening layer applied to the beam web | Reported clear enhancement in shear resistance together with delayed diagonal cracking and improved failure progression, indicating that the strengthening layer actively modified damage development in the original member. |
| Abadel et al. (2025) | Hybrid strengthening of deep beams with square openings using UHPFRC, CFRP, and WWM | Combined strengthening configuration around openings | Hybrid action produced one of the strongest overall responses because the high-performance matrix and external reinforcement complemented each other in resisting both compressive and tensile disturbances around the opening. |
| Yousef et al. (2018) | UHPFRC deep beams with minimum shear reinforcement | Interaction between fiber-rich matrix and conventional steel reinforcement | Showed that fibers reduce brittleness and improve shear performance, but do not eliminate the need for rational reinforcement detailing and |

| | | | |
|---|---|---|---|
| | | | proper control of the internal load path. |

Table 2. 8: Comparative Summary of UHPC and UHPFRC Studies Relevant to Deep Beams and Beams with Openings

As shown in **Table 2.8**, UHPC and UHPFRC provide both strength enhancement and improved crack control, with effectiveness depending on fiber content, compressive strength, and interaction with reinforcement.

### 2.5.3 UHPC/UHPFRC Versus CFRP: Difference in Structural Contribution

CFRP and UHPC/UHPFRC improve deep-beam behavior through fundamentally different mechanisms. Chen and Teng (2003) showed that CFRP acts mainly as an external tensile reinforcement that becomes effective after cracking. El Maaddawy and Sherif (2009) and Jasim et al. (2020) confirmed that CFRP improves crack control but does not restore the compression strut.

In contrast, Chen et al. (2022) showed that UHPC enhances the compression field directly through its high strength. Al-Osta (2018) and Mirzaaghabeik et al. (2025) further demonstrated that UHPFRC improves both tensile and compressive behavior, thereby stabilizing the internal load-transfer mechanism. This explains why UHPC-based strengthening often leads to a more distributed cracking pattern and improved structural stability.

This distinction becomes critical in beams with openings. El Maaddawy and Sherif (2009) showed that CFRP is effective when disturbance is moderate, while Abadel and Alharbi (2025) and Elghany et al. (2025) demonstrated that UHPFRC is more effective when the compression strut is severely disrupted. Hybrid systems combine both advantages by improving both tensile and compressive resistance.

To clarify these differences, a comparative interpretation of CFRP and UHPFRC strengthening systems is presented in **Table 2.9**.

| Criterion | CFRP systems | UHPC/UHPFRC systems | Interpretation for thesis context |
|---|---|---|---|
| **Primary structural role** | Supplementary tensile reinforcement and crack restraint | Improves both compression-field continuity and post-cracking tensile resistance | UHPC/UHPFRC tends to modify the core load-transfer mechanism more directly. |
| **Installation and geometry** | Fast installation with minimal increase in member dimensions | Requires additional material thickness, placement, | CFRP is attractive where construction access is |

| | | | |
|---|---|---|---|
| | | and curing, but can reconstruct the damaged region | limited and section enlargement is undesirable. |
| **Typical reported gain** | Commonly reported as providing moderate-to-significant improvement, depending on opening size, bond condition, fiber orientation, and strengthening layout | Frequently reported as providing moderate-to-large enhancement; jacketing and hybrid systems may exceed the gains achieved by CFRP alone | Selection should be governed by the severity of load-path disruption, not only by peak-load increase. |
| **Main limitation** | Premature debonding and sensitivity of the epoxy interface | Higher cost, casting and curing demands, and greater practical complexity in retrofit applications | A purely numerical comparison is insufficient; failure mode, bond behavior, and constructability must also be considered. |
| **Best suited condition** | Post-formed openings and relatively accessible retrofit situations | Severely weakened shear zones, durability-demanding environments, or high-performance new designs | Hybrid strengthening becomes attractive when both strength recovery and robustness are required. |

Table 2. 9 : Comparative Interpretation of CFRP and UHPFRC Strengthening in Deep Beams with Openings

As indicated in **Table 2.9**, CFRP provides efficient tensile reinforcement and crack control, while UHPC/UHPFRC directly enhances the compression field and overall load-transfer mechanism. The selection between the two systems should therefore depend on the degree of disturbance in the original diagonal load path.

## 2.6 Codes, Standards, and Design Guidance

The available experimental and numerical literature on deep beams is broader in scope than the current code framework. ACI Committee 318 (2019) provides a rational design basis for reinforced concrete deep beams through strut-and-tie provisions, which represent internal force transfer in

discontinuity regions. Schlaich et al. (1987) established the theoretical foundation of this approach by demonstrating that deep beams should be interpreted through force-path models rather than sectional stress assumptions. However, Abbood (2023) emphasized that recent research extends beyond these provisions, particularly in areas involving web openings and advanced strengthening systems.

Despite this, the treatment of web openings and advanced materials remains limited in current design provisions. ACI-ASCE Committee 426 (1974) is useful for understanding the historical development of shear behavior, but it does not address modern strengthening systems. Chen and Teng (2003) showed that CFRP strengthening introduces bond-dependent mechanisms not explicitly covered in codes. Graybeal (2014) demonstrated that UHPC introduces tensile and post-cracking contributions that are not represented in conventional design equations. Al-Osta (2018) and Abadel and Alharbi (2025) further confirmed that current provisions do not provide a unified design approach for deep beams with openings strengthened using advanced materials.

To summarize the applicability and limitations of the main design approaches, the relevant codes and guidance documents are presented in **Table 2.10**.

| Document / guidance | Primary relevance | What it captures well | Main limitation for the present topic |
|---|---|---|---|
| **ACI 318-19** | Deep-beam design through the strut-and-tie model and minimum web reinforcement provisions | Provides a rational force-path framework for conventional reinforced concrete deep beams | Does not provide a direct and dedicated design procedure for deep beams with openings strengthened using CFRP or UHPC/UHPFRC systems. |
| **ACI-ASCE 426R-74** | Historical development of shear concepts in reinforced concrete members | Useful as a background reference for understanding the development of shear-resistance mechanisms in reinforced concrete | Not a modern, dedicated design tool for deep beams with openings or for members incorporating advanced strengthening materials. |
| **STM-based design practice (Schlaich et al.; Park & Kuchma)** | Idealization of disturbed regions, nodal behavior, and force transfer in deep beams | Highly effective for conceptualizing load paths, opening effects, and reinforcement | Requires significant engineering judgment and often needs supplementary interpretation when advanced |

| | | | |
|---|---|---|---|
| | | requirements in disturbed regions | materials or strengthening systems are involved. |
| **AFGC and FHWA guidance for UHPC** | Material design and structural interpretation of UHPC/UHPFRC contribution | Better reflects the tensile behavior, post-cracking response, and structural role of fiber-rich cementitious matrices | Not yet fully integrated into mainstream building design practice for ordinary reinforced concrete strengthening applications. |

Table 2. 10: Main Design Guidance Relevant to Deep Beams, Strengthening, and High-Performance Materials

As shown in **Table 2.10**, existing frameworks provide a solid basis for conventional deep-beam design, but they do not offer a complete design methodology for beams with openings strengthened using CFRP or UHPC/UHPFRC systems. This gap justifies the adoption of a mechanics-based numerical approach in the present study.

## 2.7 Integrated Synthesis and Thesis-Oriented Research Gap

When the reviewed studies are considered collectively, a consistent structural interpretation emerges. Schlaich et al. (1987) showed that deep-beam behavior is governed by the integrity of the diagonal compression strut. Campione and Minafò (2012) demonstrated that openings weaken this mechanism by interrupting the internal load path. Jasim et al. (2020) further showed that cracking and failure progression are directly related to the disturbance introduced by openings, while Mirzaaghabeik et al. (2025) confirmed that strengthening becomes effective when it stabilizes both the compression and tensile fields.

The literature also highlights a gap in integrated studies. Liu and Mihaylov (2016) showed that parameters such as a/d ratio, reinforcement, and material strength significantly affect behavior, while Ma et al. (2022) demonstrated that these variables interact rather than act independently. Abbood (2023) emphasized that many studies examine these parameters in isolation, whereas Ali et al. (2023) showed that real structural behavior results from their combined interaction. This indicates a need for integrated analysis within a single framework.

A second gap is methodological. Jasim et al. (2018) and Jasim et al. (2020) showed that experimental studies provide valuable insight but remain limited in scope. Al-Osta (2018) and Elghany et al. (2025) demonstrated that strengthening effectiveness depends on interaction between materials and structural mechanisms, which is difficult to capture experimentally alone. This supports the use of nonlinear numerical modeling to trace load transfer, crack development, and damage evolution.

A third gap concerns the relationship between local strengthening and global behavior. Jasim et al. (2020) showed that local reinforcement improves performance near openings, while Abadel and Alharbi (2025) and Yousef et al. (2023) demonstrated that more extensive strengthening may be required when the compression strut is severely disrupted. This distinction is critical for selecting appropriate strengthening strategies.

Accordingly, the present study adopts an integrated approach in which deep beams are evaluated not only in terms of ultimate capacity, but also through load–displacement response, crack development, and damage distribution, in relation to the continuity of the diagonal compression strut.

### 2.7.1 Concluding Remarks for the Present Part

The reviewed literature shows that CFRP and UHPFRC operate through different structural mechanisms rather than acting as interchangeable solutions. CFRP primarily enhances tensile resistance and crack control, while UHPFRC improves both compressive and tensile behavior and can modify the internal load-transfer mechanism. As a result, their effectiveness depends on the degree of disturbance in the original compression strut and the required level of structural intervention.

For the present thesis, this supports a comparative analytical framework in which strengthening effectiveness is interpreted through changes in the diagonal compression strut, crack development, and damage redistribution, rather than through ultimate load capacity alone.

# Chapter3 :Finite Element Modeling

## 3.1 General

The finite element method (FEM) is one of the most effective numerical tools for simulating the nonlinear behavior of reinforced concrete members, especially when full experimental testing is costly or time-consuming. By dividing the structure into smaller elements and assigning appropriate material constitutive laws, FEM can predict stiffness, cracking, load-carrying capacity, and failure mode with reasonable accuracy.

In the present study, ABAQUS was used to model reinforced concrete deep beams with and without web openings. The numerical work was carried out in two stages. First, a finite element model was developed and calibrated against the experimental results reported by Jasim et al. (2018) in order to verify the adopted modeling approach. After validation, the verified model was used to perform a parametric study on the main variables considered in this research, namely opening size, opening location, strengthening using UHPC and CFRP, concrete compressive strength, and steel yield strength.

The beam response was evaluated in terms of load-displacement behavior, ultimate load, cracking development, and damage distribution.

## 3.2 Experimental Program Used for Model Validation

To verify the accuracy of the developed numerical model, the experimental study reported by Jasim et al. (2018) was adopted as the basis for validation. The study investigated reinforced concrete deep beams under two-point loading, including both solid beams and beams with web openings.

All specimens had the same overall dimensions of 1500 mm length, 500 mm depth, and 150 mm width. The beams were simply supported, with a pin support at one end and a roller support at the other. Two concentrated loads were applied symmetrically within the shear spans, The geometry and dimensions of the solid reference beam (DP-S2) are illustrated in Figure 3.1. This specimen was used as a control beam without openings to establish a baseline for comparison.

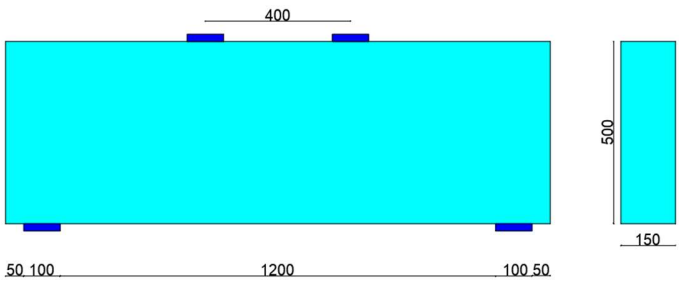


Figure 3. 1: Geometry and dimensions of deep beam DP-S2

The validation program included a control specimen without openings and beams with square web openings of different sizes and locations. Two opening sizes were considered: 200 × 200 mm and 230 × 230 mm. The openings were located either at the center of the shear span or near the inner edge

of the shear span, The configuration of these specimens is presented in Figure 3.2, where each specimen is identified according to its opening size and location.

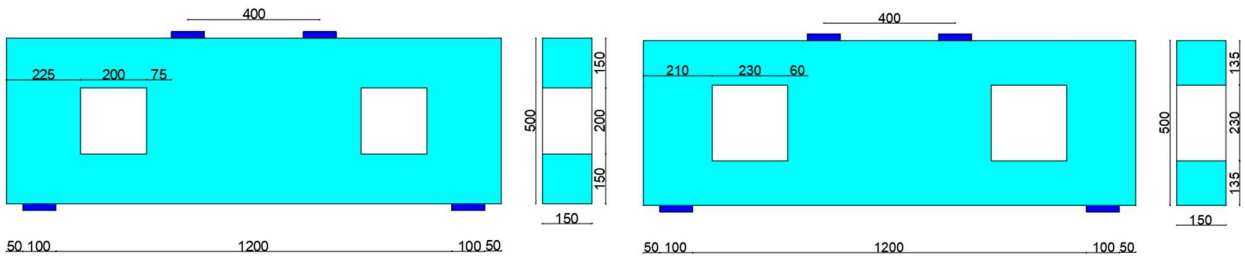


a: DP-S2-C-O1 b: DP-S2-C-O2

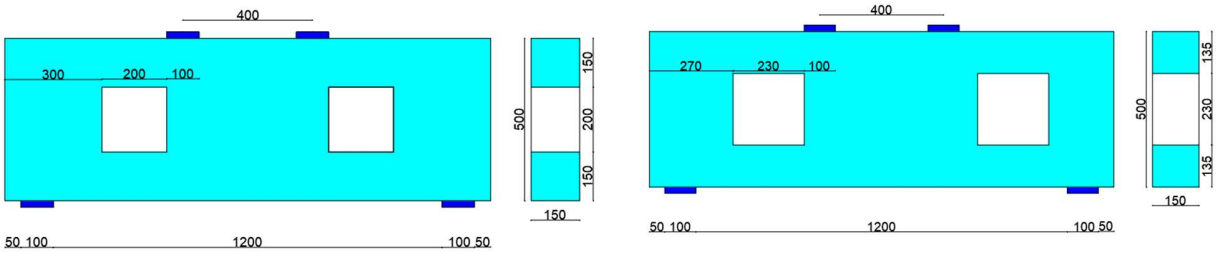


c: DP-S2-E-O1 d : DP-S2-E-O2

Figure 3. 2 Opening size and location of the deep beam specimens with web openings: (a) DP-S2-C-O1, (b) DP-S2-C-O2, (c) DP-S2-E-O1, and (d) DP-S2-E-O2.

These opening configurations were selected because of their direct influence on the diagonal compression strut, which governs the structural behavior of deep beams.

### 3.2.1 Reinforcement Details

All specimens were reinforced using the same reinforcement layout in order to isolate the influence of the studied parameters. The longitudinal reinforcement consisted of three Ø16 mm bars, while the transverse reinforcement consisted of Ø6 mm stirrups spaced at 86 mm. In addition, horizontal reinforcement was provided within the beam web in the form of a reinforcement mesh using Ø6 mm bars distributed along the

depth, in order to enhance transverse tensile resistance and control crack propagation.

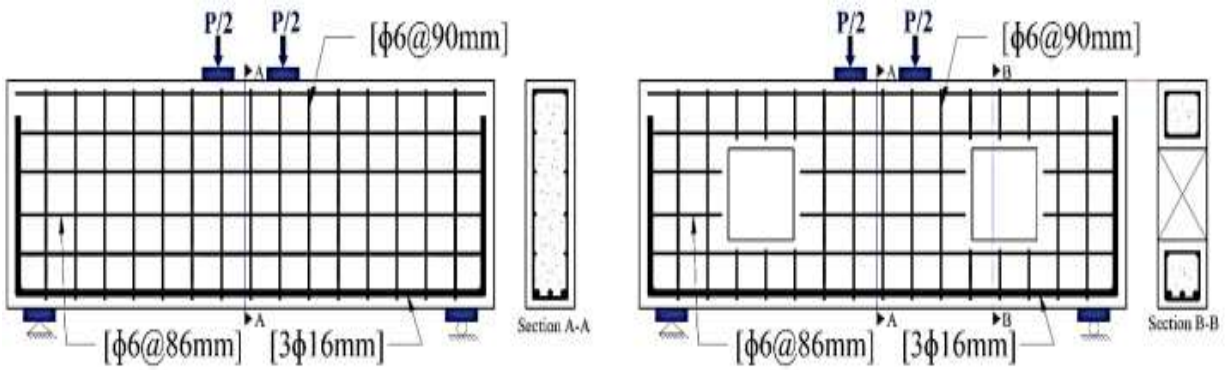


Figure 3. 3: Reinforcement details

This reinforcement arrangement was intended to maintain shear-dominated behavior and to make the effect of openings and strengthening methods more evident.

## 3.3 Parameters Considered in the Numerical Study

After completing the validation stage, a parametric study was conducted to examine the influence of the main variables affecting the response of reinforced concrete deep beams. The variables considered in this study were:

- opening size
- opening location
- strengthening using UHPC
- strengthening using CFRP
- concrete compressive strength (30, 40, and 50 MPa)
- steel yield strength (420, 500, 570, and 620 MPa)

These parameters were selected because they directly affect the continuity and efficiency of the diagonal compression strut and, consequently, the shear resistance of the beam.

## 3.4 Finite Element Modeling in ABAQUS

### 3.4.1 Geometry and Part Definition

The deep beams were modeled in ABAQUS as three-dimensional deformable bodies. The concrete beam was defined as a solid part, whereas the internal steel reinforcement was modeled separately and then embedded within the concrete body. For the strengthened specimens, the UHPC zones and CFRP sheets were introduced according to the required strengthening configuration.

The three-dimensional finite element models of the reference beam and the beams with web openings are shown in Figure 3.4. The solid reference beam (DP-S2) was modeled first, followed by the beams with web openings representing different opening sizes and locations.

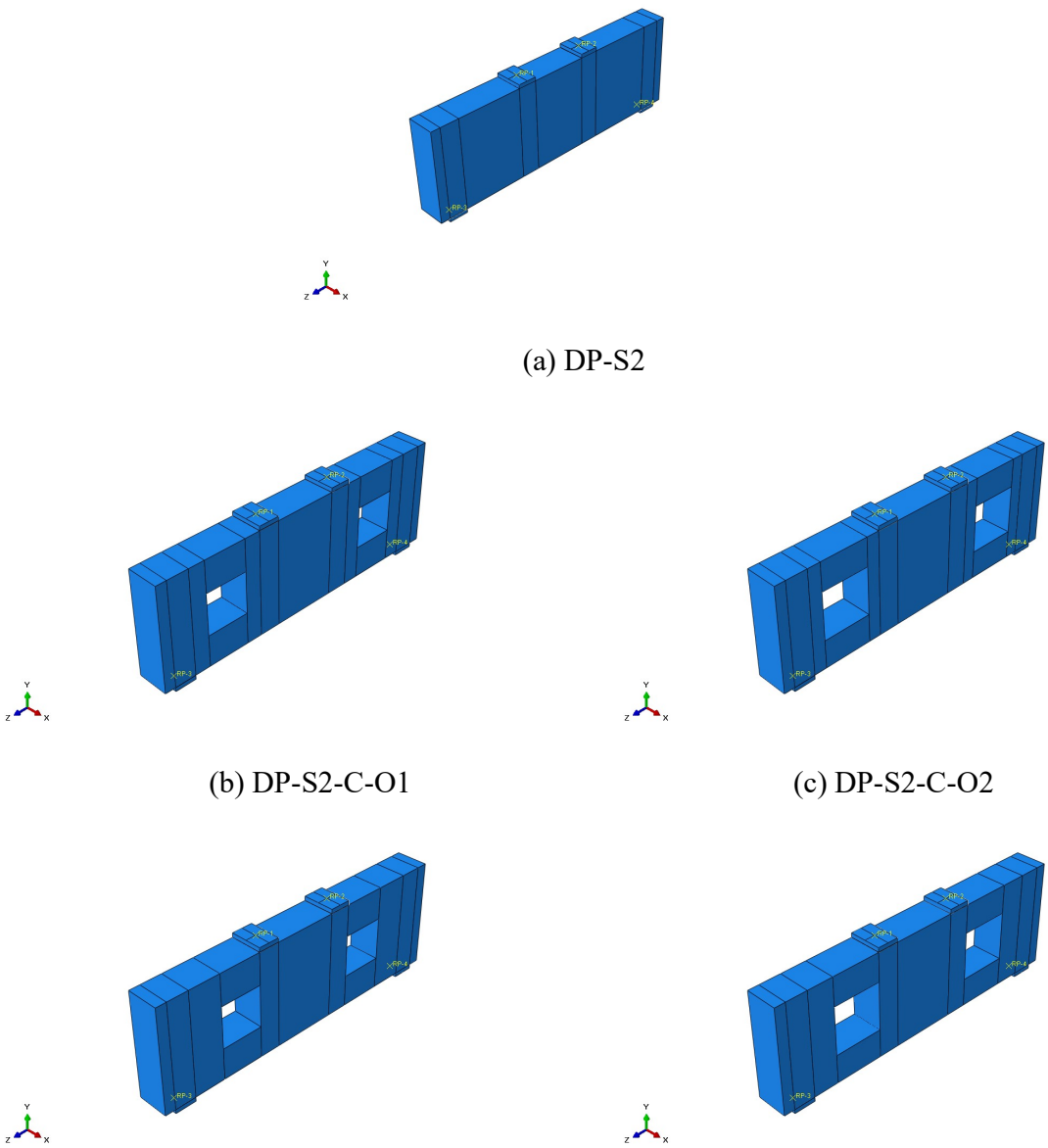

(a) DP-S2

(b) DP-S2-C-O1

(c) DP-S2-C-O2

(d) DP-S2-E-O1

(e) DP-S2-E-O2

Figure 3. 4: Three-dimensional finite element models of the validation specimens: (a) DP-S2, (b) DP-S2-C-O1, (c) DP-S2-C-O2, (d) DP-S2-E-O1, and (e) DP-S2-E-O2.

For beams with openings, the openings were modeled by removing the corresponding volume from the web region, ensuring that both the size and location of the openings were accurately represented in the numerical model.

The strengthening configurations adopted in this study are presented in Figures 3.5 and 3.6, where UHPC and CFRP strengthening systems are illustrated, respectively.

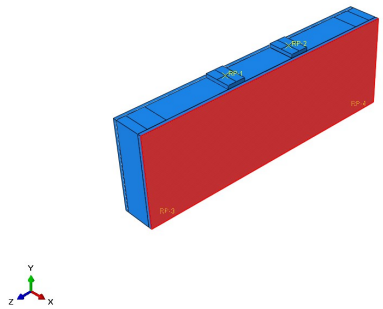

Figure 3. 5: UHPC strengthening configurations adopted in the numerical models

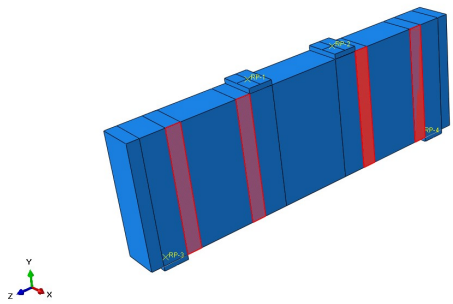

Figure 3. 6: CFRP strengthening configurations adopted in the numerical models

### 3.4.2 Element Types and Meshing

Concrete and UHPC were modeled using three-dimensional solid elements, while the reinforcing steel bars were represented using truss elements. This approach is appropriate because concrete and UHPC require volumetric elements capable of capturing stress distribution and damage evolution, whereas the reinforcement mainly resists axial forces and can be efficiently modeled using truss elements. The CFRP sheets were modeled using shell elements, which are suitable for thin orthotropic laminates and allow accurate representation of their tensile behavior.

A mesh size of approximately 20 mm was adopted in most regions of the model. Additional refinement was applied in the regions around the openings and the loading zones, where high stress concentrations and localized damage were expected.

Representative finite element meshes for the solid beam and a beam with a web opening are shown in Figure 3.7.

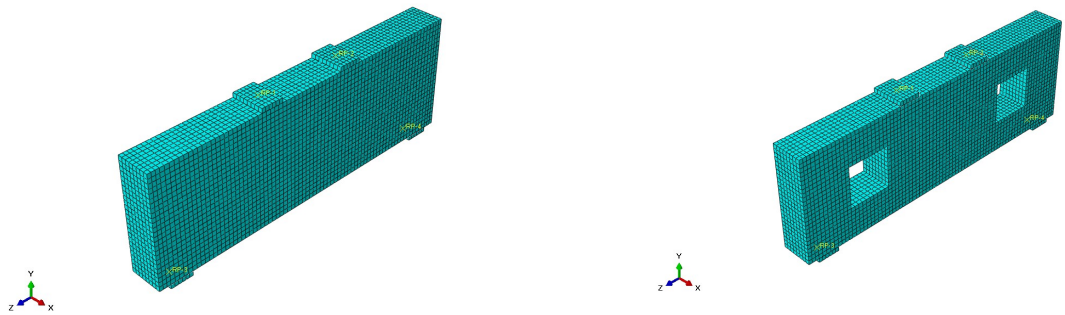

(a) DP-S2 (b) DP-S2-C-O1

Figure 3. 7: Finite element mesh of the deep beam models: (a) DP-S2, (b) DP-S2-C-O1

This mesh was found to provide a suitable balance between numerical accuracy and computational efficiency.

### 3.4.3 Material Modeling

#### *3.4.3.1 Concrete*

Concrete was modeled using the Concrete Damage Plasticity (CDP) model available in ABAQUS. This model is capable of representing nonlinear concrete behavior under both compression and tension, including crushing, cracking, and stiffness degradation.

The adopted CDP parameters were selected in line with the modeling approach reported by (ALmassri, 2024)These parameters were: dilation angle ψ = 34°, eccentricity e = 0.1, f_b0/f_c0 = 1.16, K = 0.667, and viscosity parameter μ = 0.0001. The same study also indicated that the compression and tension damage relations can be generated based on the elastic modulus and compressive strength of concrete.

| Parameter | Value |
|---|---|
| Dilation angle ψ | 34° |
| Eccentricity e | 0.1 |
| fb0/fc0 | 1.16 |
| K | 0.667 |
| Viscosity parameter μ | 0.0001 |

Table 3. 1*: CDP parameters for concrete*

To define the concrete material in ABAQUS, the complete stress-strain response under both compression and tension was first established. After that, the data were converted into the format required by the CDP model. As explained in the uploaded CDP reference, ABAQUS requires the compressive response to be entered in the form of inelastic strain-stress data, while the tensile response is introduced as cracking strain-stress data. The damage variables are then entered separately for compression and tension.

The elastic modulus of normal-weight concrete was calculated from Eq. (3.1):

$$E_c = 4700\sqrt{f'_c} \quad (3.1)$$

The ascending branch of the compressive stress-strain curve was represented using a Hognestad-type parabolic model, as given in Eq. (3.2):

$$\sigma_c / f'_c = 2(\varepsilon_c/\varepsilon_0) - (\varepsilon_c/\varepsilon_0)^2 \quad (3.2)$$

The descending branch was defined using a linear softening relationship consistent with the modified Hognestad representation, as given in Eq. (3.3):

$$\sigma c = f'c\,[1 - 0.15\,(\varepsilon_c - \varepsilon_0)/(\varepsilon_u - \varepsilon_0)] \quad (3.3)$$

where ε0 = 0.002 and εu = 0.0035.

After defining the total compressive stress-strain curve, the corresponding compressive inelastic strain was calculated from Eq. (3.4):

$$\varepsilon_{in} = \varepsilon_c - \sigma_c / E_c \quad (3.4)$$

Similarly, after defining the tensile response, the cracking strain was obtained from Eq. (3.5):

$$\varepsilon_{cr} = \varepsilon_t - \sigma_t / E_c \quad (3.5)$$

The scalar damage variables for compression and tension were then evaluated and introduced into ABAQUS in the form of compression damage versus inelastic strain and tension damage versus cracking strain, respectively. The uploaded CDP reference also shows that the damage parameter may be estimated approximately from the stress degradation when detailed unloading-reloading data are not available.

Accordingly, the concrete material definition in the present study was prepared in two stages. First, the total stress-strain curves were generated to represent the physical constitutive behavior of concrete. Second, these curves were converted into the CDP input format required by ABAQUS, namely compression hardening, tension stiffening, compression damage, and tension damage.

#### 3.4.3.2 Generated Concrete CDP Input Data

The concrete input data were generated for 27, 30, 40, and 50 MPa. The 27 MPa case corresponds to the validation model, while the remaining strengths were used in the parametric study. For each strength level, the total stress-strain response was first generated, and then transformed into the ABAQUS CDP format. This means that the tables used in the numerical model do not directly represent the original total stress-strain curve, but rather the processed material input required by the software.

| Compressive stress (MPa) | Total strain | Inelastic strain | Compression damage dc |
|---|---|---|---|
| 8.1 | 0.000327 | 0.000000 | 0.000000 |
| 16.2 | 0.000735 | 0.000072 | 0.097608 |
| 21.6 | 0.001106 | 0.000221 | 0.200006 |
| 27 | 0.002000 | 0.000894 | 0.447218 |
| 24.975 | 0.002750 | 0.001727 | 0.628128 |
| 22.95 | 0.003500 | 0.002560 | 0.731506 |

Table 3. 2: Compression hardening and compression damage data for f'c = 27 MPa

| Tensile stress (MPa) | Total strain | Cracking strain | Tension damage dt |
|---|---|---|---|
| 1.714730 | 0.000070 | 0.000000 | 0.000000 |
| 1.371784 | 0.000150 | 0.000094 | 0.625532 |
| 0.857365 | 0.000350 | 0.000315 | 0.899696 |
| 0.342946 | 0.000800 | 0.000786 | 0.982447 |
| 0.085737 | 0.001200 | 0.001196 | 0.997074 |

Table 3. 3: Tension stiffening and tension damage data for f'c = 27 MPa

| Compressive stress (MPa) | Total strain | Inelastic strain | Compression damage dc |
|---|---|---|---|
| 9 | 0.000327 | 0.000000 | 0.000000 |
| 18 | 0.000735 | 0.000036 | 0.048795 |
| 24 | 0.001106 | 0.000173 | 0.156732 |
| 30 | 0.002000 | 0.000835 | 0.417316 |
| 27.75 | 0.002750 | 0.001672 | 0.608013 |
| 25.5 | 0.003500 | 0.002509 | 0.716982 |

Table 3. 4: Compression hardening and compression damage data for f'c = 30 MPa

| Tensile stress (MPa) | Total strain | Cracking strain | Tension damage dt |
|---|---|---|---|
| 1.807484 | 0.000070 | 0.000000 | 0.000000 |
| 1.445988 | 0.000150 | 0.000094 | 0.625532 |
| 0.903742 | 0.000350 | 0.000315 | 0.899696 |
| 0.361497 | 0.000800 | 0.000786 | 0.982447 |
| 0.090374 | 0.001200 | 0.001196 | 0.997074 |

Table 3. 5: Tension stiffening and tension damage data for f'c = 30 MPa

| Compressive stress (MPa) | Total strain | Inelastic strain | Compression damage dc |
|---|---|---|---|
| 12 | 0.000327 | 0.000000 | 0.000000 |
| 24 | 0.000735 | 0.000000 | 0.000000 |
| 32 | 0.001106 | 0.000029 | 0.026278 |
| 40 | 0.002000 | 0.000654 | 0.327175 |
| 37 | 0.002750 | 0.001505 | 0.547372 |
| 34 | 0.003500 | 0.002356 | 0.673199 |

Table 3. 6 :Compression hardening and compression damage data for f'c = 40 MPa

| Tensile stress (MPa) | Total strain | Cracking strain | Tension damage dt |
|---|---|---|---|
| 2.087103 | 0.000070 | 0.000000 | 0.000000 |
| 1.669683 | 0.000150 | 0.000094 | 0.625532 |
| 1.043552 | 0.000350 | 0.000315 | 0.899696 |
| 0.417421 | 0.000800 | 0.000786 | 0.982447 |
| 0.104355 | 0.001200 | 0.001196 | 0.997074 |

Table 3. 7: Tension stiffening and tension damage data for f'c = 40 MPa

| Compressive stress (MPa) | Total strain | Inelastic strain | Compression damage dc |
|---|---|---|---|
| 15 | 0.000327 | 0.000000 | 0.000000 |
| 30 | 0.000735 | 0.000000 | 0.000000 |
| 40 | 0.001106 | 0.000000 | 0.000000 |
| 50 | 0.002000 | 0.000496 | 0.247759 |
| 46.25 | 0.002750 | 0.001358 | 0.493947 |
| 42.5 | 0.003500 | 0.002221 | 0.634626 |

Table 3. 8: Compression hardening and compression damage data for f′c = 50 MPa

| Tensile stress (MPa) | Total strain | Cracking strain | Tension damage dt |
|---|---|---|---|
| 2.333452 | 0.000070 | 0.000000 | 0.000000 |
| 1.866762 | 0.000150 | 0.000094 | 0.625532 |
| 1.166726 | 0.000350 | 0.000315 | 0.899696 |
| 0.466690 | 0.000800 | 0.000786 | 0.982447 |
| 0.116673 | 0.001200 | 0.001196 | 0.997074 |

Table 3. 9: Tension stiffening and tension damage data for f′c = 50 MPa

#### 3.4.3.3 UHPC

UHPC was modeled as a high-performance cementitious strengthening material with properties superior to those of normal concrete. Its use in the present study was intended to improve the continuity of the disturbed load-transfer path around the opening region.

The UHPC material was represented using the same general CDP framework, but with enhanced mechanical properties. In the present study, the adopted UHPC compressive strength was 146 MPa, while the corresponding elastic modulus was taken as 56.79 GPa and the tensile strength used in the constitutive model was 3.99 MPa.

The UHPC constitutive tables were generated using the same procedure adopted for conventional concrete. After defining the total compressive and tensile stress-strain relationships, the corresponding inelastic strain, cracking strain, and damage parameters were calculated and introduced into ABAQUS in the CDP format.

| Property | Value |
|---|---|
| Compressive strength f′c | 146 MPa |
| Tensile strength f_t | 10 MPa |
| Elastic modulus E | 56.79 GPa |

Table 3. 10 :UHPC material properties

| Compressive stress (MPa) | Total strain | Inelastic strain | Compression damage d_c |
|---|---|---|---|
| 43.8 | 0.000327 | 0.000000 | 0.000000 |
| 87.6 | 0.000735 | 0.000000 | 0.000000 |
| 116.8 | 0.001106 | 0.000000 | 0.000000 |
| 146 | 0.002000 | 0.000000 | 0.000000 |
| 135.05 | 0.002750 | 0.000372 | 0.135256 |
| 124.1 | 0.003500 | 0.001315 | 0.375648 |

Table 3. 11: UHPC compression hardening and compression damage data

| Tensile stress (MPa) | Total strain | Cracking strain | Tension damage d_t |
|---|---|---|---|
| 3.987405 | 0.000070 | 0.000000 | 0.000000 |
| 3.189924 | 0.000150 | 0.000094 | 0.625532 |
| 1.993703 | 0.000350 | 0.000315 | 0.899696 |
| 0.797481 | 0.000800 | 0.000786 | 0.982447 |
| 0.199370 | 0.001200 | 0.001196 | 0.997074 |

Table 3. 12: UHPC tension stiffening and tension damage data

#### *3.4.3.4 Reinforcing Steel*

The reinforcing steel was modeled as an elastic-plastic material with a modulus of elasticity of 200 GPa and Poisson's ratio of 0.30. The yield strength was varied as 420, 500, 570, and 620 MPa according to the parametric study.

#### *3.4.3.5 CFRP*

CFRP was used as an external strengthening material to improve the load-carrying capacity of the beams and to enhance stress redistribution around the disturbed regions caused by web openings. In the numerical model, CFRP was represented using shell elements and was defined as an orthotropic lamina material, consistent with the directional and brittle nature of fiber-reinforced polymers. The CFRP strips were applied around the openings, such that they were placed along both sides of each opening on both faces of the beam, with a width of 100 mm, in order to improve load transfer around the discontinuity and reduce stress concentrations at the opening corners, as illustrated in Figure 3.6.

The adopted CFRP properties were taken from Almassri (2024). The cured laminate properties included a thickness of 0.12 mm, tensile strength of 3200 MPa, elastic modulus of 220 GPa, and ultimate elongation of 1.35%. The orthotropic elastic constants used in the model were E11 = 220 GPa, E22 = 17 GPa, ν12 = 0.32, G12 = 4.5 GPa, G13 = 4.5 GPa, and G23 = 2.5 GPa.

For the present analysis, CFRP debonding was not modeled explicitly, and perfect bonding between the CFRP and the concrete substrate was assumed. The material response of CFRP was idealized as linear elastic up to failure.

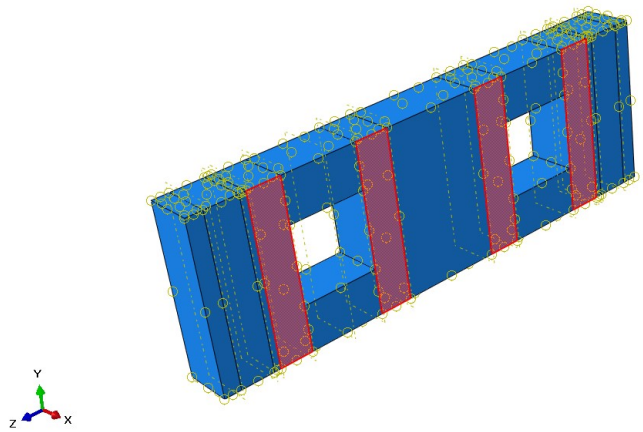


Figure 3. 8 :Strengthening configuration using CFRP strips around the web openings

| Property | Value |
|---|---|
| Thickness | 0.12 mm |
| Tensile strength | 3200 MPa |
| Elastic modulus in fiber direction E11 | 220 GPa |
| Transverse elastic modulus E22 | 17 GPa |
| Poisson's ratio Nu12 | 0.32 |
| Shear modulus G12 | 4.5 GPa |
| Shear modulus G13 | 4.5 GPa |
| Shear modulus G23 | 2.5 GPa |

Table 3. 13: CFRP material properties

### 3.4.4 Interaction Between Components

The reinforcing bars were connected to the concrete using the embedded region constraint, which assumes perfect bond between steel and surrounding concrete.

For the strengthening materials, a tie constraint was used to simulate full composite action between the concrete substrate and the strengthening layers. This assumption was adopted to focus on the overall structural response of the beam rather than on local interface failure.

The interaction definitions used in the numerical model are shown in Figure 3.9, including the interaction between concrete and reinforcement steel, concrete and UHPC, and concrete and CFRP.

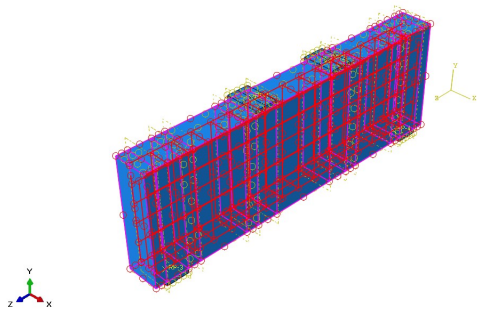

(a) Interaction between concrete and reinforcement steel

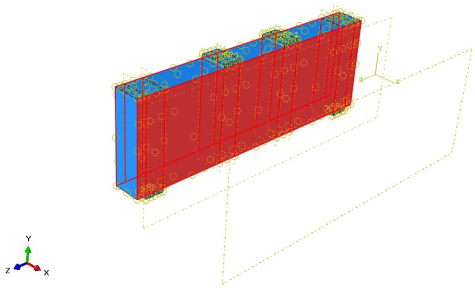

(b) Interaction between concrete and UHPC

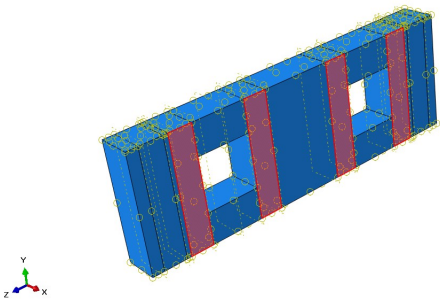

(c) Interaction between concrete and CFRP

Figure 3. 9: Interaction definitions used in the numerical model: (a) concrete and reinforcement steel, (b) concrete and UHPC, and (c) concrete and CFRP.

Accordingly, debonding between CFRP and concrete was not considered in the present study.

### 3.4.5 Boundary Conditions and Loading

The boundary conditions were defined to match the experimental setup used in the validation study, as illustrated in Figure 3.10. One end of the beam was modeled as a pin support, while the other end was modeled as a roller support. The loading configuration was applied through steel loading plates under displacement control, as shown in Figure 3.11, in order to improve numerical convergence and to capture the complete structural response up to failure.

The use of displacement-controlled loading was particularly important for tracing the post-peak response and ensuring a stable nonlinear analysis

The boundary conditions were defined to match the experimental setup used in the validation study. One end of the beam was modeled as a pin support, while the other end was modeled as a roller support. The load was applied through loading plates under displacement control to improve convergence and to capture the full response up to failure.

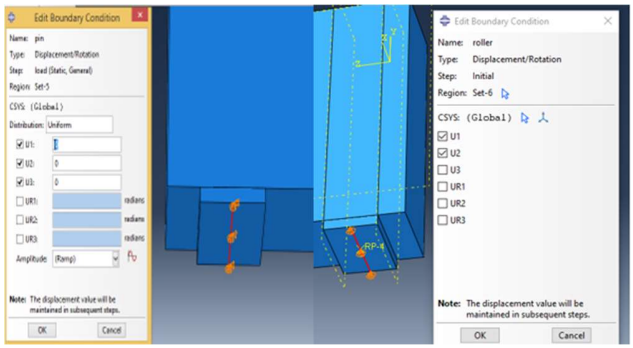


Figure 3. 10: Boundary conditions

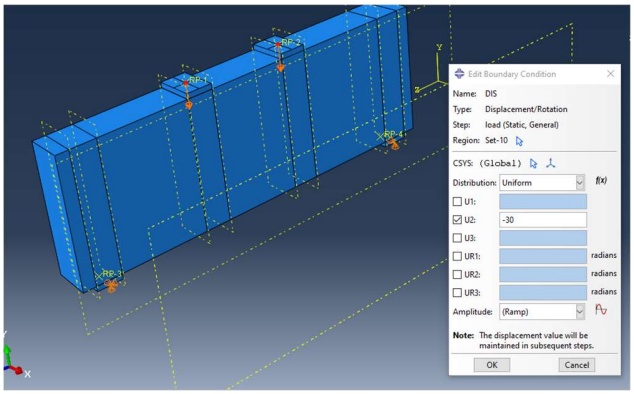


Figure 3. 11 Loading configuration

The use of displacement-controlled loading was particularly important for tracing the post-peak response and achieving stable nonlinear analysis.

### 3.5 Modeling Assumptions

Several assumptions were adopted in the numerical modeling in order to maintain stability and reduce computational complexity. The main assumptions were:

- concrete was assumed homogeneous and isotropic at the macro level
- perfect bond was assumed between concrete and reinforcement
- perfect bond was assumed between concrete and strengthening materials through the tie constraint
- CFRP debonding was neglected
- time-dependent effects such as creep and shrinkage were not considered
- the analysis was performed under monotonic static loading

These assumptions are consistent with the objective of the present study, which is to evaluate the influence of openings, strengthening systems, and material properties on the global behavior of reinforced concrete deep beams.

# Chapter4 :Results and Discussion

## 4.1 Introduction

This chapter presents and discusses the numerical results obtained from the finite element models developed in ABAQUS. The discussion begins with validation of the numerical model against available experimental results to assess its ability to predict the structural response of reinforced concrete deep beams with and without web openings.

After validation, the influence of opening size and opening location on beam behavior is examined in terms of load–displacement response, ultimate load capacity, first cracking, and damage distribution. The effectiveness of the adopted strengthening techniques is then evaluated, with particular emphasis on the structural response of beams strengthened using UHPC and CFRP.

In addition, the effects of the main parametric variables considered in this study, namely transverse reinforcement ratio, concrete compressive strength, and reinforcement yield strength, are investigated. The results are interpreted in relation to the continuity and stability of the diagonal compression strut, which governs the structural behavior of deep beams.

Finally, a comparative assessment is provided to highlight the differences between UHPC and CFRP in terms of strength, stiffness, ductility, and damage evolution, followed by a comparison between the present results and the findings reported in previous studies.

## 4.2 Validation of the Numerical Model Against the Experimental Results

### 4.2.1 Reference Experimental Program

The numerical model was validated against the experimental program reported by Jasim et al. (2018), which included reinforced concrete deep beams with a clear span of 1500 mm, an overall depth of 500 mm, and a width of 150 mm. The program considered one solid reference beam and four beams with square web openings. Two opening sizes were investigated, namely 200 × 200 mm and 230 × 230 mm. These openings were located either at the center of the shear span or near the inner edge of the shear span.

For the S2 series, the shear span-to-depth ratio was 0.9. The experimentally recorded ultimate loads were 560 kN for the solid beam DP-S2, and 240, 200, 250, and 210 kN for specimens DP-S2-C-O1, DP-S2-C-O2, DP-S2-E-O1, and DP-S2-E-O2, respectively. Most of the experimental specimens failed by diagonal splitting, while specimen DP-S2-E-O1 exhibited a shear-compression failure mode.

### 4.2.2 Numerical–Experimental Ultimate Load Comparison

The comparison between the experimental ultimate loads and the numerical predictions obtained from the ABAQUS model is presented in **Table 4.1**.

| Specimen | Experimental load (KN) | ABAQUS load (KN) | Difference (%) |
|---|---|---|---|
| DP-S2 | 560 | 612 | +9.29 |
| DP-S2-C-O1 | 240 | 220 | -8.33 |
| DP-S2-C-O2 | 200 | 210 | +5.00 |
| DP-S2-E-O1 | 250 | 230 | -8.00 |
| DP-S2-E-O2 | 210 | 215 | +2.34 |

Table 4 .1: compares the experimental ultimate loads with the corresponding numerical predictions obtained from the ABAQUS models

As shown in **Table 4.1**, the numerical model provided good agreement with the experimental results for all validation specimens. The maximum overestimation was 9.29% for the solid beam DP-S2, while the maximum underestimation was 8.33% for specimen DP-S2-C-O1. For the remaining specimens, the differences ranged between -8.00% and +5.00%, indicating that the developed finite element model was able to predict the ultimate load capacity with acceptable accuracy.

To further illustrate the level of agreement between the experimental and numerical results, Figure 4.X presents a visual comparison of the ultimate load values for all validation specimens.

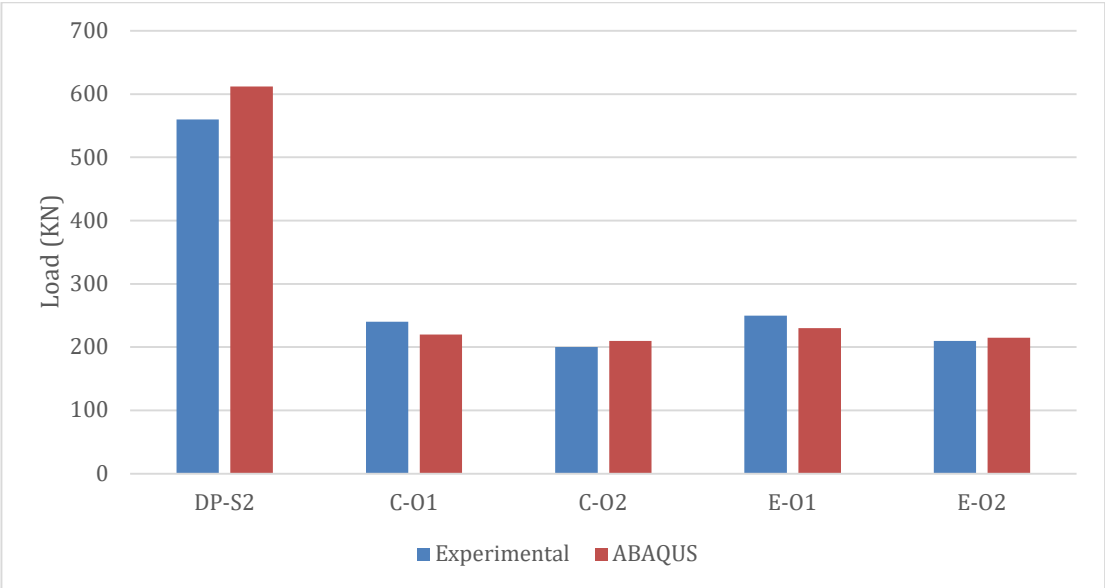


Figure 4. 1: Comparison between the experimental and ABAQUS ultimate loads for the validation specimens

Overall, the comparison confirms that the numerical model can reliably simulate the global structural response of reinforced concrete deep beams with and without web openings, and therefore can be used in the subsequent parametric study.

### 4.2.3 Numerical–Experimental Failure Mode Comparison

The ABAQUS simulations were also able to reproduce the observed failure mechanisms with good agreement. For the solid specimen DP-S2, the compression damage appeared as a diagonal band extending from the loading point toward the support, while the tensile damage was concentrated along the inclined cracking path. This numerical behavior agrees well with the experimentally observed diagonal splitting failure mode.

For the beams with web openings, the corners of the openings were identified as the main regions where tensile damage initiated, while the compression field became visibly disturbed around the opening. This response is consistent with the experimental observations, which showed that the openings interrupted the natural diagonal load-transfer path and caused localized cracking around their boundaries. In addition, the numerical results indicated a more critical compression zone above the opening in specimen DP-S2-E-O1, which is consistent with the experimentally reported shear-compression response.

A comparison between the experimental and numerical failure characteristics of the reference specimen DP-S2 is presented in Figure 4.2.

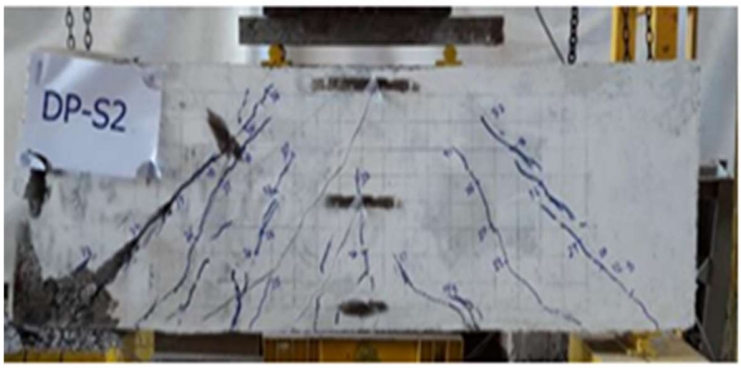


**(a)** Experimental failure of DP-S2(Jasim,2018)

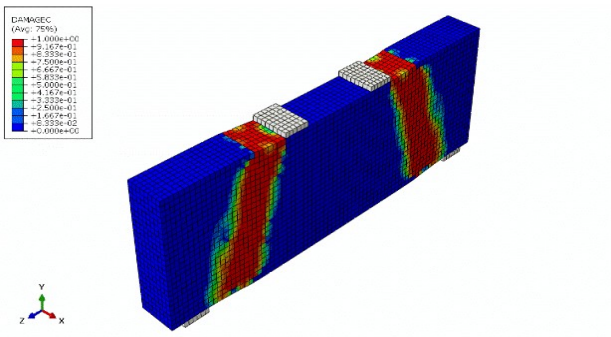

**(b)** Compression damage contour for DP-S2

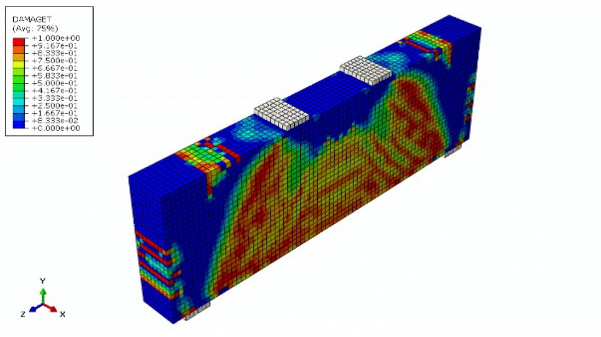

**(c)** Tensile damage contour for DP-S2

Figure 4. 2: Numerical–experimental failure mode comparison for specimen DP-S2: (a) experimental failure of DP-S2, (b) compression damage contour, and (c) tensile damage contour.

### 4.2.4 Numerical–Experimental Load–Displacement Comparison

In addition to the comparison of ultimate load and failure mode, the validation of the numerical model was further assessed by comparing the load–displacement responses obtained from the ABAQUS simulations with those reported in the experimental study.

Figure 4.3 presents the load–displacement curves for the reference beam and the beams with web openings. As shown in the figure, the numerical model was able to reproduce the general shape of the experimental curves with good agreement.

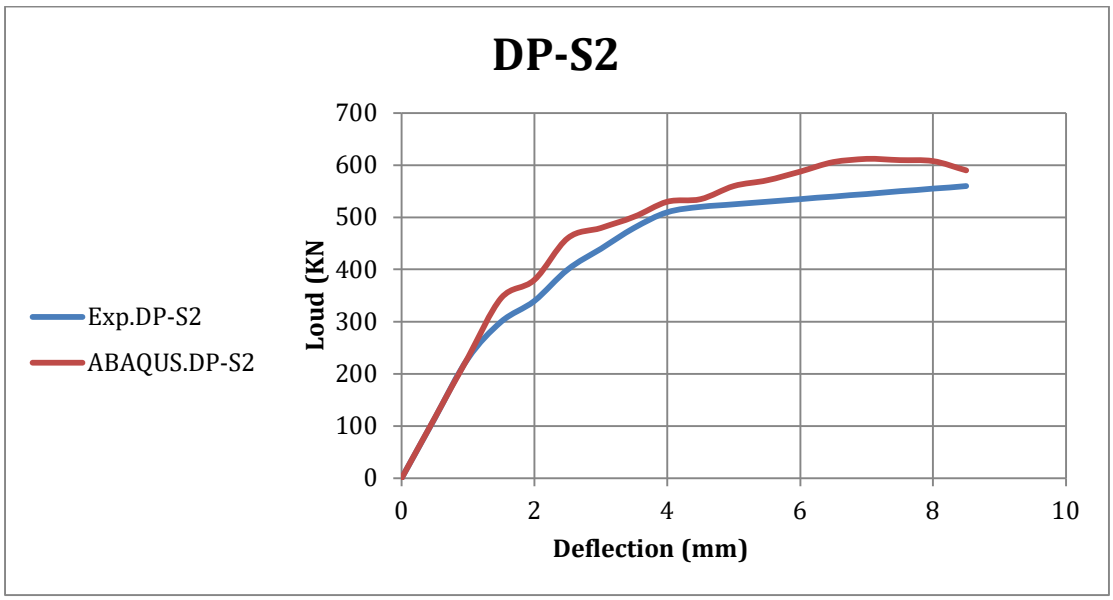


(a) DP-S2

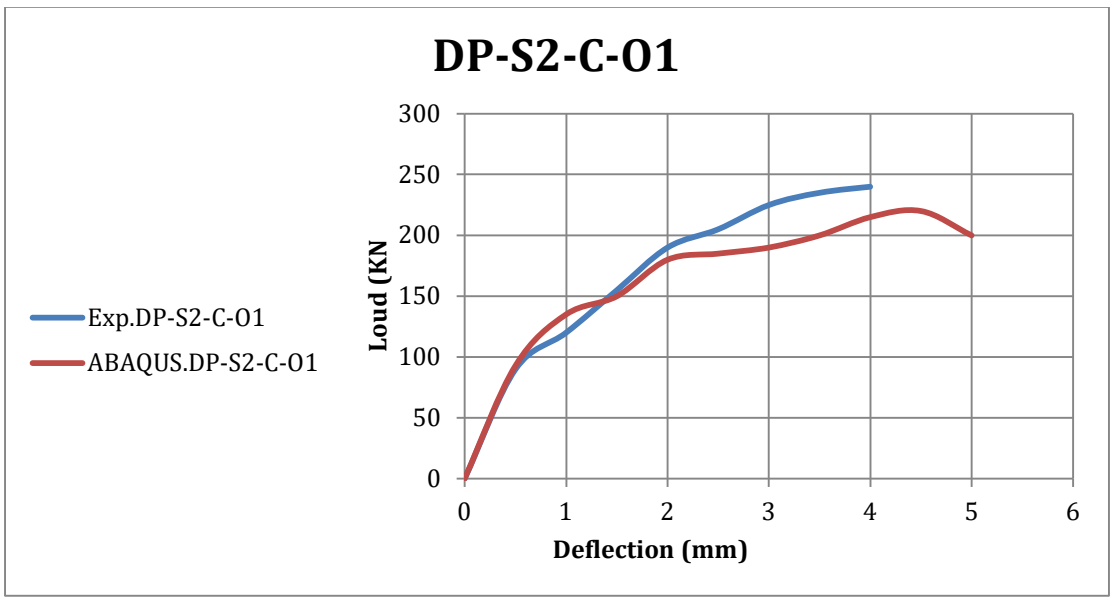


(b) DP-S2-C-O1

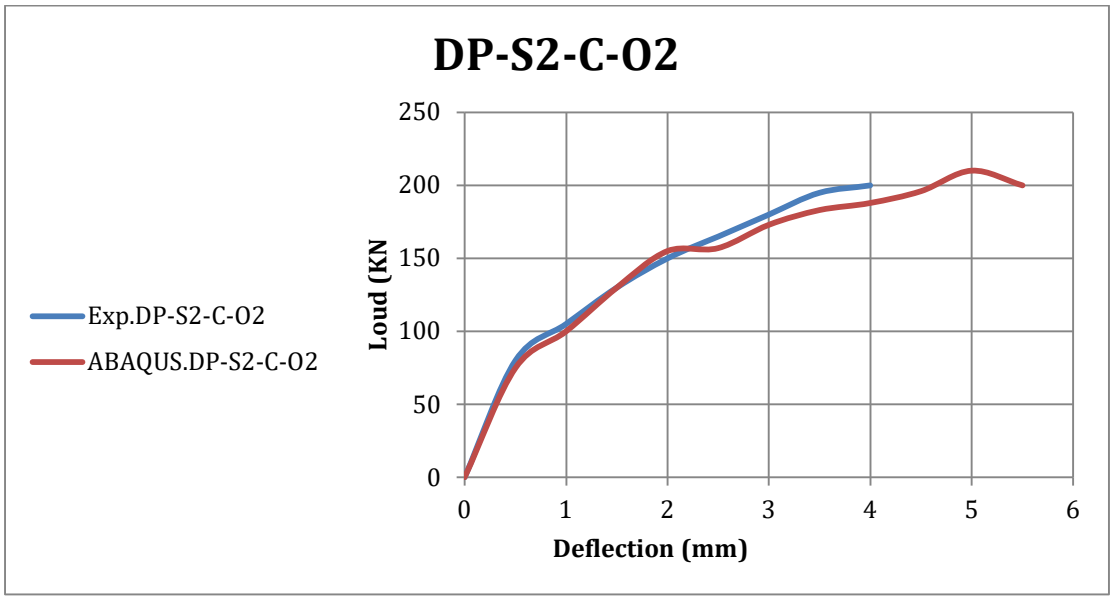


(c) DP-S2-C-O2

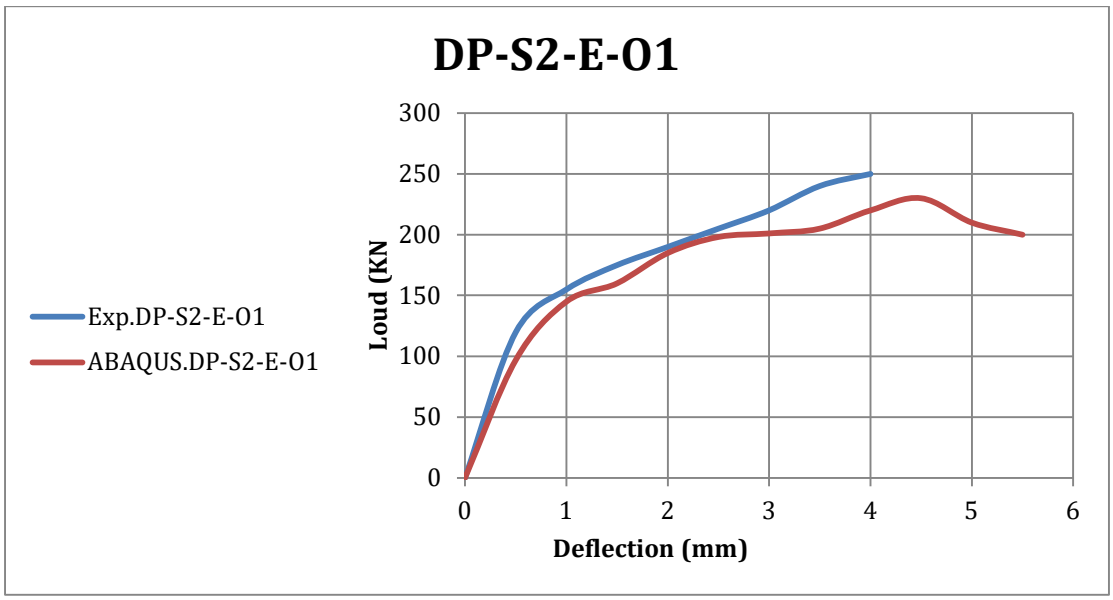


(d) DP-S2-E-O1

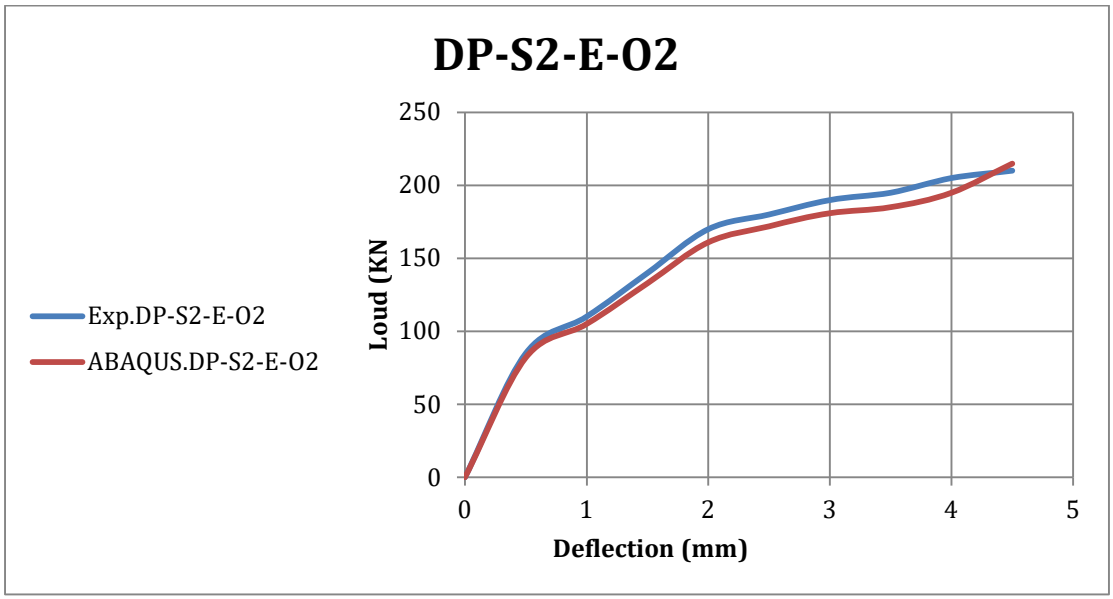


(e) DP-S2-E-O2

Figure 4. 3: Comparison of load–displacement curves between experimental results and ABAQUS predictions for the validation specimens: (a) DP-S2, (b) DP-S2-C-O1, (c) DP-S2-C-O2, (d) DP-S2-E-O1, and (e) DP-S2-E-O2.

For the solid beam DP-S2, the numerical model slightly overestimated the stiffness and ultimate load; however, the overall response, including the linear elastic stage, cracking behavior, and post-peak trend, was well captured.

For the beams with openings, the numerical curves followed a similar trend to the experimental results, showing reduced stiffness and lower ultimate load compared with the solid beam. Minor deviations were observed in the post-cracking stage, which may be attributed to modeling assumptions such as perfect bond between materials.

Overall, the comparison confirms that the developed numerical model is capable of accurately predicting not only the ultimate load but also the global structural response of reinforced concrete deep beams, including stiffness, cracking behavior, and deformation characteristics.

### 4.2.5 Manual STM-Based Verification of the Solid Beam DP-S2

A simplified manual verification was carried out for the solid reference beam DP-S2 using the Strut-and-Tie Model (STM). This verification was not intended to replace the nonlinear finite element analysis, but to provide a mechanics-based check of whether the Abaqus response is consistent with the expected internal load-transfer mechanism of a reinforced concrete deep beam.

For the solid reference beam DP-S2, the load-transfer mechanism can be idealized by a direct diagonal compression strut extending from the loading region to the support, together with a bottom tension tie represented by the longitudinal reinforcement. Since the beam behaves as a disturbed region, the STM approach provides a suitable simplified representation of the dominant compression and tension force paths.

The beam had an overall depth of h = 500 mm, a web width of bw = 150 mm, concrete compressive strength of f'c = 27 MPa, and a shear span of a = 450 mm, measured from the center of the support to the center of the applied load. The bottom longitudinal reinforcement consisted of three bars with diameter $\phi$ = 16 mm, and the steel yield strength was taken as fy = 570 MPa.

The effective depth was estimated from the beam geometry as follows:

$d = h - (c + \phi/2)$

$d = 500 - (40 + 16/2) = 452$ mm

The internal lever arm was estimated by subtracting an approximate compression-zone or nodal depth from the effective depth. This approximation represents the location of the resultant compressive force beneath the loading plate and avoids assuming that the compression resultant acts exactly at the extreme compression face. Therefore:

$z \approx d - 50$

$z = 452 - 50 = 402$ mm

Accordingly, the inclination angle of the diagonal compression strut was obtained from the geometry of the STM mechanism:

$\tan \theta = z/a$

$\tan \theta = 402/450 = 0.893$

$\theta = 41.78°$

The area of the bottom longitudinal reinforcement was calculated as:

$As = 3(\pi\phi 2/4)$

$As = 3[\pi(16)2/4] = 603.2$ mm2

The nominal tensile resistance of the bottom tie was then calculated using the yield strength of the longitudinal reinforcement:

$Tn = Asfy$

$Tn = 603.2 \times 570 = 343.8$ kN

For the symmetrical two-point loading arrangement, the total applied load corresponding to the tensile resistance of the bottom longitudinal tie can be expressed as:

$Ptie = 2Tn \tan \theta$

$Ptie = 2 \times 343.8 \times 0.893 = 614.3$ kN

The calculated tie-based capacity, Ptie = 614.3 kN, is very close to the ultimate load obtained from the Abaqus model for beam DP-S2, which was approximately 612 kN. The percentage difference between the simplified STM estimate and the numerical result is:

$Difference = [(614.3 - 612)/612] \times 100 = 0.38\%$

This close agreement indicates that the numerical response of the solid beam is mechanically consistent with the development of a direct diagonal compression field and a bottom tension tie. In other words, the Abaqus model captured the expected internal force-transfer mechanism of the solid deep beam.

A simplified compression-strut check was also considered. The effective compressive stress in the strut may be expressed as:

$f_{ce} = 0.85\beta_s f'_c$

where $\beta_s$ is the strut efficiency factor. When a conservative value of $\beta_s$ is used, the calculated strut capacity becomes lower than the Abaqus ultimate load. This is expected because conservative STM provisions are mainly intended for design purposes and include reductions to account for cracking, transverse tensile strain, and disturbance in the concrete compression field. Therefore, the conservative strut check should be interpreted as a lower-bound design estimate rather than an exact prediction of the nonlinear ultimate load.

The nodal zones were also checked to ensure that local bearing failure did not govern the response. The nodal capacity was evaluated using the general STM expression:

$F_{nn} = f_{ce}A_n$

$f_{ce} = 0.85\beta_n f'_c$

where $\beta_n$ is the nodal efficiency factor and $A_n$ is the effective bearing area of the nodal zone. For the support node, idealized as a C-C-T node, the conservative nodal capacity was approximately 550.8 kN. For the loading node, idealized as a C-C-C node, the corresponding nodal capacity was approximately 688.5 kN. The support-node capacity is close to the experimental ultimate load of 560 kN, whereas the loading-node capacity is higher than both the experimental and numerical ultimate loads. This indicates that crushing at the loading node was not the governing mechanism of the solid beam.

Overall, the manual STM verification supports the validity of the numerical response obtained for the solid beam DP-S2. The calculated tie-based capacity of 614.3 kN is almost identical to the Abaqus ultimate load of 612 kN, while the conservative nodal and strut checks provide lower-bound design-type estimates. Therefore, the response of the solid beam can be interpreted as being mechanically consistent with a stable strut-and-tie action. However, the tie-based STM estimate should be considered an equilibrium-based verification rather than a direct prediction of the actual failure mode, the experimental response was governed mainly by diagonal splitting/shear-compression behavior rather than pure yielding of the bottom tie.

## 4.3 Effect of Openings: Influence of Location and Size

### 4.3.1 General Structural Interpretation

The introduction of web openings significantly affects the structural behavior of reinforced concrete deep beams. In the solid reference beam, load transfer is governed mainly by a diagonal compression strut extending between the loading point and the support. However, when an opening is introduced within the shear span, this load path becomes disturbed, leading to a noticeable reduction in load-carrying capacity.

The severity of this reduction depends mainly on the size and location of the opening. When the compression strut is partially interrupted, the applied load is forced to follow a less efficient and more localized transfer path. As a result, stress concentration increases, cracking initiates earlier, and the structural response becomes weaker compared with the solid beam.

The influence of web openings on the global structural response is clearly reflected in the load–displacement curves. As shown in **Figure 4.4**, all beams with openings exhibited lower stiffness and lower ultimate load capacity than the solid reference beam.

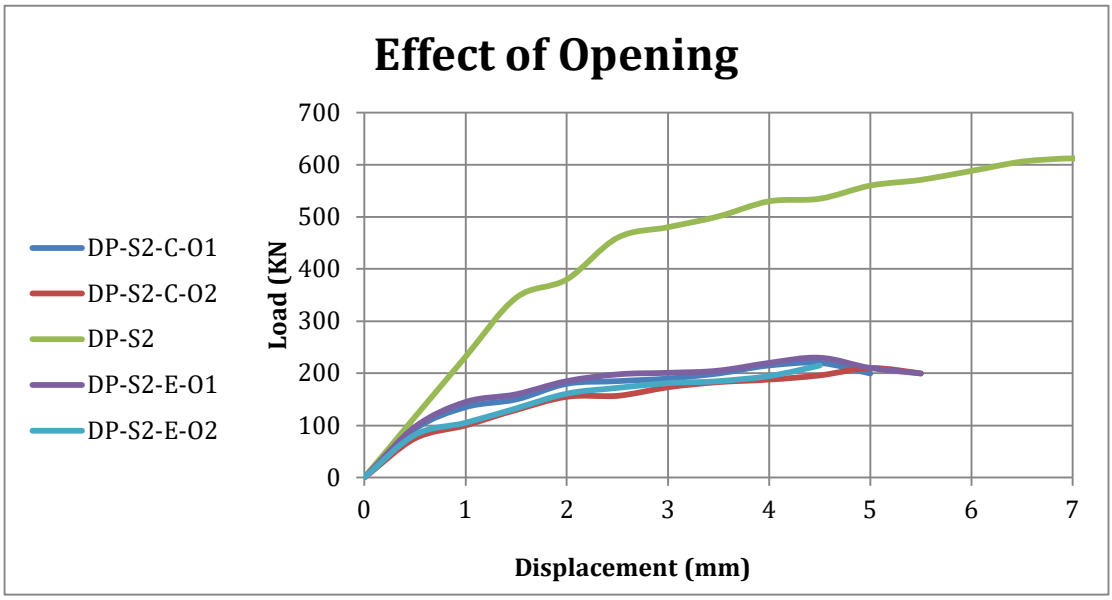


Figure 4. 4 : Load–displacement curve for DP-S2, DP-S2-C-O1, DP-S2-C-O2, DP-S2-E-O1 and DP-S2-E-O2.

### 4.3.2 Effect of Opening Location

For a given opening size, the location of the opening had a noticeable but limited influence on the structural response of the beam. The numerical results showed that beams with edge openings consistently exhibited slightly higher load-carrying capacity than those with centrally located openings.

For the smaller opening size, the ultimate load of specimen DP-S2-E-O1 was approximately 4.54% higher than that of specimen DP-S2-C-O1. This indicates that moving the opening away from

the central region of the shear span slightly reduced the disturbance in the load-transfer mechanism. The same trend is reflected in the load–displacement response shown in Figure 4.5, where the edge-opening specimen sustained a slightly higher load and showed marginally better stiffness.

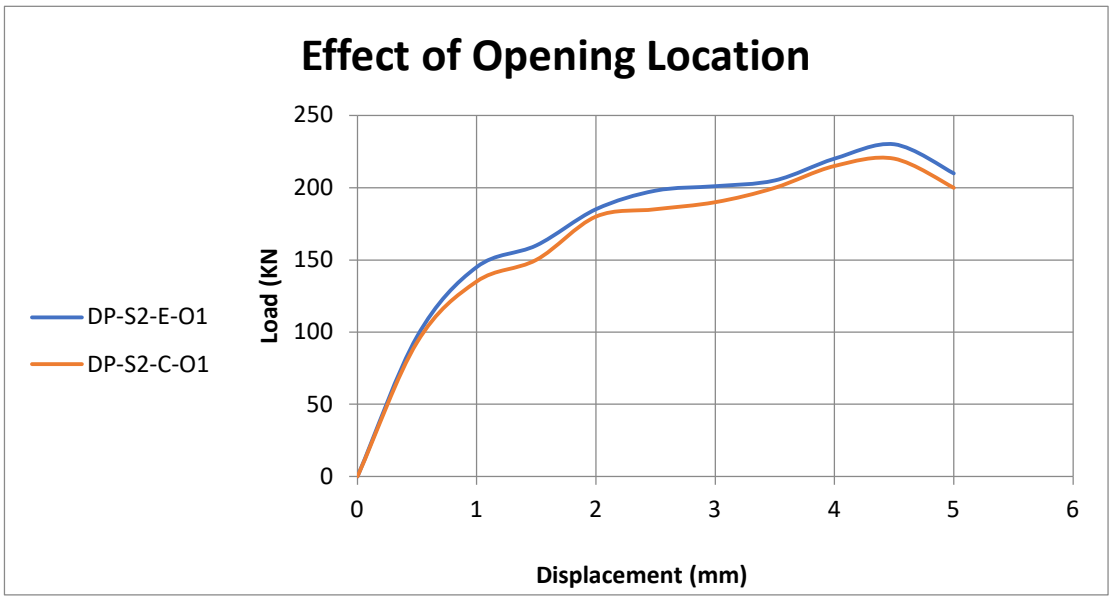


Figure 4. 5: Load–displacement curve of DP-S2-E-O1 and DP-S2-C-O1.

For the larger opening size, specimen DP-S2-E-O2 also showed a slightly better response than specimen DP-S2-C-O2, as illustrated in Figure 4.6. This confirms that the edge-opening configuration was less detrimental than the central-opening configuration, although the difference remained limited.

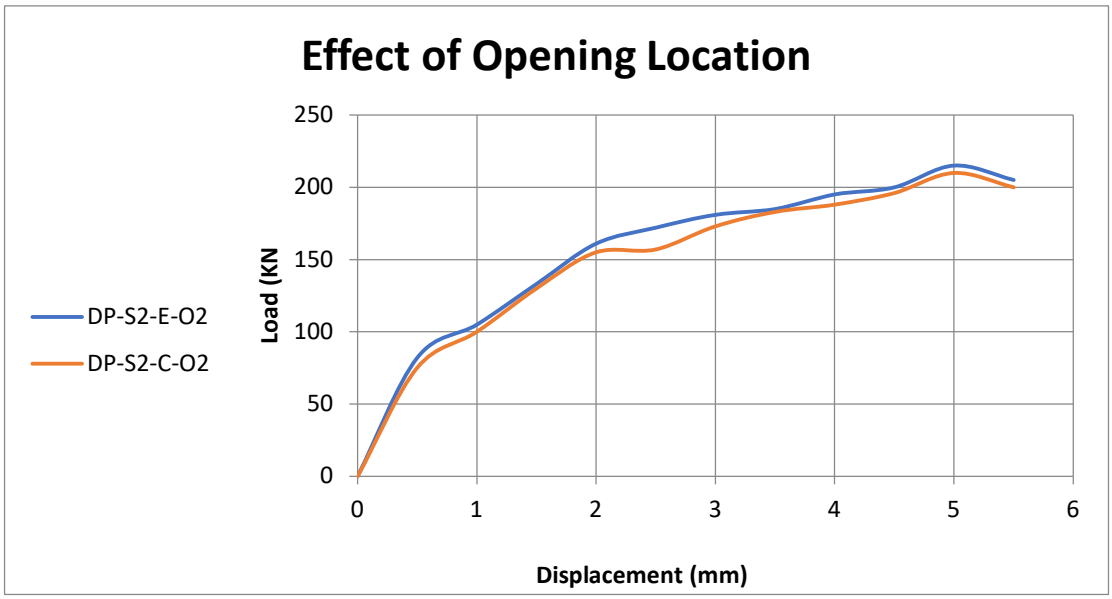


Figure 4. 6:Load–displacement curve of DP-S2-E-O2 and DP-S2-C-O2.

This behavior can be attributed to the interaction between the opening and the diagonal compression strut. Centrally located openings intersect the main load-transfer path more directly,

causing greater disturbance to the internal force flow. In contrast, edge openings allow a relatively larger portion of the compression field to remain continuous. However, because both opening locations were still within the disturbed shear span, both configurations disrupted the compression field and generated stress concentrations around the opening corners. Therefore, the presence of the opening itself was the dominant factor, while the change in opening location had a secondary effect.

This interpretation is supported by the damage contours shown in Figure 4.7. The central-opening specimen exhibited more concentrated tensile damage and a more distorted compression field, whereas the edge-opening specimen maintained a relatively more continuous compression zone. This agrees with previous studies, such as Campione and Minafò (2012) and Jasim et al. (2018), which reported that openings located closer to the principal stress path are more detrimental to deep beam behavior.

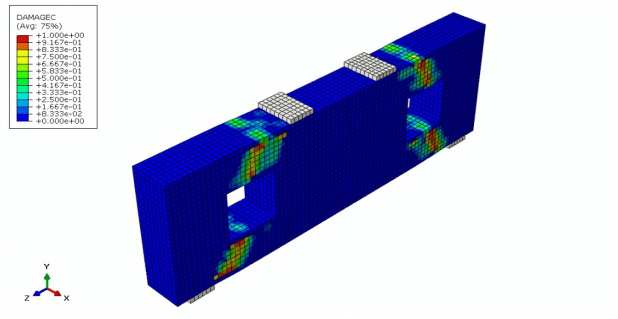

**(a)** Compression damage contour of DP-S2-C-O1

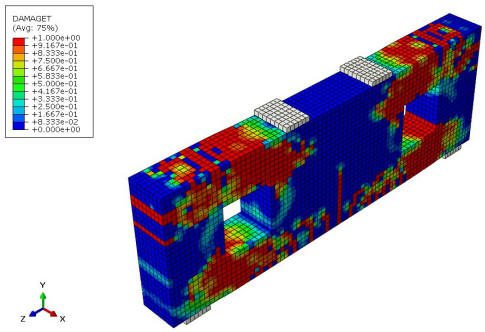

**(b)** Tensile damage contour of DP-S2-C-O1

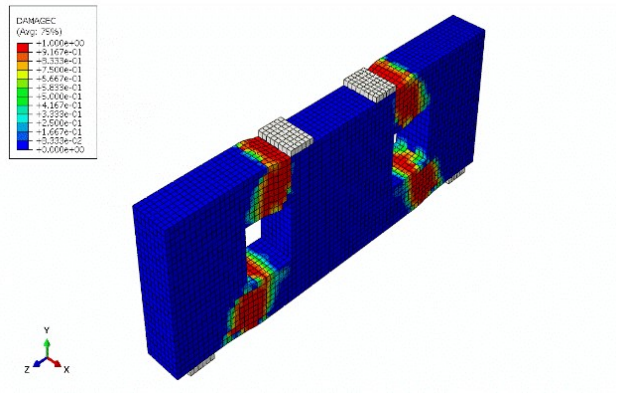

**(c)** Compression damage contour of DP-S2-E-O1

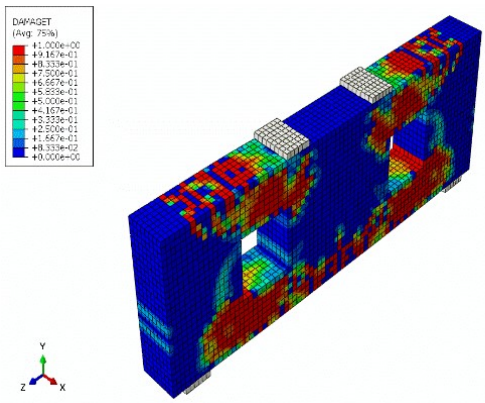

**(d)** Tensile damage contour of DP-S2-E-O1

Figure 4. 7: Effect of opening location on damage distribution: (a) compression damage contour of DP-S2-C-O1, (b) tensile damage contour of DP-S2-C-O1, (c) compression damage contour of DP-S2-E-O1, and (d) tensile damage contour of DP-S2-E-O1.

### 4.3.3 Effect of Opening Size

The numerical results clearly indicate that increasing the opening size led to a consistent reduction in the load-carrying capacity of the investigated deep beams, regardless of the opening location.

For the beams with centrally located openings, increasing the opening size from 200 × 200 mm to 230 × 230 mm resulted in a reduction in ultimate load of approximately 4.55%. This difference is clearly reflected in the load–displacement response shown in **Figure 4.8**, where specimen DP-S2-C-O2 exhibited lower strength and a less stable response than specimen DP-S2-C-O1.

A similar trend was observed for the beams with edge openings. As shown in **Figure 4.9**, increasing the opening size from 200 × 200 mm to 230 × 230 mm reduced the ultimate load by approximately 6.52%, confirming that the adverse influence of increasing opening size remained consistent for both opening locations.

From a mechanical point of view, a larger opening removes a greater portion of the web and causes more severe disturbance to the diagonal compression strut. As a result, the applied load is transferred through a narrower and less efficient compression zone, leading to higher stress concentration, earlier crack development, and lower structural capacity. This finding is consistent with previous studies **(Yang et al., 2006; Rahim et al., 2020)**.

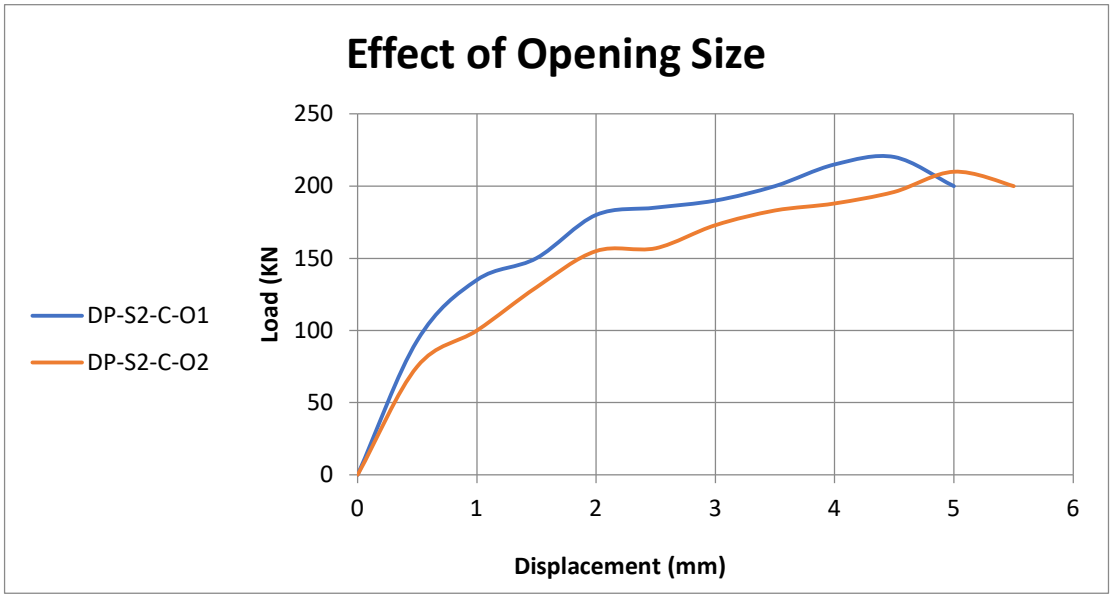


**Figure 4. 8:Load–displacement curve of DP-S2-C-O1 and DP-S2-C-O2**

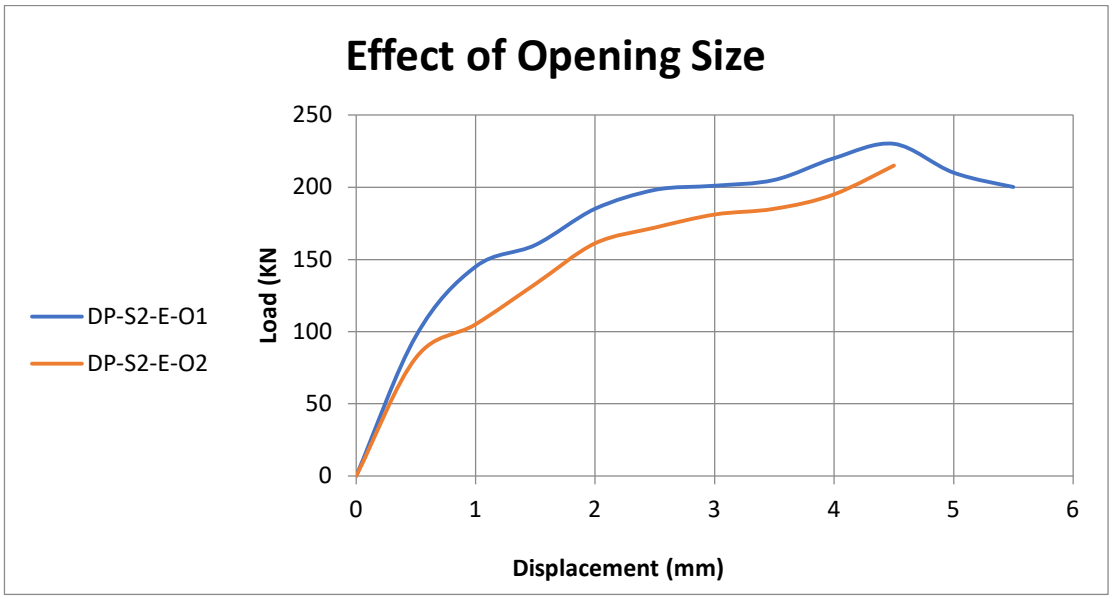


**Figure 4. 9:Load–displacement curve of DP-S2-E-O1 and DP-S2-E-O2.**

### 4.3.4 Combined Interpretation of Location and Size

Based on the numerical results, the different opening configurations can be ranked in terms of structural performance (from best to worst) as follows:

- E-O1 (small edge opening)
- C-O1 (small central opening)
- E-O2 (large edge opening)
- C-O2 (large central opening)

This ranking reflects the degree to which each configuration disrupts the diagonal compression strut. The small edge opening causes the least disturbance and therefore maintains a more efficient load-transfer mechanism, whereas the large central opening directly interrupts the primary load path, resulting in the most significant reduction in structural performance.

## 4.4 First Cracking Behavior

### 4.4.1 Identification of First Cracking

Crack initiation represents a critical transition point in the behavior of reinforced concrete deep beams, marking the departure from near-linear elastic response toward nonlinear behavior dominated by damage and cracking.

In this study, the first-cracking load was identified using a combined numerical approach based on two criteria. The first criterion is the deviation of the load–displacement curve from its initial linear trend, while the second criterion is the initiation of tensile damage as indicated by the CDP damage variables in ABAQUS.

This combined method provides a more reliable identification of crack initiation, particularly in deep beams where localized stress concentrations may produce early microcracking that later governs the global structural response

### 4.4.2 Extracted First Cracking Load Results

The extracted first-cracking loads for the investigated beam specimens are summarized in **Table 4.2**. These values represent practical indicators of the onset of nonlinear behavior rather than strict material limits.

As shown in Table 4.2, the solid reference beam (DP-S2) had the highest first-cracking load among the unstrengthened specimens, while the opened beams cracked earlier. The reduction was more evident for central and larger openings because these configurations intensified local stress concentration around the opening corners.

The strengthened specimens showed higher first-cracking loads, with UHPC producing the largest improvement and CFRP providing a more moderate delay in crack initiation.

| Case | First-cracking load (kN) | Structural interpretation |
|---|---|---|
| DP-S2 | 345 | Baseline unstrengthened solid beam |
| DP-S2-C-O1 | 150 | Moderate reduction due to central opening |
| DP-S2-C-O2 | 130 | Most severe reduction among central-opening cases |
| DP-S2-E-O1 | 160 | Higher than C-O1 due to less disturbance in the load path |
| DP-S2-E-O2 | 133 | Large edge opening still causes early cracking |
| DP-S2-UHPC | 517 | Significant delay in crack initiation |
| DP-S2-C-O1-UHPC | 210 | Clear improvement through restoration of the disturbed zone |
| DP-S2-C-O2-UHPC | 155 | Improvement remains but is limited by larger opening |
| DP-S2-E-O1-UHPC | 192 | Improved crack resistance in edge-opening case |
| DP-S2-E-O2-UHPC | 170 | Moderate to strong increase in cracking load |
| DP-S2-CFRP | 400 | Moderate delay in crack initiation |
| DP-S2-C-O2-CFRP | 136 | Limited improvement mainly through crack control |
| DP-S2-E-O2-CFRP | 151 | Slightly better than central-opening CFRP case |

Table 4. 2 :Extracted first-cracking loads for the reference, opened, and strengthened beams.

The influence of the main parametric variables on the first-cracking load is presented separately in **Table 4.3**.

The results indicate that increasing the transverse reinforcement ratio and concrete compressive strength leads to a clear improvement in cracking resistance. In contrast, the effect of reinforcement yield strength on crack initiation remains limited.

| Parameter | Value | First-cracking load (kN) | Structural interpretation |
|---|---|---|---|
| Transverse reinforcement ratio (Av/s) | 0.65 | 345 | Reference value |
| Transverse reinforcement ratio (Av/s) | 1.2 | 460 | Significant improvementin cracking resistance |
| Transverse reinforcement ratio (Av/s) | 1.8 | 510 | Further increase with diminishing returns |
| Concrete compressive strength (f'c) | 30 MPa | 375 | Strong increase in cracking resistance |
| Concrete compressive strength (f'c) | 40 MPa | 430 | |
| Concrete compressive strength (f'c) | 50 MPa | 485 | |
| Reinforcement yield strength (fy) | 420 MPa | ≈162 | Negligible influence on crack initiation |
| Reinforcement yield strength (fy) | 620 MPa | ≈162 | |

Table 4. 3: Effect of the main parametric variables on first-cracking load

These trends agree with previous studies reporting that openings accelerate cracking through stress concentration, whereas high-performance strengthening materials improve cracking resistance by enhancing crack control and local tensile capacity (Yang et al., 2006; Jasim et al., 2018; Graybeal, 2014; Elghany et al., 2025; Rahim et al., 2020).

### 4.4.3 Effect of Openings on First Cracking

Web openings reduced the first-cracking load because the opening corners acted as stress-concentration zones and disturbed the early-stage force flow around the void.

Central and larger openings produced the lowest cracking loads, confirming that both location and size control the onset of damage.

These results are consistent with the earlier load-displacement trends in Figure 4.4, where beams with openings departed from the initial linear response earlier than the solid beam.

### 4.4.4 Effect of Strengthening Techniques on First Cracking

UHPC produced the clearest improvement in first-cracking performance by increasing the stiffness and tensile resistance of the strengthened region.

For opened beams, this improvement reduced stress concentration near the opening corners and delayed the transition from linear behavior to damage development.

CFRP also delayed cracking, but its influence was more moderate because it acted mainly through external crack restraint and local confinement.

#### 4.4.5 Effect of Transverse Reinforcement Ratio on First Cracking

Increasing the transverse reinforcement ratio (Av/s) increased the first-cracking load, but the improvement followed a diminishing-return pattern.

The first increase in Av/s improved diagonal crack control noticeably, whereas further increase provided smaller additional benefits once adequate crack restraint had been achieved.

#### 4.4.6 Effect of Concrete Compressive Strength on First Cracking

Concrete compressive strength (f'c) had a strong influence on first cracking because higher concrete strength improved both local tensile resistance and the stability of the diagonal compression field.

The effect was clearer in the solid beam; in opened beams, the same positive trend remained but was partly limited by the geometric disturbance caused by the opening (Yang et al., 2006).

#### 4.4.7 Effect of Reinforcement Yield Strength on First Cracking

The influence of reinforcement yield strength (fy) on first cracking was limited because crack initiation occurred before the longitudinal reinforcement reached yielding.

Therefore, the early-stage response was governed mainly by concrete tensile resistance and force-path integrity rather than by steel yielding characteristics.

#### 4.4.8 Concluding Interpretation of First Cracking

Overall, the first-cracking results show that early damage is controlled by the integrity of the internal force path and the local tensile resistance around critical regions.

Consequently, UHPC strengthening and higher concrete compressive strength were the most effective parameters for delaying crack initiation, while CFRP, Av/s, and fy had comparatively smaller effects at this stage.

### 4.5 Effect of UHPC Strengthening

#### 4.5.1 General Observation

UHPC strengthening produced the most substantial improvement among the investigated strengthening measures, and the benefit observed at first cracking continued into the global load-displacement response.

Its main contribution was the strengthening of the disturbed zone itself, which improved stiffness, ultimate capacity, and damage stability.

#### 4.5.2 UHPC Effect on the Solid Beam

For specimen DP-S2, the ultimate load increased from 612 kN to 761 kN after UHPC strengthening, corresponding to an improvement of approximately 24.34%, as shown in Figure 4.10.

The load-displacement response indicates that UHPC increased both stiffness and ultimate capacity, as reflected by the steeper initial slope and higher peak load.

The damage contours in Figure 4.11 show a more stable diagonal compression-damage pattern and reduced tensile damage compared with the unstrengthened beam.

Thus, UHPC improved the solid beam by enhancing strength, stiffness, and damage stability, which agrees with previous studies (Elghany et al., 2025; Al-Enezi et al., 2023).

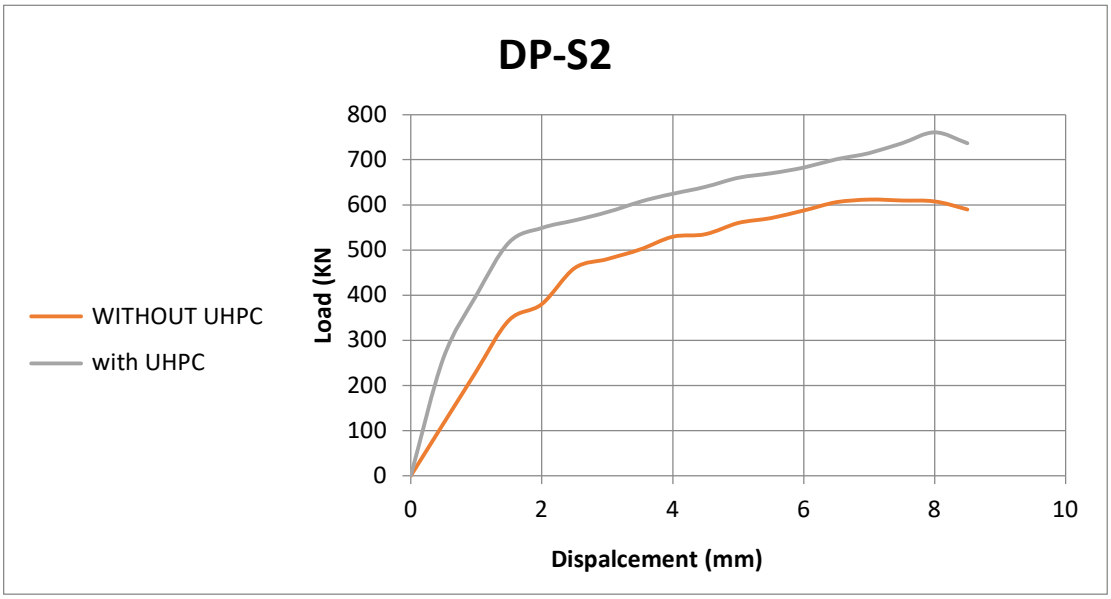


Figure 4. 10:Load–displacement curve of DP-S2 before and after UHPC strengthening.

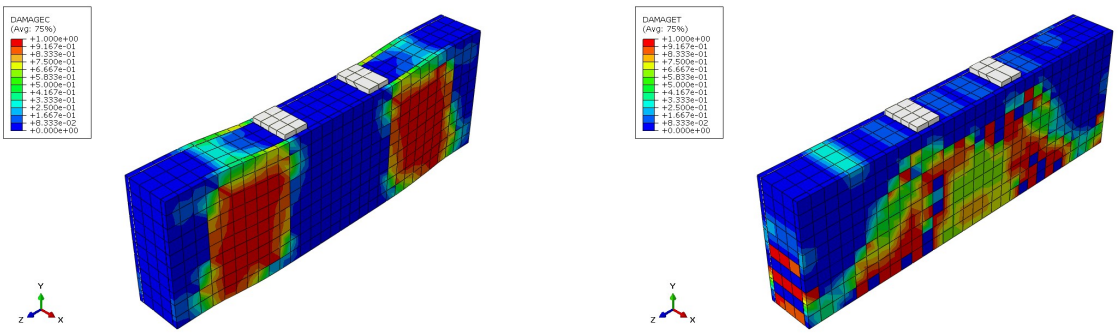

(a) compression damage contour (b) tensile damage contour

Figure 4. 11: Damage contours of specimen DP-S2 after UHPC strengthening: (a) compression damage contour and (b) tensile damage contour.

### 4.5.3 UHPC Effect on Beams with Openings

For beams with web openings, UHPC significantly improved the ultimate load capacity for all investigated configurations, as summarized in Table 4.4.

The increase ranged from approximately 27.27% to 32.61%, indicating that UHPC was particularly effective when the beam response was weakened by a disturbed web regions.

| Specimen | Reference load (KN) | UHPC load (KN) | Difference (%) |
|---|---|---|---|
| DP-S2 | 612 | 761 | +24.34 |
| DP-S2-C-O1 | 220 | 280 | +27.27 |
| DP-S2-C-O2 | 210 | 268 | +27.62 |
| DP-S2-E-O1 | 230 | 305 | +32.61 |
| DP-S2-E-O2 | 215 | 282 | +31.16 |

Table 4. 4:Comparison of ultimate load capacity between reference and UHPC-strengthened deep beam specimens

The load–displacement curves presented in **Figures 4.12–4.15** show that the UHPC-strengthened beams exhibited higher stiffness, delayed crack initiation, and improved post-peak stability compared with the corresponding unstrengthened specimens.

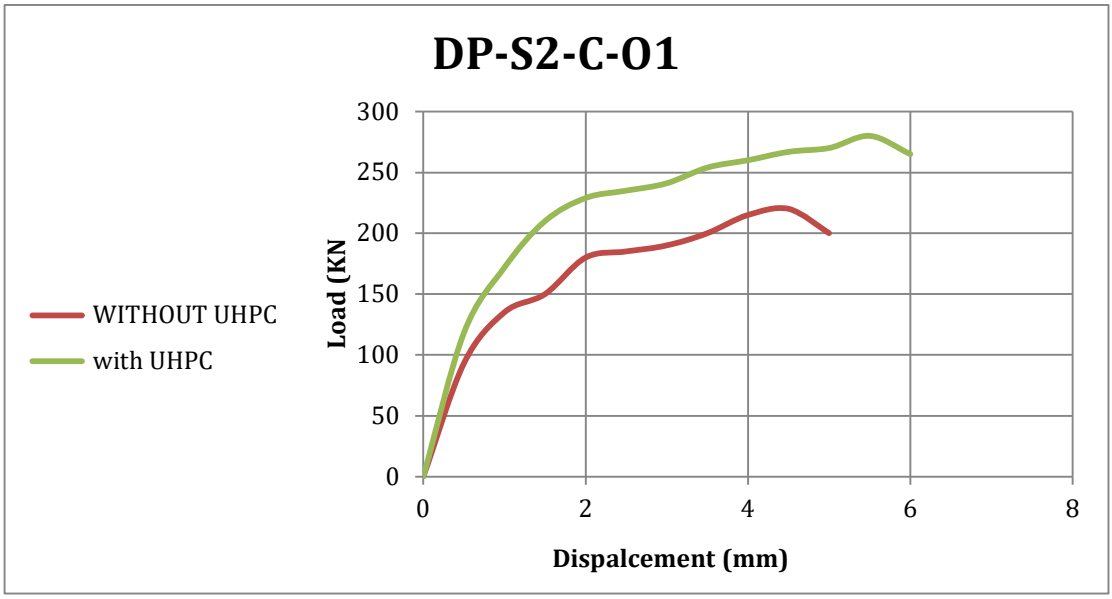


**Figure 4. 12:Load–displacement curve of DP-S2-C-O1 before and after UHPC strengthening.**

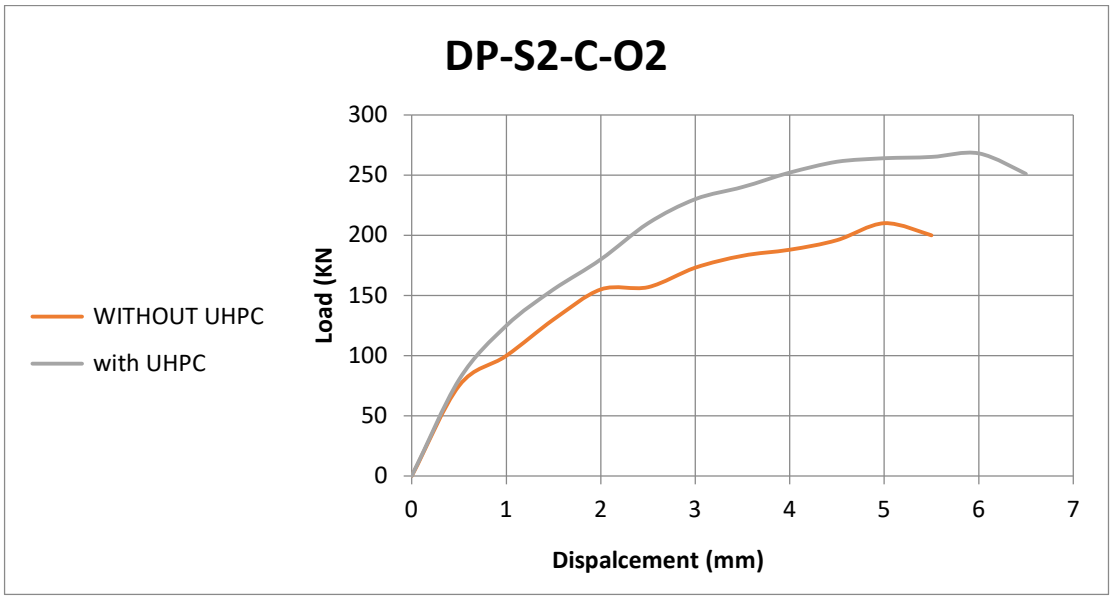


**Figure 4. 13:Load–displacement curve of DP-S2-C-O2 before and after UHPC strengthening.**

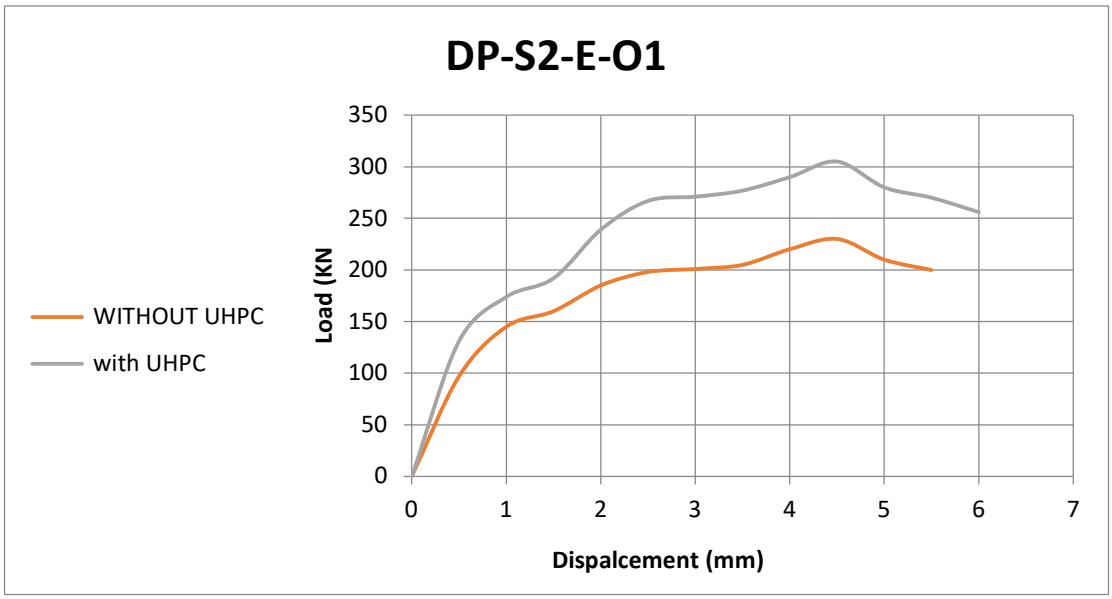


**Figure 4. 14:Load–displacement curve of DP-S2-E-O1 before and after UHPC strengthening.**

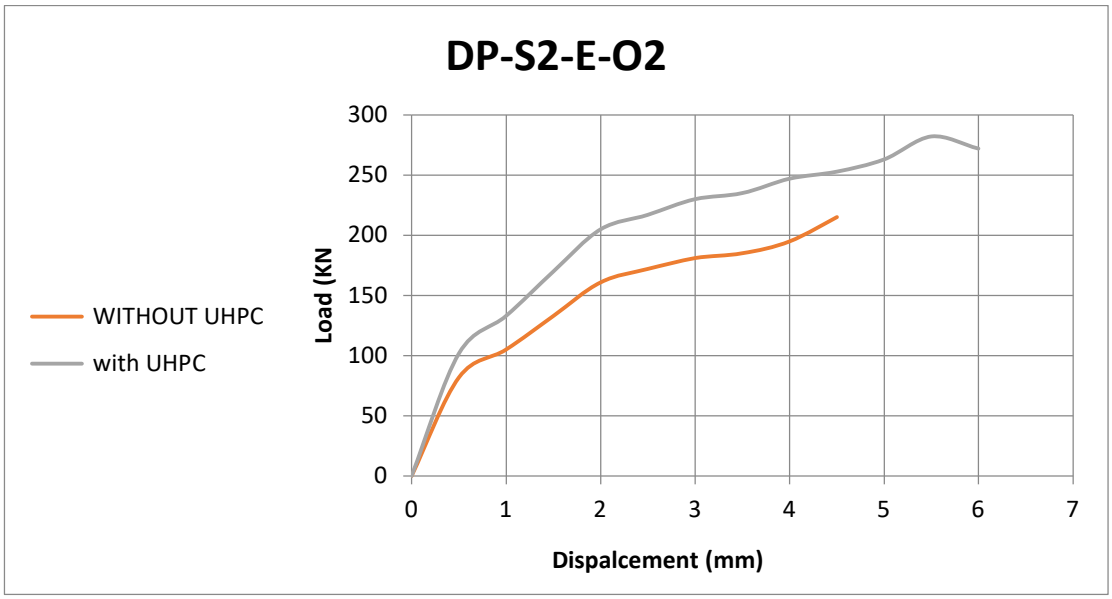


**Figure 4. 15:Load–displacement curve of DP-S2-E-O2 before and after UHPC strengthening.**

The improvement was more pronounced in beams with edge openings. Specimens DP-S2-E-O1 and DP-S2-E-O2 exhibited the highest gains, which can be attributed to the fact that edge openings preserve a larger portion of the original compression field. This allows UHPC to effectively strengthen and reconnect a load path that remains partially intact.

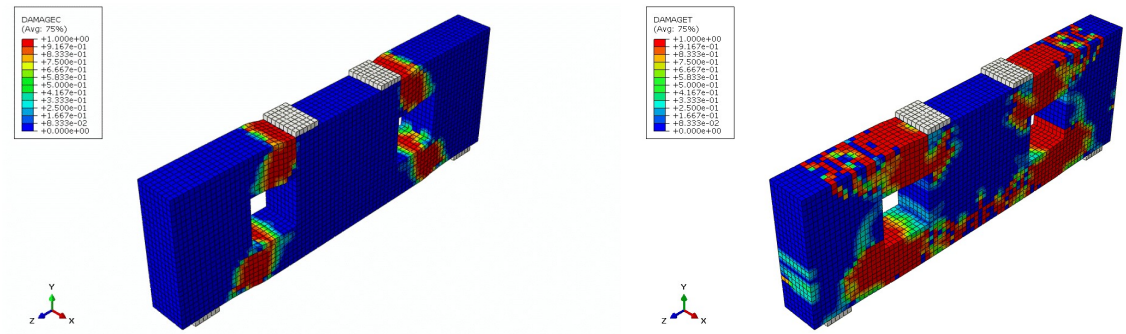

(a) Compression damage contour of DP-S2-E-O1-UHPC

(b) Tensile damage contour of DP-S2-E-O1-UHPC

Figure 4. 16: Damage contours of specimen DP-S2-E-O1-UHPC: (a) compression damage contour and (b) tensile damage contour.

Figure 4.16 supports this observation by showing a more continuous compression field and lower tensile-damage concentration around the edge opening.

For central openings, UHPC still improved the response, but the benefit was reduced because the original force path was more severely interrupted.

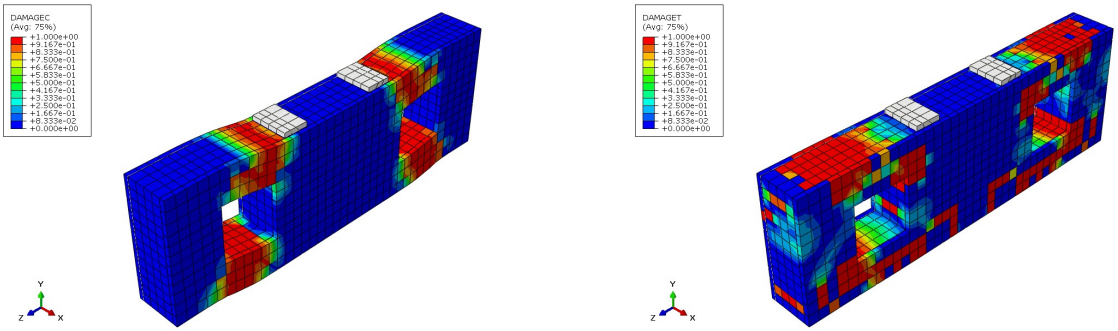

(a) Compression damage contour of DP-S2-C-O1-UHPC (b) Tensile damage contour of DP-S2-C-O1-UHPC

Figure 4. 17: Damage contours of specimen DP-S2-C-O1-UHPC: (a) compression damage contour and (b) tensile damage contour.

Figure 4.17 illustrates this limitation, where the central-opening specimen still shows a more disturbed compression field around the opening.

Overall, UHPC was highly effective for beams with openings, especially when some continuity of the original compression field remained. This agrees with previous studies (Elghany et al., 2025; Al-Enezi et al., 2023).

## 4.6 Effect of CFRP Strengthening

### 4.6.1 General Observation

CFRP strengthening improved the response of the investigated beams by increasing ultimate load and reducing crack severity, but its effect remained more moderate than UHPC.

This is because CFRP acted mainly as an external tensile-strengthening and crack-control system..

### 4.6.2 CFRP Effect on the Solid Beam

For specimen DP-S2, CFRP strengthening increased the ultimate load from 612 kN to 685 kN, corresponding to an improvement of approximately 11.9%, as shown in Figure 4.18.

The load-displacement response indicates that CFRP increased the ultimate load and improved crack control, while the change in stiffness remained limited.

As shown in Figure 4.19, CFRP reduced tensile damage, whereas the compression-damage pattern remained broadly similar to that of the reference beam.

Overall, CFRP enhanced the solid beam mainly through crack control and tensile-force redistribution, consistent with previous studies (El Maaddawy & Sherif, 2009; Rahim et al., 2020).

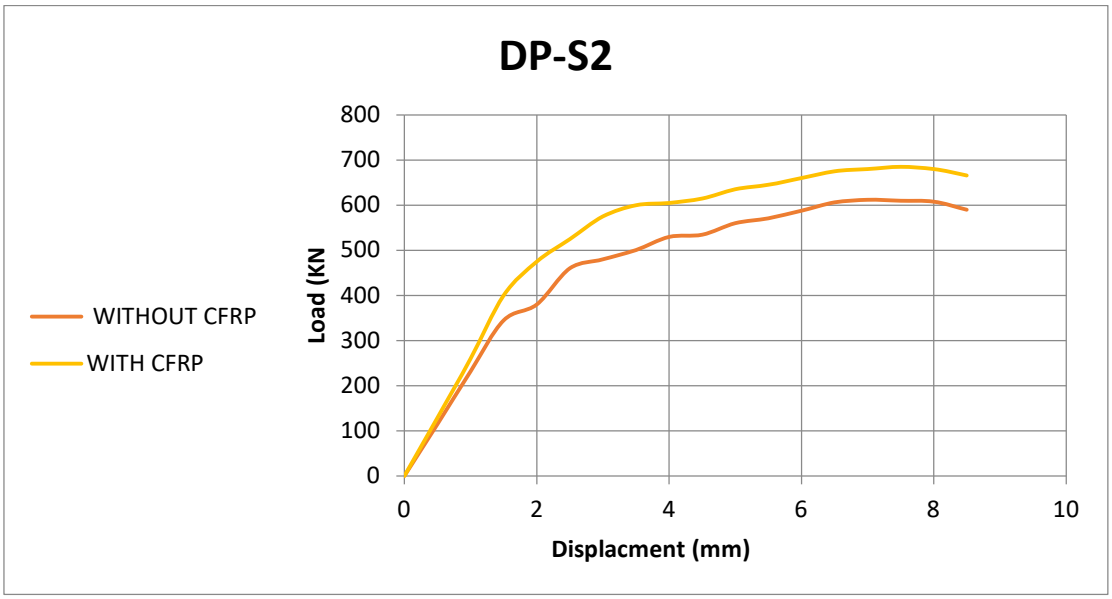


Figure 4. 18:Load–displacement curve of DP-S2 before and after CFRP strengthening.

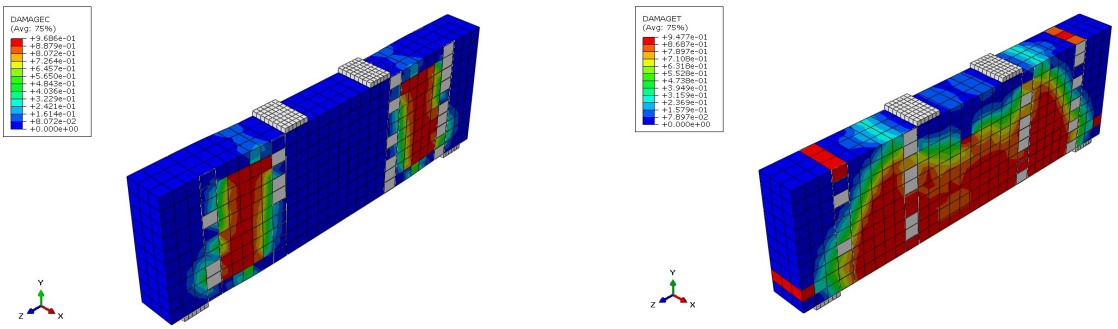

**(a)** Compression damage contour of DP-S2 after CFRP strengthening

**(b)** Tensile damage contour of DP-S2 after CFRP strengthening

Figure 4. 19: Damage contours of specimen DP-S2 after CFRP strengthening: (a) compression damage contour and (b) tensile damage contour.

### 4.6.3 CFRP Effect on Beams with Openings

For specimen DP-S2-C-O2, CFRP strengthening increased the ultimate load from 210 kN to 240 kN, corresponding to an improvement of approximately 14.3%. For specimen DP-S2-E-O2, the ultimate load increased from 215 kN to 248 kN, corresponding to an improvement of approximately 15.35%, as shown in Figures 4.20 and 4.21.

The slightly better response of the edge-opening specimen indicates that CFRP was more effective when the internal load path was less severely disturbed.

Figure 4.22 supports this interpretation: tensile damage was reduced, but the compression-field pattern remained broadly similar to that of the unstrengthened beam

. Overall, CFRP improved opened beams through crack control, with an efficiency that depended on the severity of the opening disturbance (El Maaddawy & Sherif, 2009; Rahim et al., 2020).

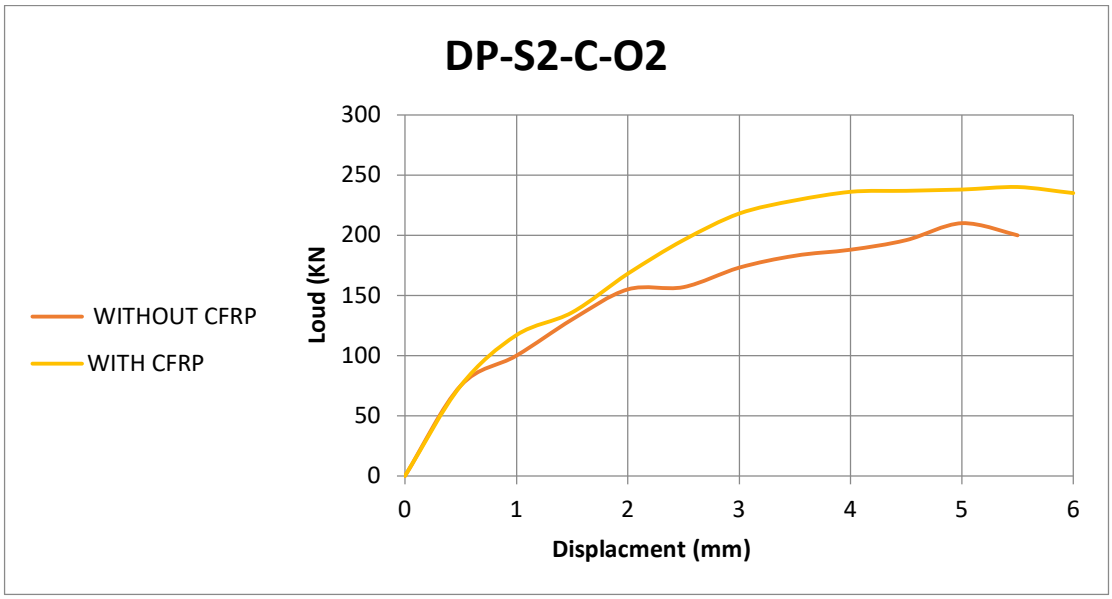


Figure 4. 20: Load–displacement curve of DP-S2-C-O2 before and after CFRP strengthening.

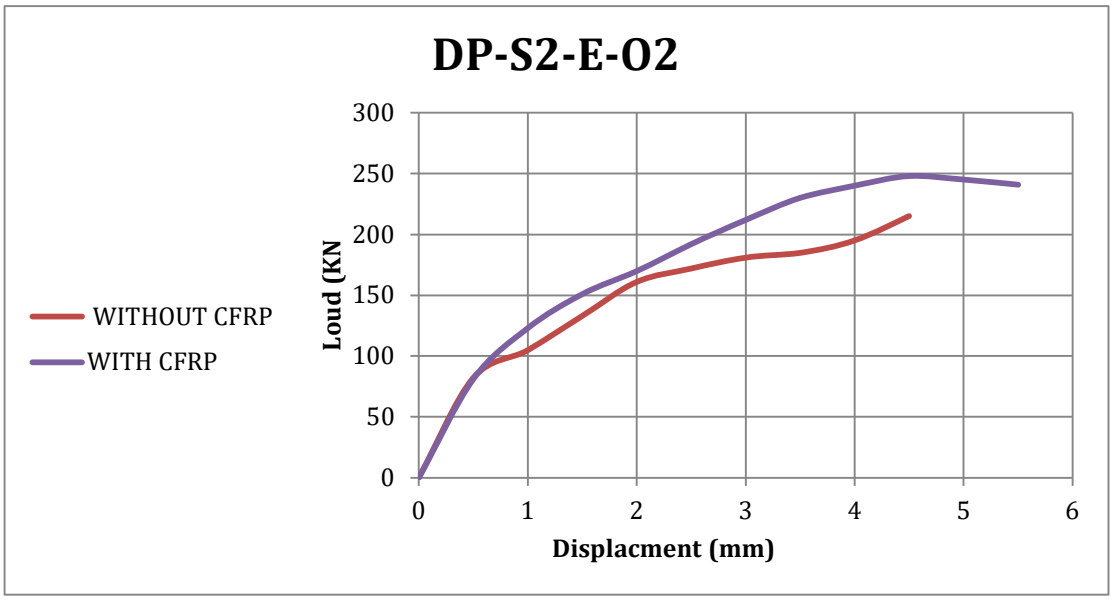


Figure 4. 21: Load–displacement curve of DP-S2-E-O2 before and after CFRP strengthening

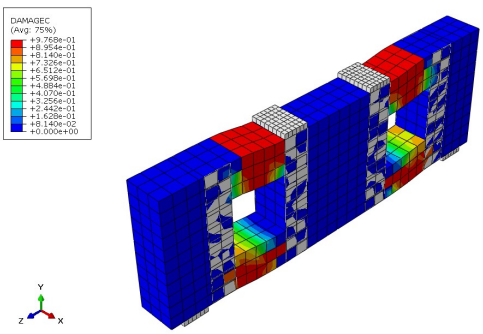

(a) compression damage contour

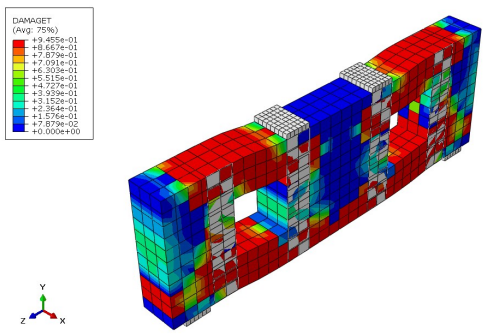

(b) tensile damage contour.

Figure 4. 22: Damage contours of specimen DP-S2-E-O2 after CFRP strengthening: (a) compression damage contour and (b) tensile damage contour.

### 4.6.4 Comparative Analysis of UHPC and CFRP Strengthening

#### *4.6.4.1 General Observation*

Both UHPC and CFRP improved beam response, but the numerical results show that their structural roles were different.

UHPC strengthened the disturbed concrete region and supported the compression field, whereas CFRP mainly provided external tensile restraint and crack control.

This distinction explains the larger strength and stiffness gains obtained with UHPC and the more moderate, post-cracking-oriented improvement obtained with CFRP.

#### *4.6.4.2 Comparison in Ultimate Load Capacity*

The comparison in ultimate load capacity shows a clear advantage for UHPC over CFRP in all selected specimens.

For DP-S2, UHPC increased the ultimate load from 612 kN to 761 kN (+24.34%), whereas CFRP increased it to about 685 kN (+11.9%).

For DP-S2-C-O2, UHPC increased the load from 210 kN to 268 kN (+27.62%), while CFRP increased it to about 240 kN (+14.3%).

For DP-S2-E-O2, UHPC increased the load from 215 kN to 282 kN (+31.16%), whereas CFRP increased it to about 248 kN (+15.35%).

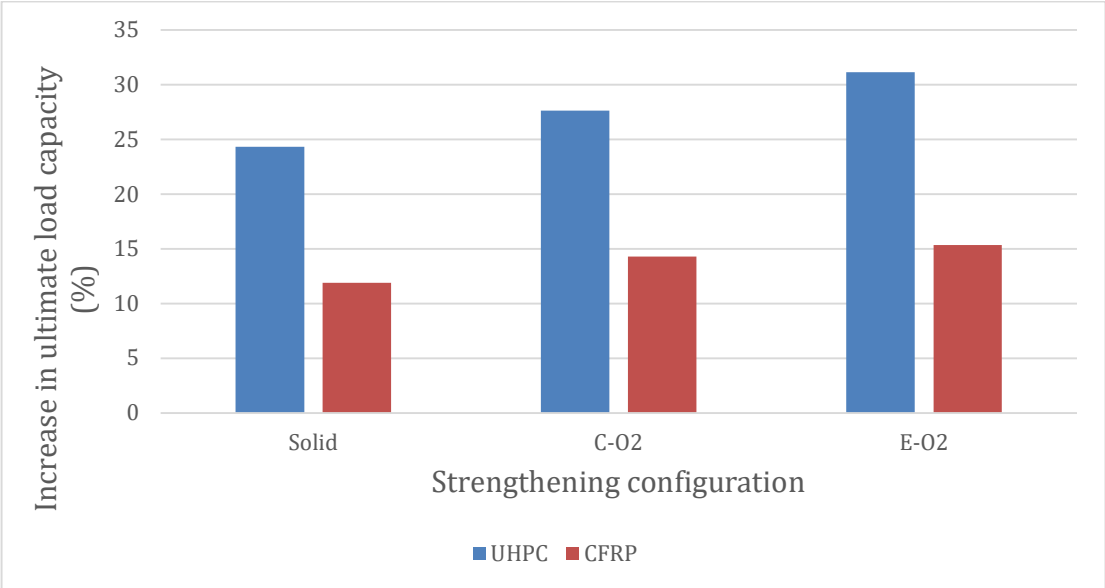


Figure 4. 23: Comparison of the increase in ultimate load capacity for deep beam specimens strengthened using UHPC and CFRP under selected configurations.

Figure 4.23 summarizes these percentage increases and confirms that UHPC consistently produced higher capacity gains than CFRP.

Mechanically, this difference reflects the ability of UHPC to improve both the compressive and tensile behavior of the disturbed region, while CFRP mainly improves crack restraint (Elghany et al., 2025; Al-Enezi et al., 2023).

#### *4.6.4.3 Comparison in Load–Displacement Response*

Figures 4.24-4.26 show that UHPC-strengthened beams had steeper initial slopes, higher peak loads, and more stable post-peak responses than the reference beams.

CFRP-strengthened beams showed a smaller increase in peak load and only limited stiffness enhancement, with curve shapes that remained closer to the reference response.

Therefore, the load-displacement results confirm that UHPC produced a stronger global enhancement, while CFRP mainly improved post-cracking behavior..

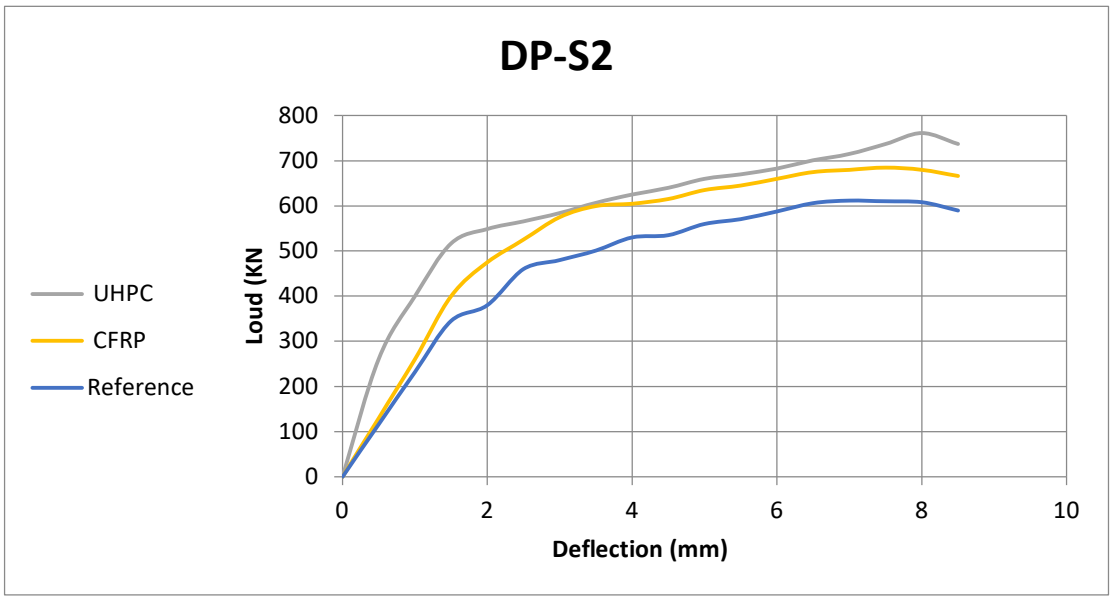


Figure 4. 24: Comparison of load–displacement curves for the reference, UHPC-strengthened, and CFRP-strengthened DP-S2 beam.

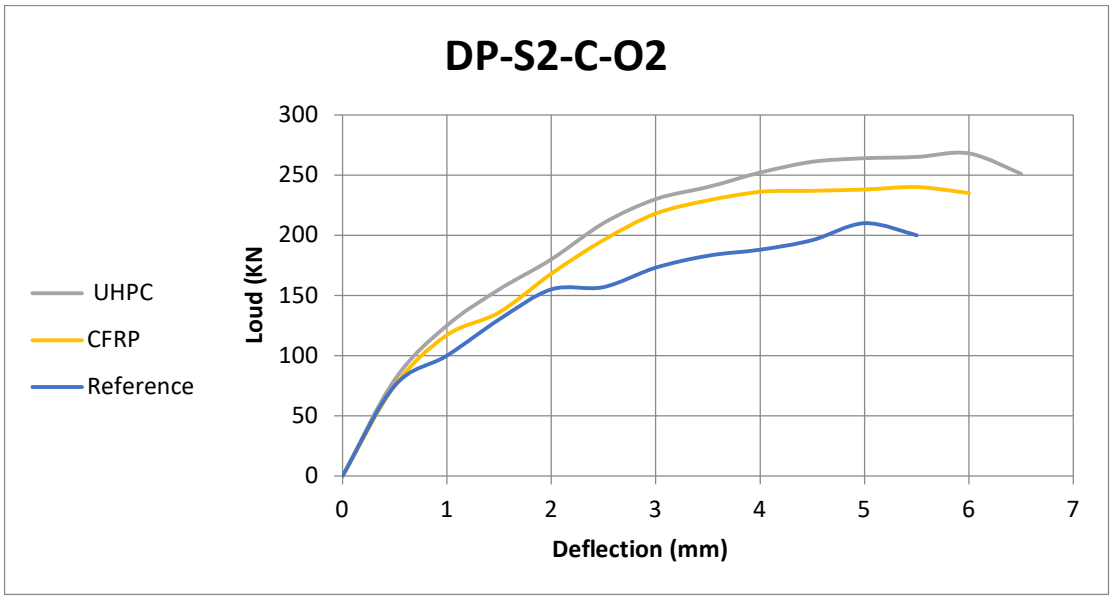


Figure 4. 25: Comparison of load–displacement curves for the reference, UHPC-strengthened, and CFRP-strengthened DP-S2-C-O2 beam.

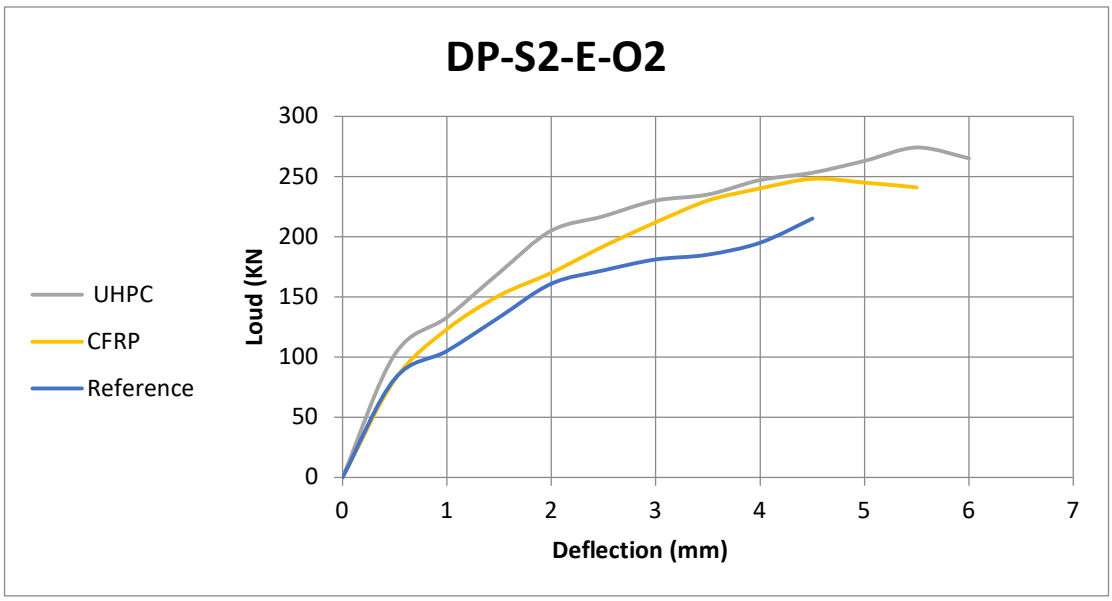


Figure 4. 26: Comparison of load–displacement curves for the reference, UHPC-strengthened, and CFRP-strengthened DP-S2-E-O2 beam.

#### *4.6.4.4 Comparison in Damage Distribution*

The difference between UHPC and CFRP strengthening becomes clearer when the damage contour distributions are examined.

As illustrated in **Figure 4.27** for the solid beam and **Figure 4.28** for the beam with opening, UHPC strengthening produced a more continuous and better-defined compression field, accompanied by a noticeable reduction in tensile damage within the critical regions.

In particular, the diagonal compression strut in the UHPC-strengthened specimens appeared more stable and less disturbed, indicating a more efficient load-transfer mechanism. This behavior reflects the ability of UHPC to improve both the compressive and tensile response of the disturbed zone.

In contrast, the CFRP-strengthened beams still showed localized tensile-damage concentration, especially near the opening corners, while the overall configuration of the compression field remained broadly similar to that of the unstrengthened beam. This indicates that CFRP mainly improved crack control and provided local tensile support, but had only a limited effect on restoring the continuity of the internal stress path.

Overall, the damage contours confirm that UHPC strengthening was more effective than CFRP in modifying the internal structural mechanism of the beam, whereas CFRP mainly improved the local crack response without substantially restoring the diagonal compression strut.

.

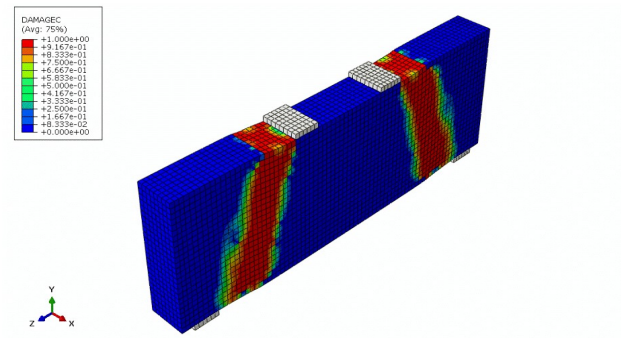

**(a)** Compression damage contour of DP-S2-reference

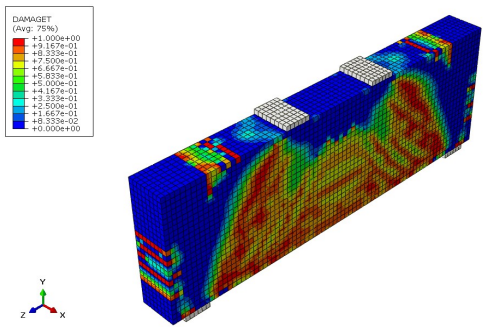

**(d)** Tensile damage contour of DP-S2-reference

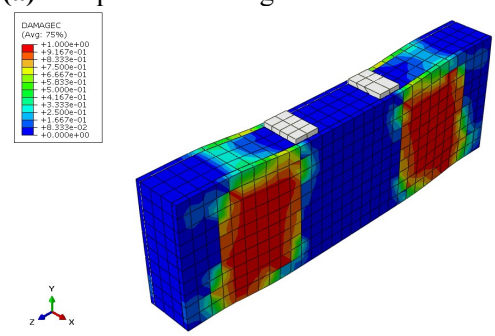

**(b)** Compression damage contour of DP-S2-UHPC

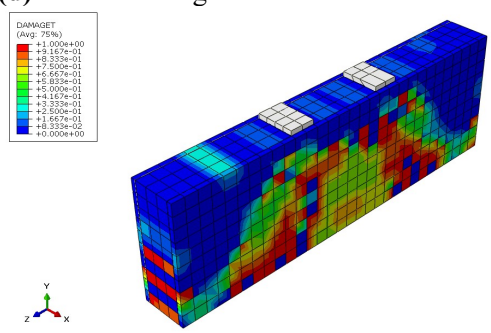

**(e)** Tensile damage contour of DP-S2-UHPC

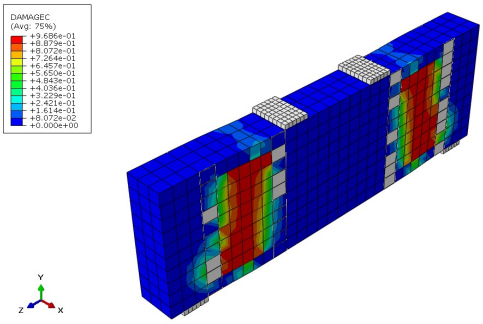

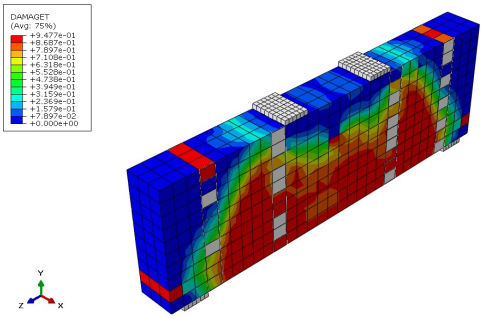

**(c)** Compression damage contour of DP-S2-CFRP **(f)** Tensile damage contour of DP-S2-CFRP

Figure 4. 27: Comparison of damage contours for specimen DP-S2: (a) compression damage contour of the reference beam, (b) compression damage contour after UHPC strengthening, (c) compression damage contour after CFRP strengthening, (d) tensile damage contour of the reference beam, (e) tensile damage contour after UHPC strengthening, and (f) tensile damage contour after CFRP strengthening.

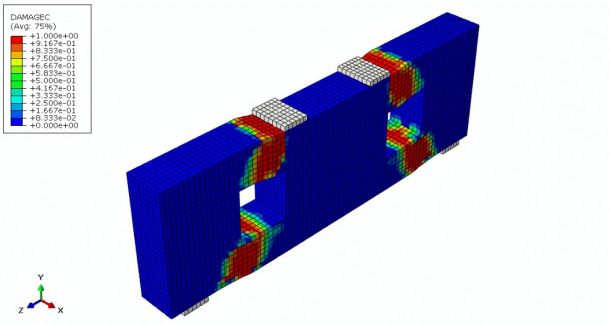

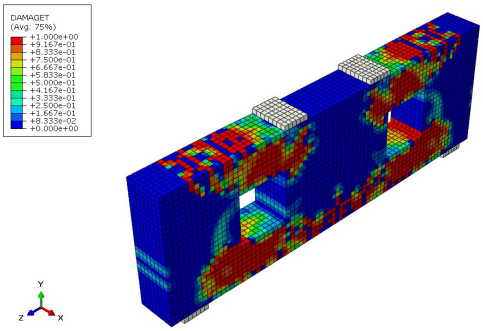

**(a)** Compression damage contour of DP-S2-E-O2-reference **(d)** Tensile damage contour of DP-S2-E-O2-reference

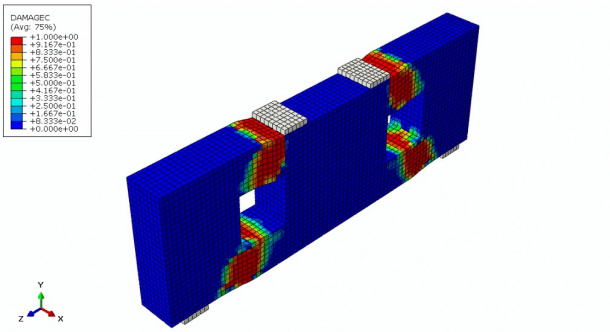

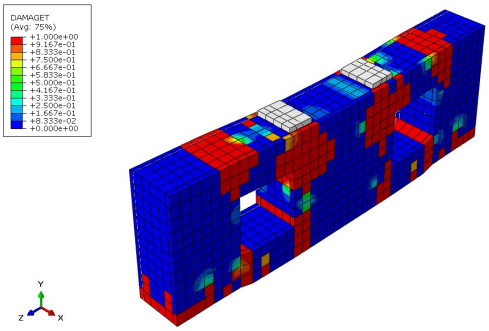

**(b)** Compression damage contour of DP-S2-E-O2-UHPC **(e)** Tensile damage contour of DP-S2-E-O2-UHPC

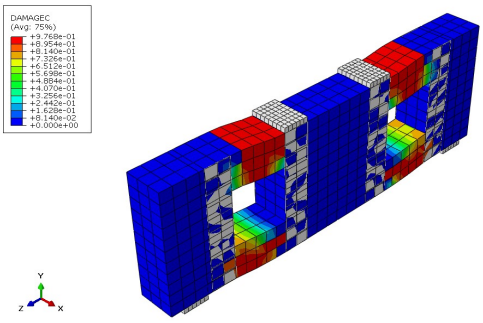

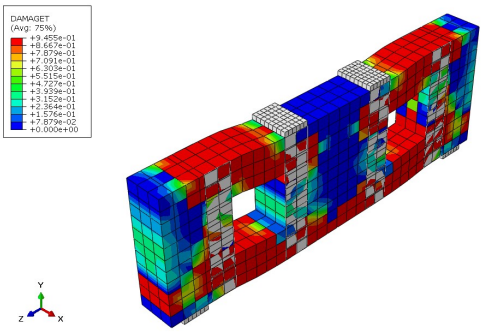

**(c)** Compression damage contour of DP-S2-E-O2-CFRP **(f)** Tensile damage contour of DP-S2-E-O2-CFRP

Figure 4. 28: Comparison of damage contours for specimen DP-S2-E-O2: (a) compression damage contour of the reference beam, (b) compression damage contour after UHPC strengthening, (c) compression damage contour after CFRP strengthening, (d) tensile damage contour of the reference beam, (e) tensile damage contour after UHPC strengthening, and (f) tensile damage contour after CFRP strengthening.

#### *4.6.4.5 Comparison in Ductility*

The difference between UHPC and CFRP strengthening can also be evaluated in terms of ductility. In the present study, ductility was quantified using the ratio between the ultimate displacement and the displacement corresponding to 75% of the ultimate load.

The results indicate that the ductility response did not follow a single uniform trend for all specimens. For the solid beam (DP-S2), UHPC strengthening increased the ductility index from approximately 2.92 for the reference beam to about 3.49, while CFRP strengthening resulted in a slightly lower value of about 3.14. This indicates that UHPC was more effective in improving both strength and deformation capacity in the solid beam.

For specimen DP-S2-E-O2, a similar trend was observed. The ductility index increased from about 2.49 for the reference beam to approximately 2.72 with UHPC strengthening, whereas CFRP strengthening resulted in a lower value of about 1.90. This suggests that UHPC was more effective in maintaining a stable post-peak response in cases where the compression field remained partially intact.

In contrast, for specimen DP-S2-C-O2, CFRP strengthening produced a slightly higher ductility index compared to UHPC. The ductility index increased from approximately 1.99 in the reference beam to about 2.50 with CFRP strengthening, whereas UHPC strengthening resulted in a lower value of approximately 2.12. This behavior can be attributed to the more severe disturbance of the compression field in centrally located openings, where CFRP provides more effective crack control and allows a more gradual post-peak response.

Overall, the results indicate that the influence of UHPC and CFRP on ductility is case-dependent and governed by the condition of the internal load-transfer mechanism. UHPC generally provides higher strength and stiffness, and in many cases improves ductility, while CFRP may offer better post-cracking deformation capacity in certain configurations due to its role in controlling crack propagation.

| Specimen | Reference | UHPC | CFRP |
|---|---|---|---|
| DP-S2 | 2.92 | 3.49 | 3.14 |
| DP-S2-C-O2 | 1.99 | 2.12 | 2.50 |
| DP-S2-E-O2 | 2.49 | 2.72 | 1.90 |

Table 4. 5: Comparison of ductility index

#### *4.6.4.6 Structural Interpretation*

From a structural mechanics perspective, the observed differences between UHPC and CFRP strengthening can be explained by the way each technique interacts with the internal load-transfer mechanism of the beam.

UHPC modifies the structural response by improving the material properties within the disturbed region itself. As a result, it enhances both the compressive and tensile behavior of the strengthened zone and contributes to restoring the continuity of the diagonal compression strut. This leads to a more efficient internal load-transfer path, higher stiffness, and a greater increase in ultimate load capacity.

In contrast, CFRP acts mainly as an external strengthening system that improves crack control, reduces tensile damage, and enhances local confinement. Although it limits crack propagation and improves the post-cracking response, it does not significantly modify the geometry or continuity of the internal compression field. Therefore, its structural contribution remains more limited than that of UHPC when the original load path has been severely disturbed.

These observations are consistent with the damage contours and load–displacement responses discussed earlier, which showed that UHPC was more effective in restoring the compression field, whereas CFRP mainly improved the local tensile response.

#### *4.6.4.7 Overall Comparison and Engineering Insight*

Overall, UHPC was the more effective technique for improving ultimate load, stiffness, and damage stability.

Its advantage was clearest in edge-opening configurations, where the remaining compression field could be strengthened more efficiently.

CFRP provided useful but more moderate enhancement and is more suitable when the main objective is crack control or when external retrofit is preferred.

Accordingly, UHPC is recommended when major recovery of the load-transfer mechanism is required, while CFRP remains a practical option for crack-control-oriented strengthening.

## 4.7 Effect of Transverse Reinforcement Ratio($A_v/s$)

### 4.7.1 General

The effect of transverse reinforcement was examined by increasing stirrup diameter while keeping spacing constant, giving Av/s values of approximately 0.65, 1.20, and 1.80 mm2/mm.

The results showed a diminishing-return trend: increasing Av/s enhanced shear resistance and post-cracking stability, but the incremental benefit became smaller at higher reinforcement levels.

### 4.7.2 Solid Beam DP-S2

For the solid beam DP-S2, the ultimate load increased from 612 kN to 724 kN when $A_v/s$increased from 0.65 to 1.20mm2/mm, corresponding to an improvement of approximately 18.3%.

When $A_v/s$was further increased to 1.80, the ultimate load reached 757 kN, which represents an additional increase of about 4.6% relative to the intermediate case and about 23.7% relative to the reference specimen, as shown in **Figure 4.29**.

The load–displacement curves in **Figure 4.29** show that increasing $A_v/s$ improved both the peak load and the ability of the beam to sustain load after cracking. This indicates that transverse reinforcement contributed not only to increasing shear resistance, but also to improving post-cracking stability.

The corresponding damage contours, shown in **Figure 4.30**, indicate a gradual reduction in diagonal tensile-damage intensity as $A_v/s$ increased. This reflects the role of transverse reinforcement in improving crack restraint and reducing the severity of diagonal tension cracking.

These observations show that transverse reinforcement is most effective when the beam is initially deficient in shear reinforcement; after adequate crack control is achieved, additional stirrups provide smaller proportional gains).

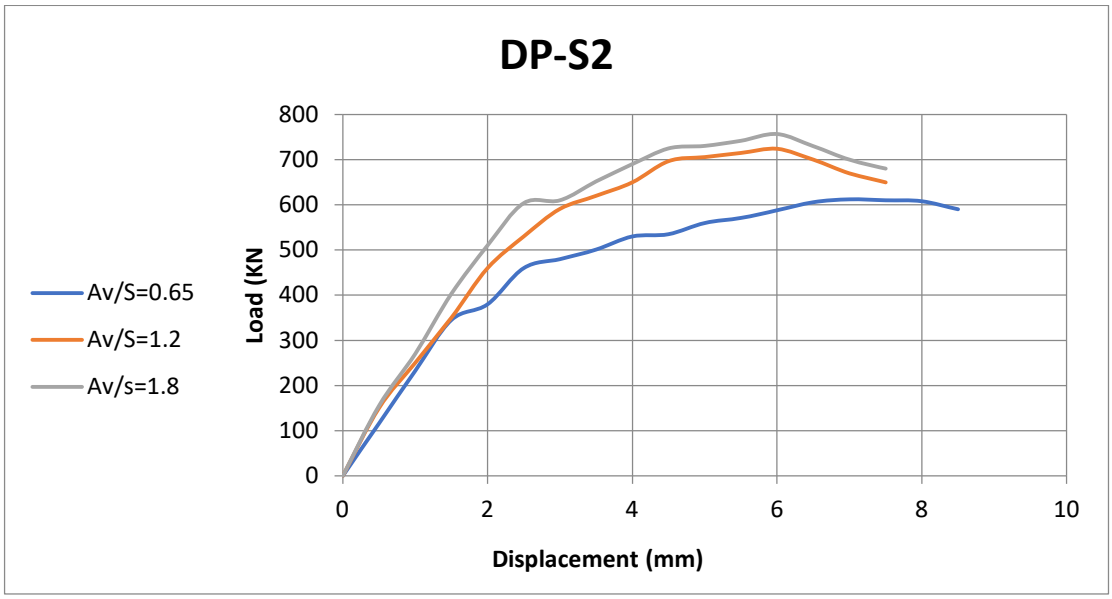


Figure 4 .29: Load-displacement curves for DP-S2 at different transverse reinforcement ratios.

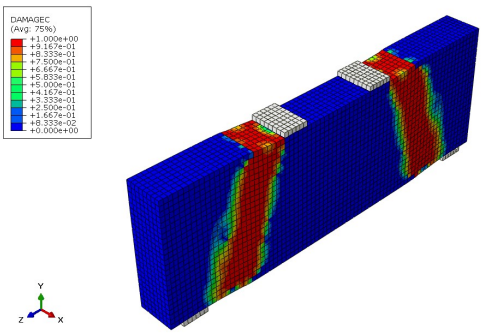

**(a)** Compression damage contour of DP-S2 at $A_v/s = 0.65$

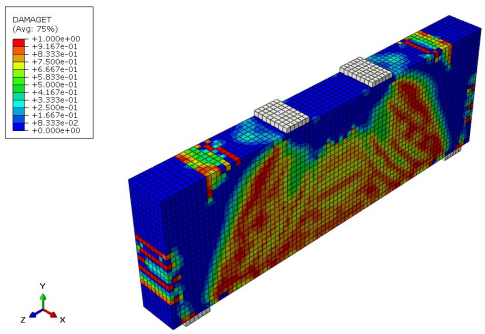

**(b)** Tensile damage contour of DP-S2 at $A_v/s = 0.65$

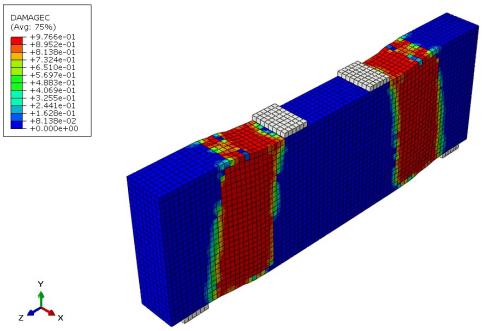

**(c)** Compression damage contour of DP-S2 at $A_v/s = 1.20$

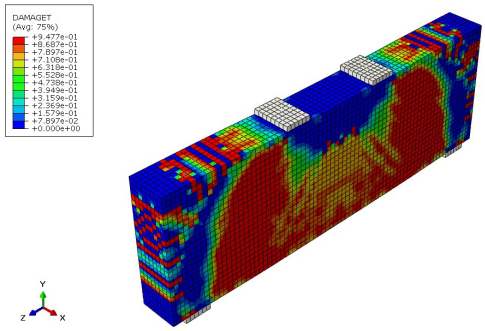

**(d)** Tensile damage contour of DP-S2 at $A_v/s = 1.20$

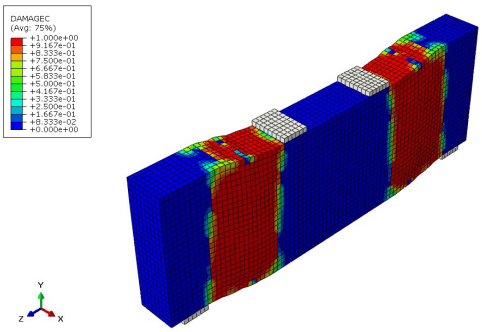

**(e)** Compression damage contour of DP-S2 at $A_v/s = 1.80$

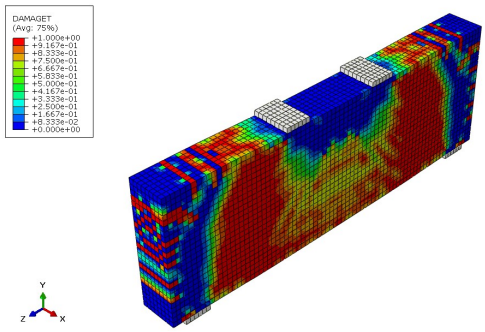

**(f)** Tensile damage contour of DP-S2 at $A_v/s = 1.80$

Figure 4. 30: Damage contours of specimen DP-S2 at different transverse reinforcement ratios: (a) compression damage contour at $A_v/s = 0.65$, (b) tensile damage contour at $A_v/s = 0.65$, (c) compression damage contour at $A_v/s = 1.20$, (d) tensile damage contour at $A_v/s = 1.20$, (e) compression damage contour at $A_v/s = 1.80$, and (f) tensile damage contour at $A_v/s = 1.80$.

### 4.7.3 Beams with Openings

For the beams with openings, the predicted ultimate loads also increased as the transverse reinforcement ratio increased. The numerical results were as follows:

DP-S2-C-O1: 230 → 279 → 290 KN

DP-S2-C-O2: 210 → 250 → 261 KN

DP-S2-E-O1: 212 → 258 → 268 KN

DP-S2-E-O2: 200 → 240 → 250 KN

These results correspond to total increases of approximately 26.1%, 24.3%, 26.4%, and 25.0%, respectively, when $A_v/s$increased from 0.65 to 1.80. In all perforated beams, most of the improvement occurred with the first increase in $A_v/s$, while the second increase produced only a limited additional gain, typically on the order of about 4%, the numerical results are summarized in **Table 4.6**

| Beam | 0.65 | 1.2 | 1.8 |
|---|---|---|---|
| DP-S2-C-O1 | 230 | 279 | 290 |

| | | | |
|---|---|---|---|
| DP-S2-C-O2 | 210 | 250 | 261 |
| DP-S2-E-O1 | 212 | 258 | 268 |
| DP-S2-E-O2 | 200 | 240 | 250 |

Table 4 .6 : Comparison of ultimate load at different $\boldsymbol{A_v/s}$values for all S2 beams with openings.

The load–displacement curves shown in **Figures 4.31–4.34** indicate that increasing $A_v/s$ improved both the ultimate load capacity and the post-cracking stability of all beams with openings.

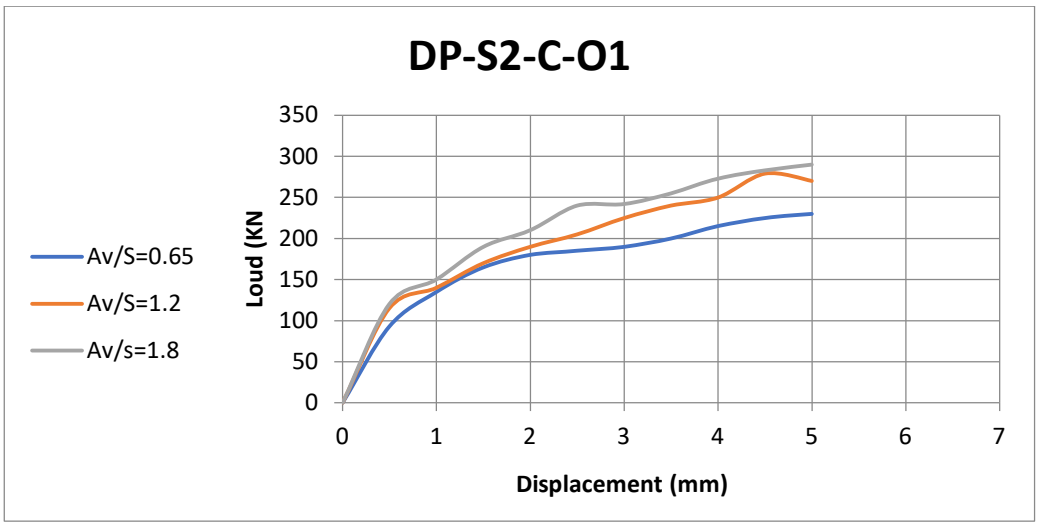


Figure 4. 31: Load-displacement curves for DP-S2-C-O1 at different transverse reinforcement ratios

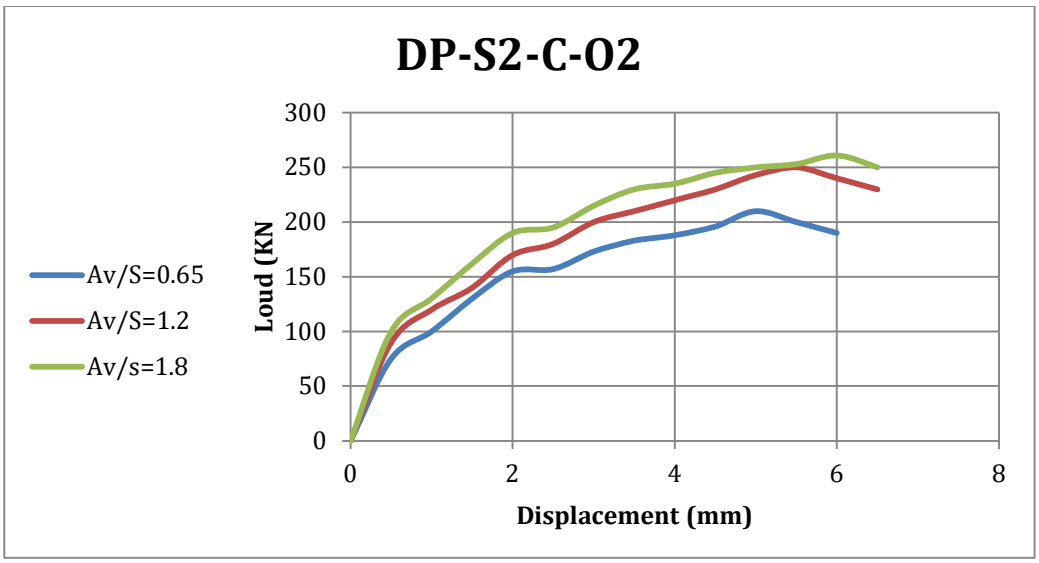


Figure 4. 32: Load-displacement curves for DP-S2-C-O2 at different transverse reinforcement ratios.

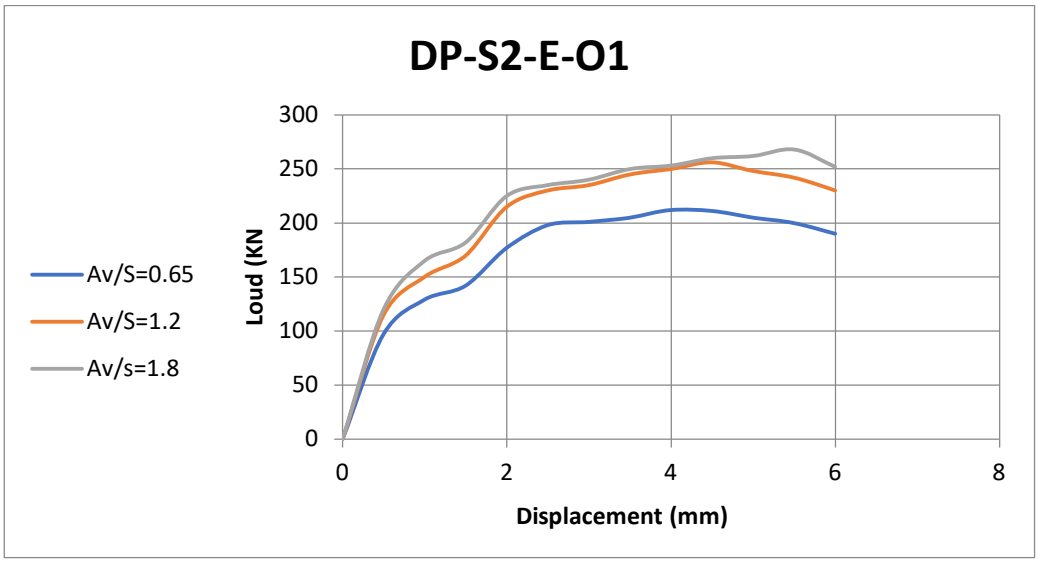


Figure 4. 33: Load-displacement curves for DP-S2-E-O1 at different transverse reinforcement ratios.

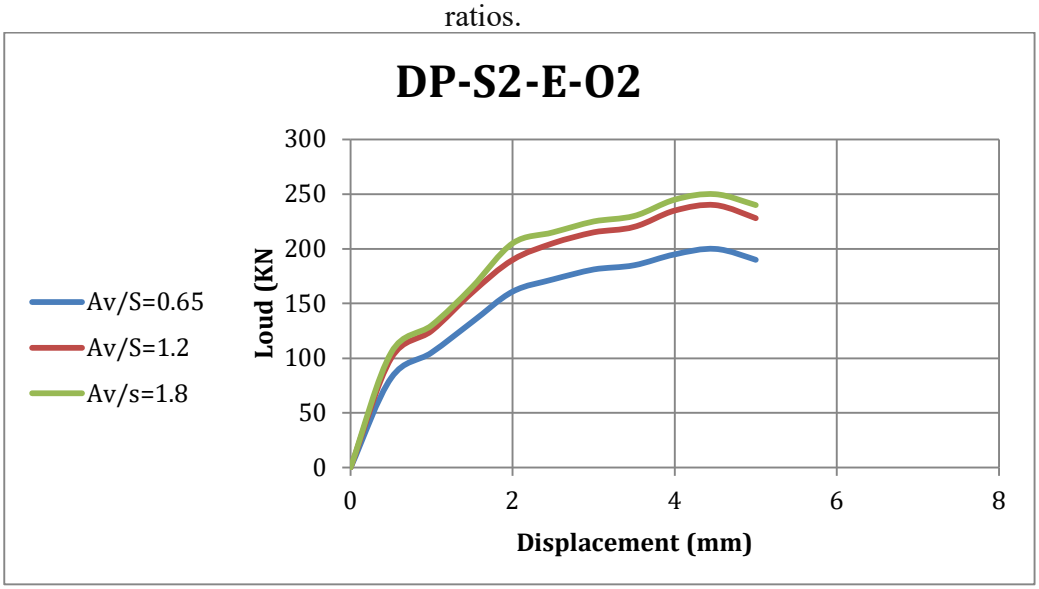


Figure 4. 34: Load-displacement curves for DP-S2-E-O2 at different transverse reinforcement ratios

Although increasing Av/s improved all beams with openings, it could not fully compensate for the opening-induced disturbance of the load path.

This agrees with previous studies showing that transverse reinforcement improves crack control and shear resistance but becomes less effective when the internal force path is strongly interrupted (Tan et al., 1997; Liu & Mihaylov, 2016; Ma et al., 2022).

### 4.7.4 Damage Contours for Beams with Openings

The damage contours for opened beams illustrate how transverse reinforcement affected crack development around the openings.

Increasing Av/s reduced tensile-damage concentration and improved diagonal crack control near the opening boundaries.

For the central-opening beam, damage still remained concentrated near the opening corners, indicating that the opening continued to govern the force-transfer mechanism.

Figure 4.35 shows that the first increase in Av/s produced the clearest reduction in crack localization, while the second increase produced only limited additional improvement.

Overall, the contours confirm that transverse reinforcement improves crack control but does not fully recover the load-transfer efficiency lost because of the opening.

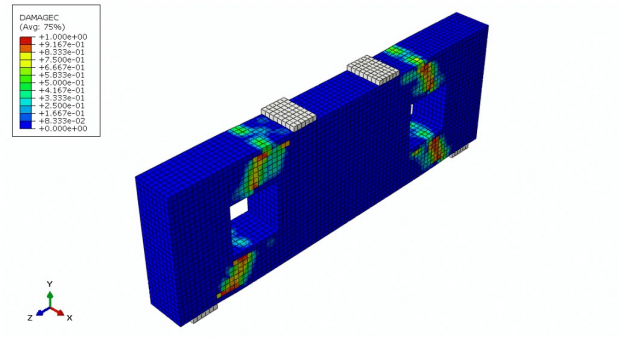

**(a)** Compression damage contour at $A_v/s = 0.65$

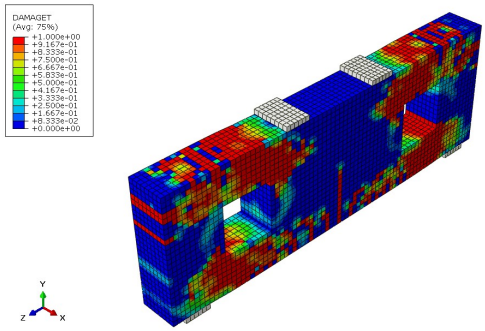

**(b)** Tensile damage contour at $A_v/s = 0.65$

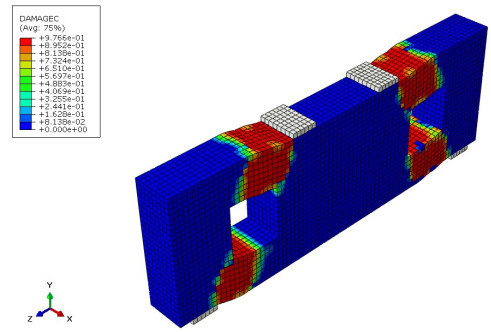

**(c)** Compression damage contour at $A_v/s = 1.20$

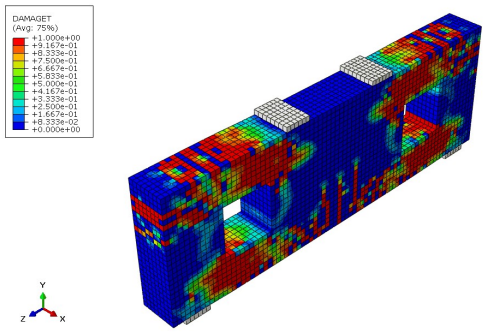

**(d)** Tensile damage contour at $A_v/s = 1.20$

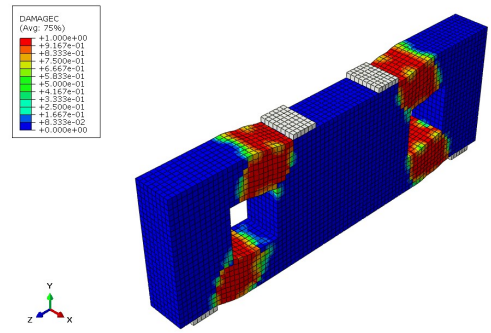

**(e)** Compression damage contour at $A_v/s = 1.80$

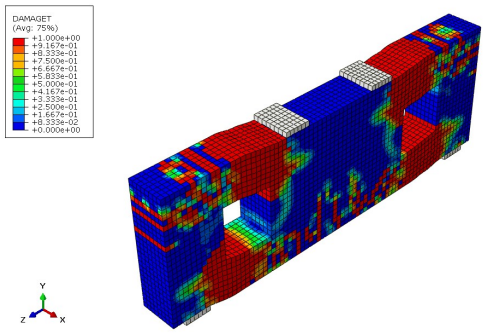

**(f)** Tensile damage contour at $A_v/s = 1.80$

Figure 4. 35: Damage contours of specimen DP-S2-C-O1 at different transverse reinforcement ratios: (a–b) $A_v/s = 0.65$, (c–d) $A_v/s = 1.20$, and (e–f) $A_v/s = 1.80$.

## 4.8 Effect of Concrete Compressive Strength($f'_c$)

### 4.8.1 General Trend

When compared to the effect of transverse reinforcement ratio, the changes in concrete compressive strength had a greater and more immediate impact. This corresponds to the cracking that seems to have started later as a result of an increased Fc', according to the first-cracking results in Section 4.4. Such a situation is perfectly in line with the idea of deep beams, where the main way of load transfer is almost entirely through the diagonal concrete compression strut. Since this compressive action is pretty much determined by concrete, a higher Fc' will, in fact, enhance the beam's capacity to withhold higher compressive stresses, maintain the strut's soundness, and postpone the crushing of the critical load path.

### 4.8.2 Solid Beam DP-S2

For the solid beam DP-S2, the influence of concrete compressive strength was clear and significant. Increasing $f'_c$ from 30 MPa to 40 MPa increased the ultimate load from approximately 655 kN to 730 kN, corresponding to an increase of about 11.5%. When $f'_c$ was further increased to 50 MPa, the ultimate load reached approximately 825 kN, representing an additional increase of about 13.0% relative to the 40 MPa case and a total increase of about 26.0% relative to the 30 MPa case, as shown in **Figure 4.36**.

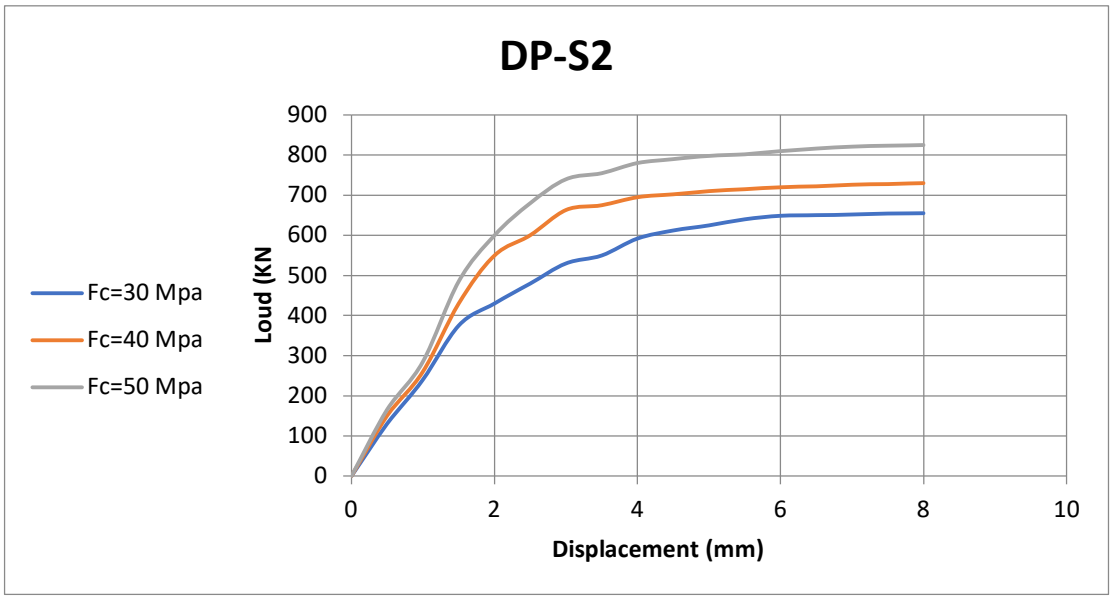


Figure 4. 36: Effect of concrete compressive strength on the load–displacement response of specimen DP-S2.

The load-displacement curves indicate that increasing f'c improved both ultimate capacity and stiffness because the solid beam transferred load through a relatively uninterrupted compression field.

The corresponding damage contours provide further evidence of this effect. As shown in Figure 4.37, increasing f'c resulted in a more stable and concentrated diagonal compression strut, with less severe compression damage in the critical load-transfer zone.

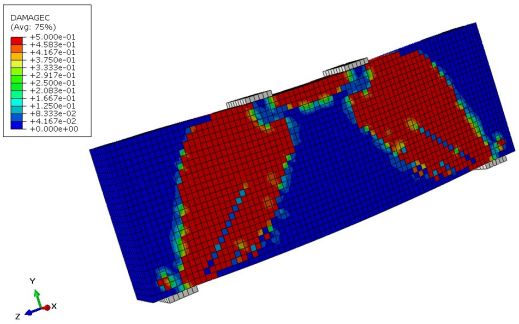

**(a)** Compression damage contour of DP-S2 at $f_c' =$ 30MPa

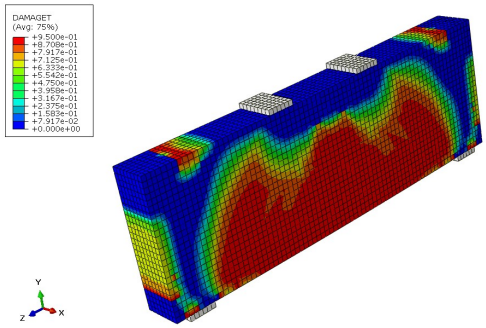

**(b)** Tensile damage contour of DP-S2 at $f_c' = 30$MPa

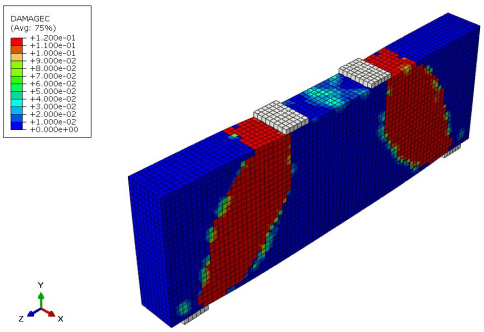

**(c)** Compression damage contour of DP-S2 at $f_c' =$ 40MPa

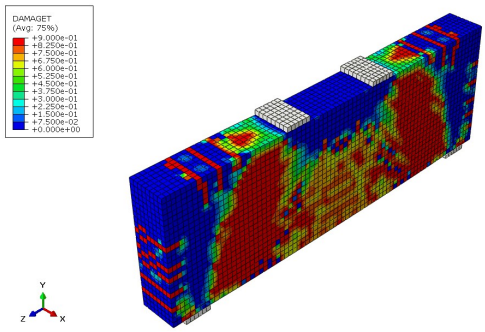

**(d)** Tensile damage contour of DP-S2 at $f_c' = 40$MPa

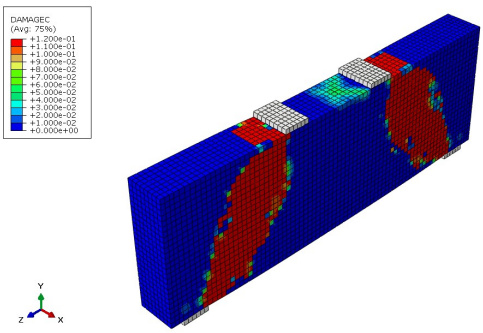

**(e)** Compression damage contour of DP-S2 at $f_c' =$ 50MPa

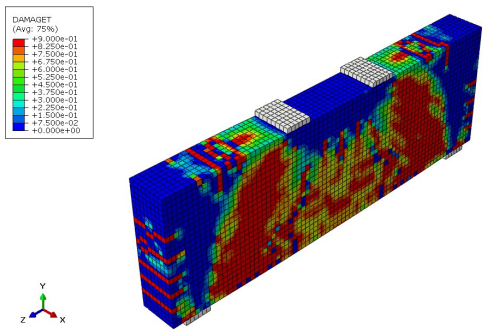

**(f)** Tensile damage contour of DP-S2 at $f_c' = 50$MPa

Figure 4. 37: Damage contours of specimen DP-S2 at different concrete compressive strengths: (a–b) $\boldsymbol{f_c' = 30}$MPa, (c–d) $\boldsymbol{f_c' = 40}$MPa, and (e–f) $\boldsymbol{f_c' = 50}$MPa.

These observations are consistent with previous studies, which reported that increasing concrete compressive strength significantly improves the shear resistance and structural stability of deep beams

by enhancing the efficiency of the diagonal compression field (Tan et al., 1995; Liu & Mihaylov, 2016; Chen et al., 2022).

### 4.8.3 Beam with Opening DP-S2-C-O1

For beam DP-S2-C-O1, the effect of concrete compressive strength was also clearly positive. Increasing $f_c'$ from 30 MPa to 40 MPa increased the ultimate load from about 263 kN to 285 kN, corresponding to an increase of approximately 8.4%. When $f_c'$ was further increased to 50 MPa, the ultimate load reached about 320 kN, representing an additional increase of about 12.3% relative to the 40 MPa case and about 21.7% relative to the 30 MPa case, as shown in **Figure 4.38**.

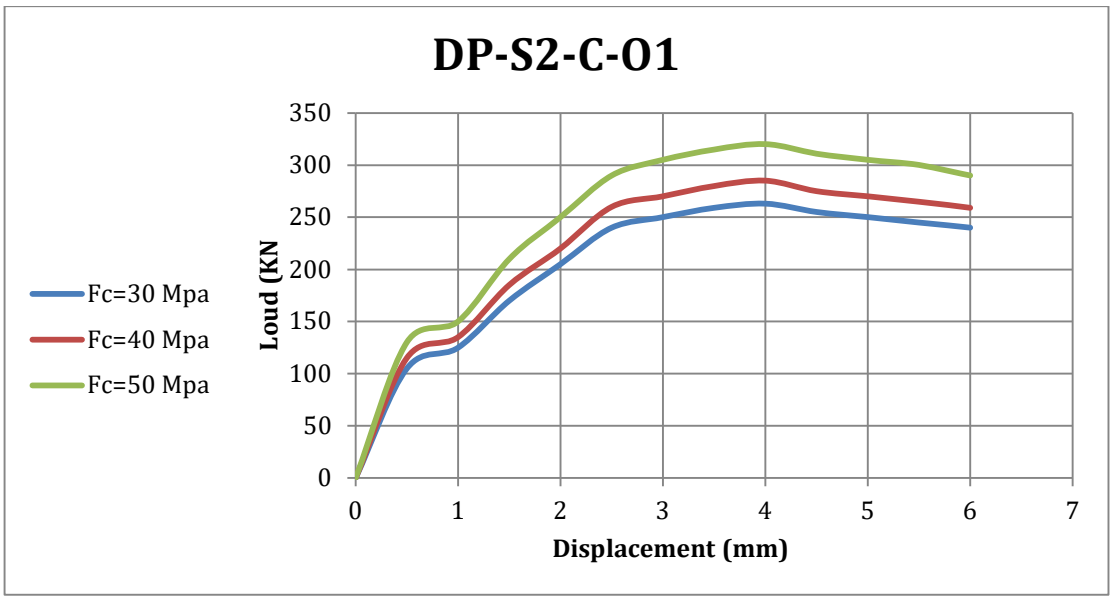


Figure 4. 38: Effect of concrete compressive strength on the load–displacement response of specimen DP-S2-C-O1.

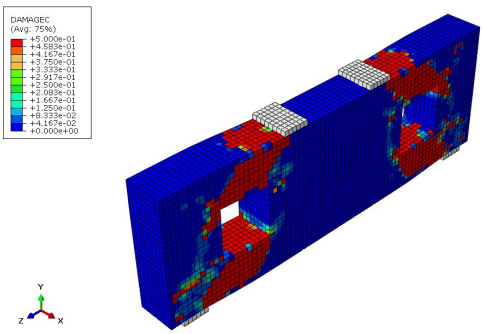

**(a)** Compression damage contour of DP-S2 at $f_c' =$ 30MPa

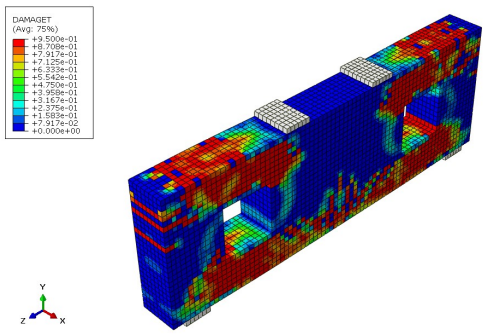

**(b)** Tensile damage contour of DP-S2 at $f_c' =$ 30MPa

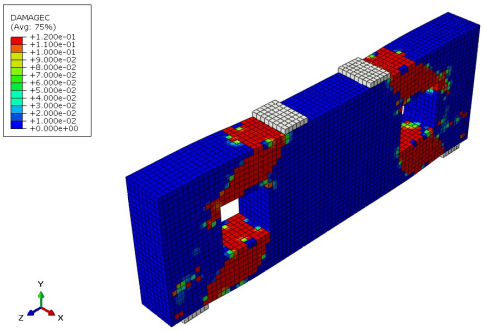


**(c)** Compression damage contour of DP-S2 at $f_c' =$ 40MPa

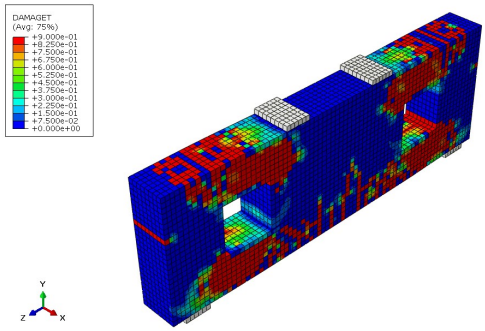


**(d)** Tensile damage contour of DP-S2 at $f_c' = 40$MPa

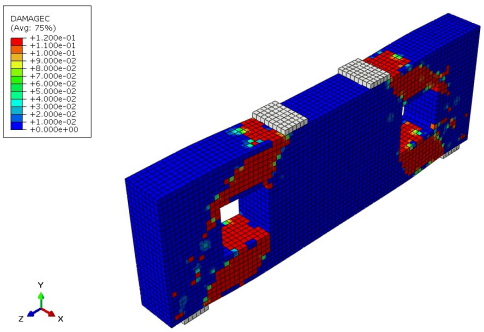


**(e)** Compression damage contour of DP-S2 at $f_c' =$ 50MPa

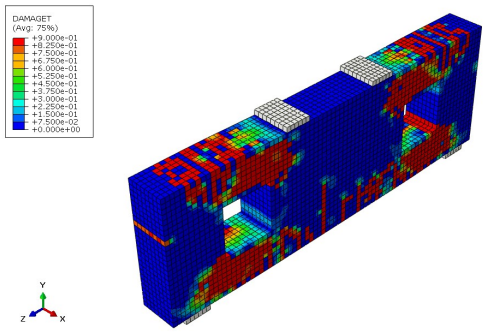


**(f)** Tensile damage contour of DP-S2 at $f_c' = 50$MPa

Figure 4. 39: Damage contours of specimen DP-S2-C-O1 at different concrete compressive strengths: (a–b) $\boldsymbol{f_c' = 30}$MPa, (c–d) $\boldsymbol{f_c' = 40}$MPa, and (e–f) $\boldsymbol{f_c' = 50}$MPa.

The load-displacement response indicates that increasing f'c improved ultimate capacity and stability, although the gain was lower than in the solid beam because the opening interrupted the compression path.

Figure 4.39 shows that lower f'c values caused stronger stress concentration around the opening, while higher f'c improved the resistance of the surrounding concrete and partially recovered the disturbed force path (Yang et al., 2006; Chen et al., 2022).

## 4.9 Effect of Reinforcement Yield Strength (fy)

### 4.9.1 General Trend

The influence of reinforcement yield strength was more limited than that of transverse reinforcement ratio and concrete compressive strength.

Although higher fy improves steel tensile resistance and may delay local yielding, it does not significantly change the main compression-field mechanism.

This explains why its effect on deep-beam capacity was modest compared with parameters that directly affect the compression field (Liu & Mihaylov, 2016; Ma et al., 2022).

### 4.9.2 Numerical Results for DP-S2

For the solid beam DP-S2, the numerical ultimate loads corresponding to different reinforcement yield strengths were approximately as follows:

420 MPa -> 600 KN

500 MPa -> 610 KN

570 MPa -> 630 KN

620 MPa -> 650 KN

These results indicate that increasing $f_y$ from 420 MPa to 620 MPa increased the ultimate load capacity by only about 8.3%. The increase was therefore gradual and relatively limited despite the substantial increase in reinforcement yield strength, as shown in **Figure 4.40**. This confirms that the global resistance of the deep beam was not strongly governed by reinforcement yielding.

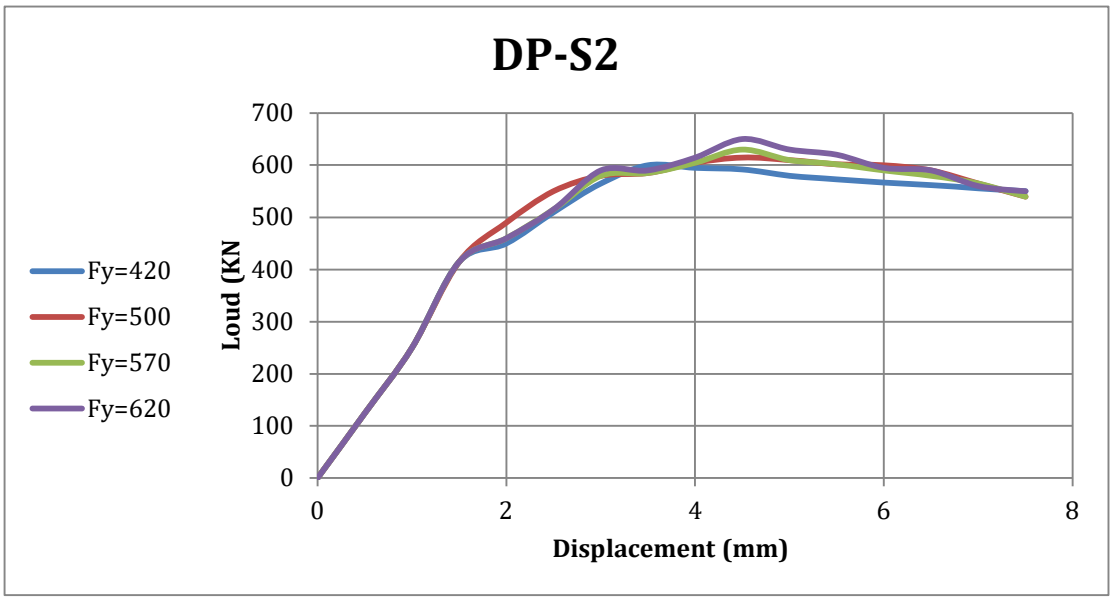


Figure 4. 40: Effect of reinforcement yield strength on the load–displacement response of specimen DP-S2.

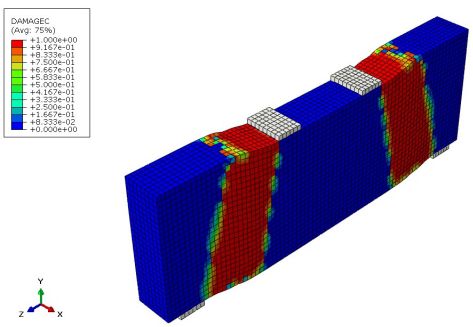

**(a)** Compression damage contour of DP-S2 at $f_y = 420\text{MPa}$

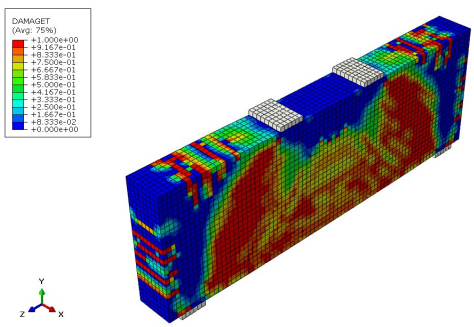

**(b)** Tensile damage contour of DP-S2 at $f_y = 420\text{MPa}$

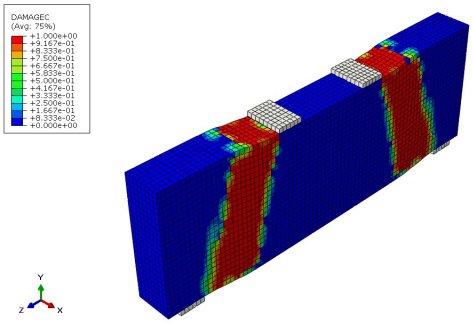

**(c)** Compression damage contour of DP-S2 at $f_y = 500$MPa

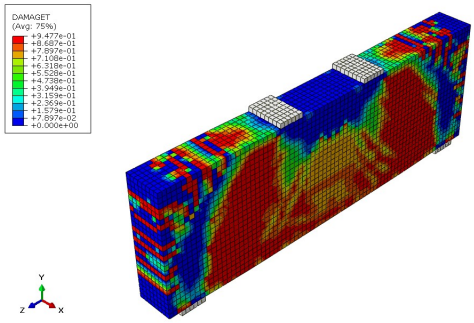

**(d)** Tensile damage contour of DP-S2 at $f_y = 500$MPa

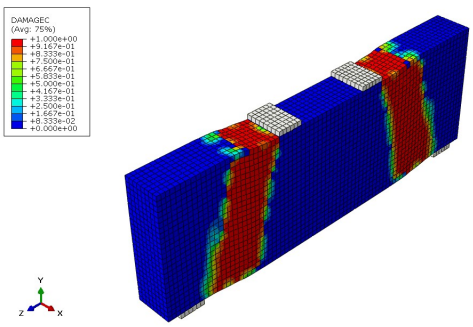

**(e)**Compression damage contour of DP-S2 at $f_y = 570$MPa

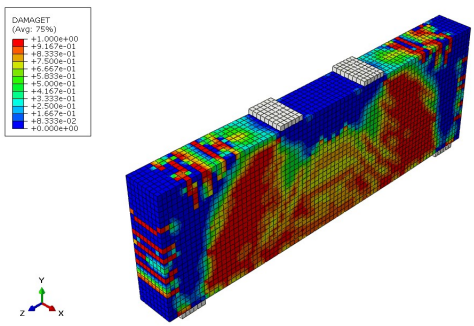

**(f)** Tensile damage contour of DP-S2 at $f_y = 570$MPa

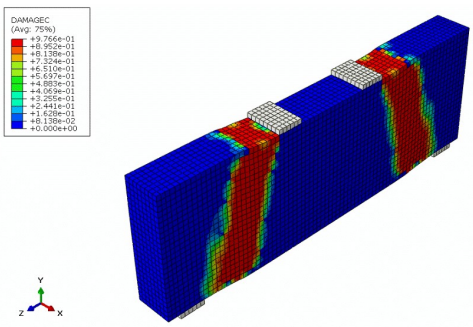

**(g)**Compression damage contour of DP-S2 at $f_y = 620$MPa

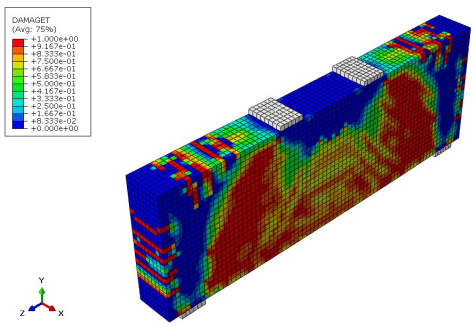

**(h)** Tensile damage contour of DP-S2 at $f_y = 620$MPa

Figure 4. 41: Damage contours of specimen DP-S2 at different reinforcement yield strengths: (a–b) $f_y = 420$MPa, (c–d) $f_y = 500$MPa, (e–f) $f_y = 570$MPa, and (g–h) $f_y = 620$MPa.

The load-displacement curves show only minor changes in initial stiffness; the benefit of higher fy appeared mainly near the ultimate stage, where reinforcement could sustain larger tensile stresses.

This agrees with Liu and Mihaylov (2016) and Ma et al. (2022), who reported that increasing reinforcement strength gives limited gains once adequate tie capacity is available.

Figure 4.41 confirms this interpretation, as the compression-strut geometry remained almost unchanged while crack control improved slightly in the tension-tie regions.

### 4.9.3 Effect of Reinforcement Yield Strength on Beam DP-S2-C-O1

For the beam with a central opening, DP-S2-C-O1, increasing reinforcement yield strength (fy) produced only modest improvement compared with concrete compressive strength and transverse

reinforcement ratio. The ultimate load increased from about 202 kN at fy = 420 MPa to about 210 kN at fy = 500 MPa, then to 213 kN at fy = 570 MPa, and finally to 218 kN at fy = 620 MPa. This corresponds to a total increase of about 7.9%, as shown in Figure 4.42.

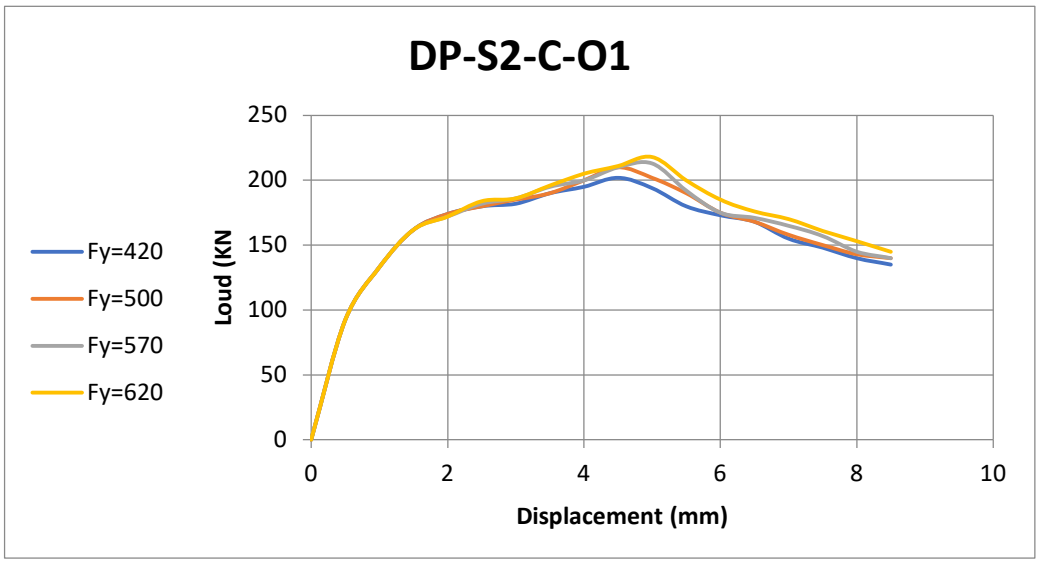


Figure 4. 42: Effect of reinforcement yield strength on the load–displacement response of specimen DP-S2-C-O1.

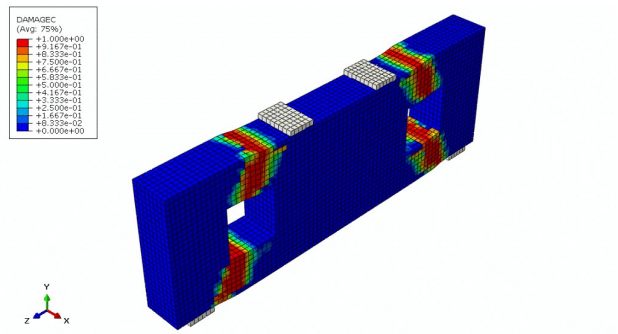

**(a)** Compression damage contour of DP-S2-C-O1 at $f_y = 420$MPa

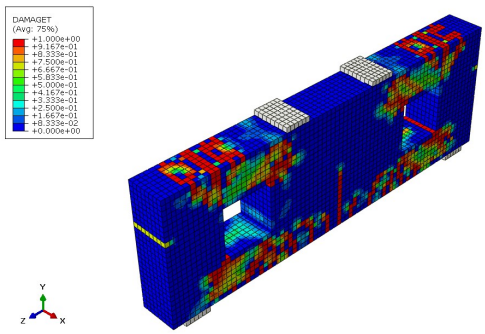

**(b)** Tensile damage contour of DP-S2-C-O1 at $f_y = 420$MPa

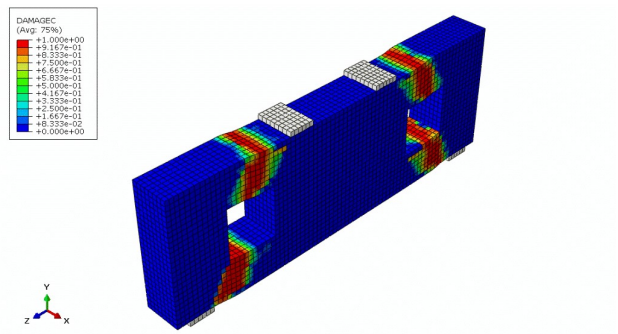

**(c)** Compression damage contour of DP-S2-C-O1 at $f_y = 500$MPa

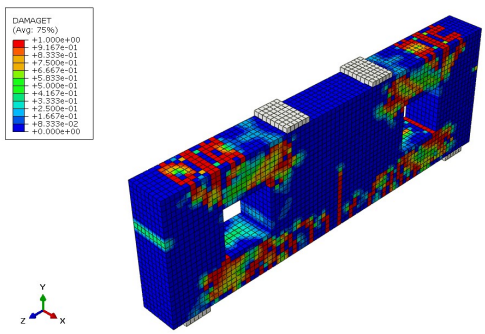

**(d)** Tensile damage contour of DP-S2-C-O1 at $f_y = 500$MPa

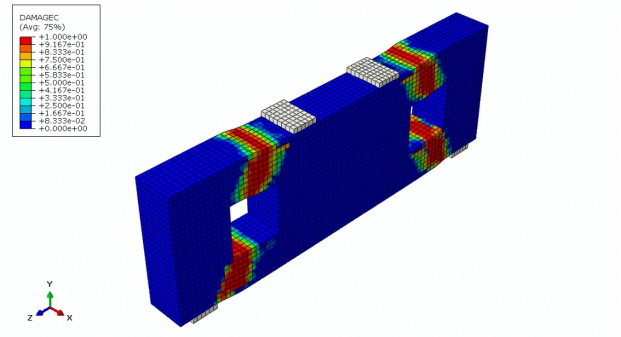

**(e)** Compression damage contour of DP-S2-C-O1 at $f_y = 570\text{MPa}$

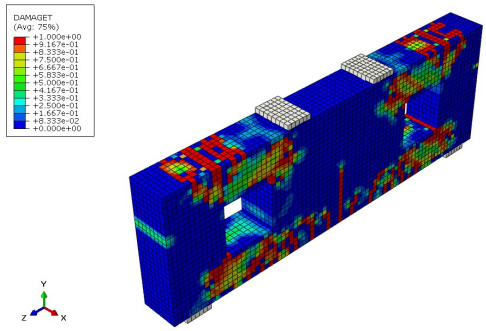

**(f)** Tensile damage contour of DP-S2-C-O1 at $f_y = 570\text{MPa}$

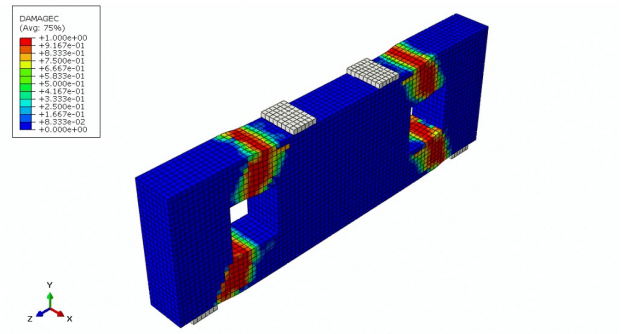

**(g)** Compression damage contour of DP-S2-C-O1 at $f_y = 620\text{MPa}$

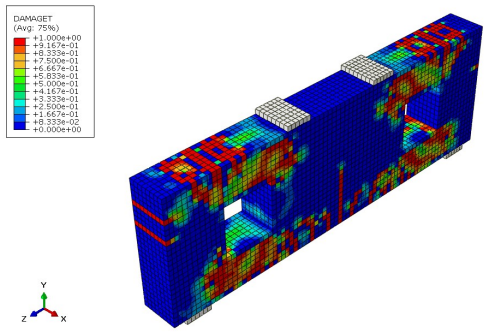

**(h)** Tensile damage contour of DP-S2-C-O1 at $f_y = 620\text{MPa}$

Figure 4. 43: Damage contours of specimen DP-S2-C-O1 at different reinforcement yield strengths: (a–b) $f_y = 420\text{MPa}$, (c–d) $f_y = 500\text{MPa}$, (e–f) $f_y = 570\text{MPa}$, and (g–h) $f_y = 620\text{MPa}$.

These results indicate that higher fy slightly improved tensile resistance and crack control, but the opening continued to govern the response by disturbing the main compression field.

The improvement was therefore insufficient to compensate for the loss of structural efficiency caused by the interrupted web.

At later stages, higher-yield reinforcement sustained greater tensile forces around the opening, producing a small increase in ultimate load and deformation resistance.

This trend is consistent with previous studies showing that reinforcement strength has limited influence when deep-beam response is controlled by the diagonal compression strut (Liu & Mihaylov, 2016; Ma et al., 2022).

Figure 4.43 further shows that increasing fy did not fundamentally modify the compression-strut trajectory around the opening; the main observable effect was slightly improved crack restraint near the opening corners.

### 4.9.4 Comparison with Concrete Compressive Strength

For DP-S2, increasing fy from 420 MPa to 620 MPa increased ultimate load by about 8.3%, whereas increasing f'c from 30 MPa to 50 MPa increased it by about 26.0%.

This comparison shows that deep-beam performance was governed more strongly by the concrete compression field than by the yield strength of the longitudinal reinforcement.

Together with Sections 4.7 and 4.8, this establishes the following order of influence: concrete compressive strength first, transverse reinforcement ratio second, and reinforcement yield strength third.

This order is consistent with studies showing that deep beams are more sensitive to parameters affecting the compression field than to those affecting reinforcement yielding capacity (Tan et al., 1995; Liu & Mihaylov, 2016; Ma et al., 2022)

## 4.10 Summary of Chapter 4

This chapter presented the ABAQUS results and validated the numerical model against experimental data. The agreement in ultimate load, load-displacement response, and failure mode confirmed that the model was suitable for the parametric study.

The results showed that web openings significantly reduced load capacity, with central and larger openings producing the most severe deterioration.

UHPC was the most effective strengthening technique because it improved the disturbed region and stabilized the compression field, while CFRP provided a more moderate improvement mainly through crack control and tensile restraint.

Among the parametric variables, concrete compressive strength had the strongest influence, followed by transverse reinforcement ratio, whereas reinforcement yield strength had the least influence.

Overall, the chapter confirms that the greatest structural benefit is achieved by variables or strengthening systems that improve the integrity and efficiency of the internal load-transfer path.

# Chapter5 : Conclusions

Based on the validated nonlinear ABAQUS models developed in this study, several important conclusions can be drawn regarding the structural behavior of reinforced concrete deep beams with and without web openings, as well as the effectiveness of the investigated strengthening techniques.

First, the presence of web openings caused a severe reduction in the ultimate load capacity of the investigated deep beams. The reduction ranged from **62.42% to 65.69%** relative to the solid reference beam, depending on the size and location of the opening. This confirms that web openings should be interpreted primarily as a disturbance to the internal load-transfer path rather than merely as a reduction in concrete area.

Second, the structural response of deep beams with openings was governed mainly by the extent to which the opening disturbed the diagonal compression strut and weakened the continuity of the internal compression field. Openings located in more critical regions produced more severe structural deterioration than those placed farther from the principal load path, while larger openings caused greater weakening of the remaining concrete ligaments and the alternative force-transfer mechanism.

Third, among the investigated strengthening techniques, **UHPC** demonstrated the highest effectiveness in improving structural performance. The increase in ultimate load capacity ranged from **24.34% to 32.61%**, indicating that UHPC provided substantial enhancement in beam response. This improvement reflects its ability to improve the continuity and efficiency of the disturbed compression field and to provide a stronger structural contribution beyond crack control alone.

In contrast, **CFRP** strengthening provided a more moderate improvement. The increase in ultimate load capacity ranged from **11.9% to 15.35%**, which confirms that CFRP can enhance the structural response, but to a lesser extent than UHPC. Its main contribution was associated primarily with crack restraint and tensile enhancement, while its effect on the disturbed internal load-transfer mechanism was less pronounced.

Fourth, among the investigated parametric variables, **concrete compressive strength** showed a much stronger influence on beam capacity than **reinforcement yield strength**. For the solid beam DP-S2, increasing the reinforcement yield strength from **420 MPa to 620 MPa** increased the ultimate load by only about **8.3%**, whereas increasing the concrete compressive strength from **30 MPa to 50 MPa** increased the ultimate load by about **26.0%**. This confirms that the behavior of deep beams is governed primarily by the capacity and stability of the concrete compression field.

Fifth, the results also showed that first-cracking behavior provides important insight into the early-stage structural response of deep beams. Parameters that disturbed the internal force path accelerated crack initiation, whereas parameters that improved the continuity of the load-transfer mechanism delayed first cracking. This indicates that serviceability-related behavior and ultimate

structural response are closely related in deep beams and should be interpreted within the same mechanical framework.

Overall, the findings of this study confirm that the structural behavior of reinforced concrete deep beams is governed mainly by the integrity, continuity, and efficiency of the diagonal compression strut. Therefore, any parameter or strengthening technique that improves this internal load-transfer mechanism has the greatest influence on structural performance.

## 5.1 Recommendations

Based on the findings of this study, the following recommendations are proposed:

- The use of UHPC is highly recommended for strengthening deep beams, particularly in cases where the structural mechanism is significantly disturbed, such as beams with large or centrally located openings.
- CFRP strengthening can be considered as a practical solution when crack control is the primary objective, especially in cases where full restoration of structural capacity is not required.
- The location and size of web openings should be carefully considered during the design stage. Edge openings are preferable to central openings, and large openings should be avoided whenever possible.
- Increasing concrete compressive strength is an effective method to enhance the load-carrying capacity and delay crack initiation in deep beams.
- Providing adequate transverse reinforcement is important for crack control and improving post-cracking behavior; however, excessively high reinforcement ratios may not be economically efficient due to diminishing returns.
- Increasing reinforcement yield strength alone is not sufficient to significantly improve the structural performance of deep beams.

## 5.2 Recommendations for Future Work

To further develop the understanding of deep beam behavior, the following areas are suggested for future research:

- Investigation of combined strengthening techniques (e.g., UHPC and CFRP together) to assess potential synergistic effects.
- Study of different opening shapes (circular, rectangular, irregular) and their influence on structural performance.
- Experimental validation of UHPC-strengthened deep beams with various opening configurations.
- Investigation of long-term behavior, including creep, shrinkage, and durability effects.
- Extension of the study to different shear span-to-depth ratios (a/d) to generalize the findings

# Chapter6 References


1. Abadel, A. A., & Alharbi, Y. R. (2025). Experimental and numerical study on strengthening of UHPFRC deep beams with square openings using CFRP and WWM configurations. Case Studies in Construction Materials, 23, e05157. https://doi.org/10.1016/j.cscm.2025.e05157
2. Abbood, I. S. (2023). Strut-and-tie model and its applications in reinforced concrete deep beams: A comprehensive review. Case Studies in Construction Materials, 19, e02643. https://doi.org/10.1016/j.cscm.2023.e02643
3. ACI Committee 318. (2019). Building Code Requirements for Structural Concrete (ACI 318-19) and Commentary.
4. ACI-ASCE Committee 426. (1974). The shear strength of reinforced concrete members (ACI 426R-74). Journal of the Structural Division, ASCE, 99(ST6), 1091–1187.
5. Al-Bayati, N. A., Muhammad, B. R., & Hasan, A. S. (2016). Structural behavior of self-compacting reinforced concrete deep beams containing openings. Engineering and Technology Journal, 34(Part A, No. 12). https://www.uotechnology.edu.iq/tec_magaz/2016/volum342016/No.12.A.2016/[13]Text.pdf
6. Al-Enezi, M. S., Yousef, A. M., & Tahwia, A. M. (2023). Shear capacity of UHPFRC deep beams with web openings. Case Studies in Construction Materials, 18, e02105. **https://doi.org/10.1016/j.cscm.2023.e02105**
7. Alhayani, A. A., & Almssad, A. (2026). Size and location influence of opening on shear capacity of RC deep beams using ANN. Journal of Asian Architecture and Building Engineering. https://doi.org/10.1080/13467581.2025.2610888
8. Ali, Y. A., Hashim, T. M., & Ali, A. H. (2023). Numerical investigation on effect of opening ratio on structural performance of reinforced concrete deep beam reinforced with CFRP enhancements. Infrastructures, 8(1), 2. https://doi.org/10.3390/infrastructures8010002
9. Almassri, B. (2024). Experimental and FE numerical analysis of RC shear walls retrofitted using CFRP and steel plates. The Open Civil Engineering Journal, 18, e18741495344620. https://doi.org/10.2174/0118741495344620240830103333
10. Al-Osta, M. A. (2018). Exploitation of ultrahigh-performance fibre-reinforced concrete for the strengthening of concrete structural members. **Advances in Civil Engineering, 2018**, 8678124. **https://doi.org/10.1155/2018/8678124**
11. Ashour, A. F., & Rishi, G. (2000). Tests of reinforced concrete continuous deep beams with web openings. ACI Structural Journal, 97(3), 418–426. https://doi.org/10.14359/4636
12. Ashour, A. F., & Rishi, G. (2000). Tests of reinforced concrete continuous deep beams with web openings. ACI Structural Journal, 97(3), 418–426. https://doi.org/10.14359/4636

13. Augustino, D. S., Mwakalesi, A. J., & Mrema, G. C. (2022). The orientation effect of opening and internal strengthening on shear performance of deep concrete beam using recycled tyre steel fibres. Results in Engineering, 15, 100561. **https://doi.org/10.1016/j.rineng.2022.100561**
14. Campione, G., & Minafò, G. (2012). Behaviour of concrete deep beams with openings and low shear span-to-depthratio. Engineering Structures, 41, 294–306. **https://doi.org/10.1016/j.engstruct.2012.03.055**

15. Chen, J. F., & Teng, J. G. (2003). Shear capacity of FRP-strengthened RC beams: FRP debonding. Construction and Building Materials, 17(1), 27–41. https://doi.org/10.1016/S0950-0618(02)00091-0
16. El Maaddawy, T., & Sherif, S. (2009). FRP composites for shear strengthening of reinforced concrete deep beams with openings. Composite Structures, 89(1), 60–69. https://doi.org/10.1016/j.compstruct.2008.06.022
17. Elghany, A. A., Elsayed, M., Elsayed, A., & Shaheen, A. (2025). Enhancement of the shear capacity of RC deep beams with ultra-high performance fiber-reinforced concrete. Engineering, Technology & Applied Science Research, 15(1), 20418–20424. https://doi.org/10.48084/etasr.9792
18. El-Kassas, A. I., Hassan, H. M., & Arab, M. A. E. S. (2020). Effect of longitudinal opening on the structural behavior of reinforced high-strength self-compacted concrete deep beams. Case Studies in Construction Materials, 12, e00348. https://doi.org/10.1016/j.cscm.2020.e00348
19. Graybeal, B. (2014). Design and construction of field-cast UHPC connections (Report No. FHWA-HRT-14-084). Federal Highway Administration (FHWA), U.S. Department of Transportation. https://www.fhwa.dot.gov/publications/research/infrastructure/structures/14084/index.cfm
20. Abbood, I. S. (2023). Strut-and-tie model and its applications in reinforced concrete deep beams: A comprehensive review. Case Studies in Construction Materials, 19, e02643. https://doi.org/10.1016/j.cscm.2023.e02643

21. Hu, B., & Wu, Y.-F. (2018). Effect of shear span-to-depth ratio on shear strength components of RC beams. Engineering Structures, 168, 770–783. https://doi.org/10.1016/j.engstruct.2018.05.017
22. Hu, O. E., Tan, K.-H., & Liu, X. H. (2007). Behaviour and strut-and-tie predictions of high-strength concrete deep beams with trapezoidal web openings. Magazine of Concrete Research, 59(7), 529–541.https://doi.org/10.1680/macr.2007.59.7.529
23. Ibrahim, M., Wakjira, T., & Ebead, U. (2020). Shear strengthening of reinforced concrete deep beams using near-surface mounted hybrid carbon/glass fibre reinforced polymer strips. Engineering Structures, 210, 110412. **https://doi.org/10.1016/j.engstruct.2020.110412**

24. Jasim, W. A., Abu Tahnat, Y. B., & Halahla, A. M. (2020). Behavior of reinforced concrete deep beam with web openings strengthened with CFRP sheet. Structures, 26, 785–800. https://doi.org/10.1016/j.istruc.2020.05.003
25. Jasim, W. A., Allawi, A. A., & Oukaili, N. K. (2018). Strength and serviceability of reinforced concrete deep beams with large web openings created in shear spans. Civil Engineering Journal, 4(11), 2560-2574. http://dx.doi.org/10.28991/cej-03091181
26. Karimzadeh, H., & Arabzadeh, A. (2021). A STM-based analytical model for predicting load capacity of deep RC beams with openings. Structures, 34, 1185–1200. https://doi.org/10.1016/j.istruc.2021.08.052
27. Khalaf, M. R., Al-Ahmed, A. H. A., Allawi, A. A., & El-Zohairy, A. (2021). Strengthening of continuous reinforced concrete deep beams with large openings using CFRP strips. Materials, 14(11), 3119. https://doi.org/10.3390/ma14113119
28. Kong, F. K., & Evans, R. H. (1987). Reinforced concrete deep beams. Blackie & Son Ltd. https://books.google.com/books?id=Nex0QgshO2wC
29. Kong, F. K., & Sharp, G. R. (1977). Structural idealization for deep beams with web openings. Magazine of Concrete Research, 29(99), 81–91. https://doi.org/10.1680/macr.1977.29.99.81.
30. Li, V. C. (2004). High performance fiber reinforced cementitious composites as durable material for concrete structure repair. International Journal for Restoration of Buildings and Monuments, 10(2), 163–180. https://www.academia.edu/84898480
31. Li, Y., Chen, H., Yi, W.-J., Peng, F., Li, Z., & Zhou, Y. (2021). Effect of member depth and concrete strength on shear strength of reinforced concrete deep beams without transverse reinforcement. Engineering Structures, 241, 112427. https://doi.org/10.1016/j.engstruct.2021.112427
32. Liu, J., & Mihaylov, B. I. (2016). A comparative study of models for shear strength of reinforced concrete deep beams. Engineering Structures, 112, 81–89. https://doi.org/10.1016/j.engstruct.2016.01.012
33. Lu, W.-Y., Lin, I.-J., & Yu, H.-W. (2013). Shear strength of reinforced concrete deep beams. ACI Structural Journal, 110(4), 671–680. https://doi.org/10.14359/51685640
34. Ma, C., Xie, C., Tuohuti, A., & Duan, Y. (2022). Analysis of influencing factors on the shear behavior of reinforced concrete deep beams. Journal of Building Engineering, 45, 103383. **https://doi.org/10.1016/j.jobe.2021.103383**
35. Mabrouk, R. T. S., Mahmoud, M. A. S., & Kassem, M. E. (2022). Behavior of reinforced concrete deep beams with openings under vertical loads using strut and tie model. Civil Engineering Journal, 7(Special Issue), 148–170. https://doi.org/10.28991/CEJ-SP2021-07-011
36. Mansour, M., & El-Maaddawy, T. (2021). Testing and modeling of deep beams strengthened with NSM-CFRP reinforcement around cutouts. Case Studies in Construction Materials, 15, e00670. https://doi.org/10.1016/j.cscm.2021.e00670

37. Mansur, M. A., & Alwis, W. A. M. (1984). Reinforced fibre concrete deep beams with web openings. International Journal of Cement Composites and Lightweight Concrete, 6(4), 263–271. https://doi.org/10.1016/0262-5075(84)90021-6
38. Megahed, K. (2024). Prediction and reliability analysis of shear strength of RC deep beams. Scientific Reports, 14, 14590. **https://doi.org/10.1038/s41598-024-64386-w**
39. Mirzaaghabeik, H., Mashaan, N. S., & Shukla, S. K. (2025). Shear behavior of ultra-high-performance concrete deep beams reinforced with fibers: A state-of-the-art review. Infrastructures, 10(3), 67. **https://doi.org/10.3390/infrastructures10030067**
40. Park, J.-W., & Kuchma, D. A. (2007). Strut-and-tie model analysis for strength prediction of deep beams. ACI Structural Journal, 104(5), 573–581. https://www.researchgate.net/publication/285744070
41. Rahim, N. I., Mohammed, B. S., Al-Fakih, A., Wahab, M. M. A., Liew, M. S., Anwar, A., & Amran, Y. H. M. (2020). Strengthening the structural behavior of web openings in RC deep beam using CFRP. Materials, 13(12), 2804. https://doi.org/10.3390/ma13122804
42. Schlaich, J., Schäfer, K., & Jennewein, M. (1987). Toward a consistent design of structural concrete. PCI Journal, 32(3), 74–150. https://doi.org/10.15554/pcij.05011987.74.150
43. Subedi, N. K., Vardy, A. E., & Kubota, N. (1986). Reinforced concrete deep beams: Some test results. Magazine of Concrete Research,38(137),206–219. https://doi.org/10.1680/macr.1986.38.137.206
44. Tan, K. H., Kong, F. K., Teng, S., & Guan, L. (1995). High-strength concrete deep beams with effective span and shear span variations. ACI Structural Journal, 92(4), 395–405. https://doi.org/10.14359/991
45. Tan, K.-H., Kong, F.-K., Teng, S., & Weng, L.-W. (1997). Effect of web reinforcement on high-strength concrete deep beams. ACI Structural Journal, 94(5), 572–582. https://doi.org/10.14359/506
46. Tan, K.-H., Tang, C. Y., & Tong, K. (2004). Shear strength predictions of pierced deep beams with inclined web reinforcement. Magazine of Concrete Research, 56(8), 443–452. https://doi.org/10.1680/macr.2004.56.8.443.
47. Tuchscherer, R. G., Birrcher, D. B., & Bayrak, O. (2011). Strut-and-tie model design provisions. ACI Structural Journal, 108(4), 465–473. https://www.researchgate.net/publication/265436203
48. Yang, K.-H., Eun, H.-C., & Chung, H.-S. (2006). The influence of web openings on the structural behavior of reinforced high-strength concrete deep beams. Engineering Structures, 28(13), 1825–1834. https://doi.org/10.1016/j.engstruct.2006.03.021

49. Yousef, A. M., Tahwia, A. M., & Al-Enezi, M. S. (2023). Experimental and numerical study of UHPFRC continuous deep beams with openings. Buildings, 13(7), 1723. https://doi.org/10.3390/buildings13071723
50. Yousef, A. M., Tahwia, A. M., & Marami, N. A. (2018). Minimum shear reinforcement for ultra-high performance fiber reinforced concrete deep beams. Construction and Building Materials, 184, 177–185. https://doi.org/10.1016/j.conbuildmat.2018.06.022